Wireless Networks

Bin Lin
Jianli Duan
Mengqi Han
Lin X. Cai

Next Generation Marine Wireless Communication Networks

Springer

Wireless Networks

Series Editor

Xuemin Sherman Shen, University of Waterloo, Waterloo, ON, Canada

The purpose of Springer's Wireless Networks book series is to establish the state of the art and set the course for future research and development in wireless communication networks. The scope of this series includes not only all aspects of wireless networks (including cellular networks, WiFi, sensor networks, and vehicular networks), but related areas such as cloud computing and big data. The series serves as a central source of references for wireless networks research and development. It aims to publish thorough and cohesive overviews on specific topics in wireless networks, as well as works that are larger in scope than survey articles and that contain more detailed background information. The series also provides coverage of advanced and timely topics worthy of monographs, contributed volumes, textbooks and handbooks.

** Indexing: Wireless Networks is indexed in EBSCO databases and DPLB **

More information about this series at https://link.springer.com/bookseries/14180

Bin Lin • Jianli Duan • Mengqi Han • Lin X. Cai

Next Generation Marine Wireless Communication Networks

Springer

Bin Lin
School of Information Science and Tech
Dalian Maritime University
Dalian, China

Jianli Duan
School of Science, Qingdao University of Technology
Qingdao, China

Mengqi Han
Illinois Institute of Technology
Chicago, IL, USA

Lin X. Cai
Illinois Institute of Technology
Chicago, IL, USA

ISSN 2366-1186 ISSN 2366-1445 (electronic)
Wireless Networks
ISBN 978-3-030-97306-3 ISBN 978-3-030-97307-0 (eBook)
https://doi.org/10.1007/978-3-030-97307-0

This Springer imprint is published by the registered company Springer Nature Switzerland AG
The registered company address is: Gewerbestrasse 11, 6330 Cham, Switzerland

Preface

In the past decades, we have witnessed the rapid development of marine programs in many countries. Marine communication and networking, as an important cornerstone of the delivery of maritime services, is deeply integrated into production and life of people in coastal countries. The next generation Marine Wireless Communication Networks (MWCNs) are expected to incorporate advanced communication and networking technologies to meet the ever-increasing demand of maritime services, and to enable many new intelligent maritime applications such as environment-adaptive navigation, intelligent cargo storage management, underwater inspection and surveillance, telemedication, and maritime emergency rescue. However, marine communications are faced with many fundamental challenges such as complex marine environments, fast-changing maritime channels, and limited spectrum resources. These challenging issues may greatly degrade the quality of service of MWCN in terms of latency, reliability, and scalability.

This book aims to address these challenges in the design and development of next generation MWCNs. Specifically, we will explore the key technologies in the following general categories to improve the network performance, including (1) the network deployment, (2) the physical layer channel coding, (3) the link layer resource management, and (4) the network layer routing design. The objective of the book is to provide a comprehensive guide for the audience to understand the design principle and development of MWCNs in support of numerous maritime services.

The book is organized as follows. An overview of MWCNs is first presented, including maritime applications and a comprehensive survey of existing MWCNs, followed by a detailed discussion of challenges of maritime communications and networking in different layers. In order to address these challenges, e.g., high deployment costs of marine sensors in a large-scale three-dimensional space, and long propagation delay of underwater acoustic channel, we first study the network deployment and management of next generation MWCNs with a multi-tier hierarchical network architecture that includes three sub-networks, namely, the underwater acoustic sub-network, the sea-surface wireless sub-network, and the air wireless sub-network. Then, a novel Orthogonal Frequency Division Multiplexing (OFDM)

autoencoder featuring CNN-based channel estimation is presented for marine communications with complex and fast-changing environments. Next, the energy sustainable performance of an underwater sensor network using a random-access protocol is analytically studied, taking into consideration the stochastic nature of energy harvesting and the unique feature of the acoustic communication channel. Furthermore, in order to monitor the marine environment and surveil the sensor ecosystem, an Energy-efficient Depth-based Opportunistic Routing Algorithm with Q-learning (EDORQ) is proposed for marine wireless sensor networks to guarantee the energy efficiency and reliable data transmissions. Finally, we summarize the book and outline the possible further research directions.

We would like to acknowledge with thanks Prof. Nan Wu (Dalian Maritime University, China), Prof. Rongxi He (Dalian Maritime University, China), Prof. Yuanguo Bi (Northeast University, China), Prof. Haibo Zhou (Nanjing University, China), and Prof. Nan Cheng (Xidian University, China) for their valuable suggestions and comments on this book. We would like to thank the helpful suggestions made by the reviewers, including Xu Hu, Shuang Qi, Chaoyue Zhang, Haocheng Wang, and Jiaye Li. Special thanks to the staffs at Springer Nature: Hemalatha Velarasu and Mary E. James, for their effort and support throughout the publication preparation process.

Dalian, China — Bin Lin
Qingdao, China — Jianli Duan
Chicago, IL, USA — Mengqi Han
Chicago, IL, USA — Lin X. Cai

Contents

Abbreviations

AANet	Adaptive aggregation network
AIS	Automatic identification system
ANO	Average network overhead
AoA	Arrival of angle
AP	Access point
APD	Average packet delay
AR	Augmented reality
ARN	Aerial relay node
ARQ	Automatic repeat request
ASM	Application specific messages
AUVs	Autonomous underwater vehicles
BDS	BeiDou navigation satellite system
BLER	Block error rate
BnB	Branch and bound
BSs	Base stations
CE	Channel estimator
CIRs	Channel impulse responses
CL	Candidate location
CNNs	Convolutional neural networks
Co-DNAR	Cooperative DNAR
CoEERD	Cooperative effective energy and reliable delivery
COSPAS/SARSAT	International satellite system for search and rescue services
CP	Cyclic prefix
CSI	Channel state information
CSMA/CA	Carrier-sense multiple access with collision avoidance
CTS	Clear to send
DART	Deep-ocean assessment and reporting of tsunamis
DBR	Depth-based routing
DEADS	Depth and energy aware dominating set based algorithm
Dense-Net	Dense convolutional neural networks

DFT	Discrete Fourier transform
DL	Deep learning
DNAR	Depth and noise-aware routing
DSC	Digital selective calling
ECN	Edge computing node
EDORQ	Energy-efficient depth-based opportunistic routing algorithm with Q-learning
EE-DBR	Energy-efficient depth-based routing algorithm
EERD	Effective energy and reliable delivery
ELF	Extremely low frequency
ELT	Emergency locator transmitter
eMBB	Enhanced mobile broadband
EPIRB	Emergency position indicating radio beacon
ESONET	European Seas Observatory Network
EW	Electromagnetic waves
FC	Full connected
FCL	Feasible candidate location
FDMA	Frequency division multiple access
FSK	Frequency-shift keying
GEO	Geostationary Earth Orbit
GMDSS	Global Maritime Distress and Safety System
GOES	Geostationary Operational Environmental Satellite
GOOS	Global Ocean Observing System
GX	Global Xpress
HAPs	High-altitude platforms
HD	High definition
HF	High frequency
HH-VBF	Hop-by-Hop vector-based forwarding algorithm
IALA	International Association of Maritime Aids to Navigation and Lighthouse Authorities
IDFT	Inverse discrete Fourier transform
IMO	International Maritime Organization
INMARSAT	International Maritime Satellite
IoV	Internet of vessels
ISI	Inter-symbol interference
ITU	International Telecommunication Union
LEO	Low Earth orbit
LMMSE	Linear minimum mean square error
LS	Least squares
LUT	Local user terminal
MASS	Maritime autonomous surface ship
MCC	Mission Control Center
MDP	Markov decision process
MEC	Mobile edge computing

MEO	Medium Earth orbit
MF	Medium frequency
MMN	Marine monitoring network
MO	Multi-objectives optimization
MSI	Maritime safety information
MWCNs	Marine wireless communication networks
NAVTEX	Navigational Telex
NBDP	Narrow band direct printing
NCC	Network Control Center
NCS	Network Coordination Station
NFV	Network functions virtualization
NS2	Network simulator version 2
OFDM	Orthogonal frequency division multiplexing
OR	Opportunistic routing
OVAR	Opportunistic void avoidance routing
PDR	Packet delivery ratio
PLB	Personal locator beacon
QDAR	Q-learning based delay-aware routing
QELAR	Q-learning-based energy-efficient and lifetime-aware routing
QKS	Q-Learning with additional kinematics and sweeping features
QoS	Quality of service
RCC	Rescue coordination center
Res-Net	Residual network
RF	Radio frequency
ROVs	Remote operated vehicles
RSS	Received signal strength
RTS	Request to send
SAGSIN	Space-air-ground-sea integrated networks
SCS	Special communications systems
SDN	Software defined network
SIFS	Shortest interframe space
SOLAS	International Convention for the Safety of Life at Sea
SOTDMA	Self-organized time division multiple access
SSN	Sea-surface node
TEC	Total energy consumption
ToA	Time of arrival
TRITON	TRI-media Telematic Oceanographic Network
UAN	Underwater acoustic network
UAVs	Unmanned aerial vehicles
UNCTAD	United Nations Conference on Trade and Development
URLLC	Ultra-reliable and low latency communication
URN	Underwater relay node
UWSNs	Underwater wireless sensor networks
VAPR	Void-aware pressure routing

VBF	Vector-based forwarding
VDE	VHF data exchange
VDES	VHF data exchange system
VDL	VHF data links
VHF	Very high frequency
VLF	Very low frequency
VR	Virtual reality
VSAT	Very small aperture terminal
WiMAX	World Interoperability for Microwave Access
WISEPORT	Wireless broadband access project
WSN	Wireless sensor network

Chapter 1
Introduction

The area of the ocean is about 360 million square kilometers, which accounts for about 71% of the earth surface area. As a huge treasure house of resources, the ocean contains rich ecosystems with mineral wealth, chemical resources, biological resources, and so on. It is not only an important place for human activities such as fishery, maritime transportation, and offshore industries, but also a potential area of human habitat in the future [1]. Therefore, the development of the marine industry is highly relevant to the growth of global economy and the maintenance of a healthy global biosphere.

Maritime economy is essential to the economic growth and prosperity worldwide. Maritime transport accounts for more than 90% of world trade. At the beginning of 2020, the total world fleet amounted to 98,140 commercial ships of 100 gross tons and above, equivalent to a capacity of 2.06 billion dead-weight tons, excluding inland waterway vessels, fishing vessels, military vessels, yachts, and fixed/mobile offshore platforms. United Nations Conference on Trade and Development (UNCTAD) estimates that the total volume of maritime trade including the tanker trade, main bulk, and other dry cargo reaches 11.08 billion tons in 2019 [2].

Marine tourism is one of the largest industries in the world marine economy. Recent developments suggest that marine tourism has become one of the fastest growing areas of the world's tourism. According to the statistics from Cruise Lines International Association, the number of cruise tourists worldwide reached 28.5 million in 2018, an increase of 74.8% over 16.3 million in 2008, with an average annual growth rate of 5.8% [3]. Despite the negative impact of COVID-19 on the world economy, the marine economy still plays an important role in global economic development. As human activities in oceans continuously increase, it becomes critical and pressing to provision reliable and cost-effective maritime services over Marine Wireless Communication Networks (MWCNs) [1].

Marine ecosystem spanning over polar, temperate, and tropical waters is an indispensable part of the global ecosystems. The stability of ocean ecosystem is important for regulating the global climate and the biological productivity of the ocean. However, some human activities in the ocean may cause damage to the

B. Lin et al., *Next Generation Marine Wireless Communication Networks*, Wireless Networks, https://doi.org/10.1007/978-3-030-97307-0_1

marine environment and ocean resources to some extent. As such, many coastal countries develop environmentally sustainable strategies to rationally exploiting marine resources while protecting marine environment. For example, the UK released the "Marine Energy Plan 2010," which presented a vision of a renewable energy strategy and a low-carbon industrial strategy [4]. In 2019, China first proposed the concept of building a maritime community with a shared future, which has charted the path and direction for global maritime governance. To protect the marine environment, marine monitoring systems are deployed to monitor the ocean environments, including Global Ocean Observing System (GOOS), Neptune, European Seas Observatory Network (ESONET), etc. The MWCNs can realize the interconnections among observation equipment, expand the observation coverage, and thus enhance the real-time ocean monitoring and surveillance.

In addition to the development of the marine industry, it is also well noted that maritime safety issues are arising. Maritime emergencies, such as a sinking ship, will cause not only heavy casualties, but also huge economic losses. For example, in 2006, the Egyptian passenger ship Al Salam Boccaccio 98 sank in the Red Sea with more than 1400 people on board, leaving more than 1000 people dead or missing. It is of great significance to improve the capability of dealing with and responding to maritime emergencies to enhance the safety of life and property at sea while promoting the steady development of the marine industry. Maritime emergency services can help emergency rescue by comprehensively utilizing various communication resources in case of maritime emergencies or marine natural disasters [5]. The Global Maritime Distress and Safety System (GMDSS) proposed by International Maritime Organization (IMO) is the most well-known system for maritime emergency.

Facing the rapid development trend of maritime activities, MWCNs are expected to provide ultra-reliable, low-latency, and low-cost communication services [6]. However, the current MWCNs can only meet the needs of some services and are not able to cope with the continued growth of marine applications. For example, the current maritime medical services can only support text message and voice transmissions due to limited bandwidth, thus complicated diagnose or surgeries that require real-time video communication cannot be performed [7]. The construction of MWCNs also faces great challenges due to the salient features of oceans. Firstly, the deployment of network infrastructure over sea is much more difficult compared with territorial networks as geographical space available for deploying Base Stations (BSs) at sea is very limited. Offshore communications rely on shore-based communication networks, while communication services in the open sea can only be provided by maritime satellites. Secondly, the communication environment in the ocean is very complicated, and the hostile weather and ocean conditions may seriously affect the communication quality. Finally, maritime nodes usually have to be operated in high humidity or seawater immersion environment for a long time under the influence of strong winds and waves. How to improve the lifetime of network equipment is another challenging task. More details will be described in Sect. 1.2. Catering to the growing needs of maritime communications, we aim at

addressing the challenges in the design and development of next generation MWCNs.

This chapter is organized as follows: Sect. 1.1 provides an overview of MWCNs, including the applications of MWCNs, the current MWCNs, and the next generation MWCNs. Section 1.2 discusses the research challenges of MWCNs. Section 1.3 presents the organization of this book.

1.1 Overview of Marine Wireless Communications and Networks (MWCNs)

1.1.1 Maritime Applications in MWCNs

Advanced wireless communication technologies enable many maritime services spanning from ocean monitoring and surveillance to emergency rescue. Digital Selective Calling (DSC), Narrow Band Direct Printing (NBDP), ship identification, and monitoring services rely on maritime communication over Medium Frequency (MF), High Frequency (HF), and Very High Frequency (VHF) bands. International Satellite System for Search and Rescue Services (COSPAS/SARSAT) and International Maritime Satellite (INMARSAT) provide emergency alarm, ship position identification, and positioning and location inquiry services. In the offshore area, the shore-based mobile communication system provides broadband data services for ports, docks, channel management, mariculture, and marine rescue. Recently, Internet of Things (IoT) technology that incorporates sensing, actuation, computation, control, and communications has been used to provide various intelligent maritime services. In this subsection, we introduce four typical intelligent maritime applications including smart transport, environmental monitoring, entertainment, and emergency rescue.

1.1.1.1 Smart Maritime Transport

The smart transport is in urgent need due to the demand of maritime traffic and port logistics tasks. A smart maritime transport system can make use of water transportation facilities and information resources to improve ship navigation efficiency and safety and to realize the socialization of water transport service and smart management. The necessity of smart maritime transport can be reflected in many application scenarios described below.

The first scenario is the situational awareness of navigation environment. According to the statistics of the International Maritime Organization (IMO), the predominant reasons for sea transport accidents are due to human mistakes (overloading, improper navigation) and/or environmental factors such as storms and cyclones. If a crew member is aware of an improper operation in time and the

weather conditions can be accurately predicted in advance, the risk of marine accidents can be greatly reduced. Thus, it is desirable for a vessel to employ a network system comprised of different information sensing nodes, e.g., to determine the numbers of passengers and freight, ship location and speed, the value of freeboard, the tidal wave height, and water current speed and direction, and to check the weather conditions and so forth to avoid marine accidents [8, 9]. Another application scenario is the operation of Maritime Autonomous Surface Ship (MASS). A MASS is a highly automated ship, which greatly reduces the demand for the number of crew, and thus releases more space for cargo for a given tonnage. The automation of MASS relies on a reliable maritime communication network. For example, in the scenario of MASS berthing and unberthing, the operators on the shore send control signals according to the real-time video from the unmanned ship, which requires very low latency and high reliability [10, 11]. The third application scenario is marine cargo storage monitoring. As there is generally no monitoring equipment in closed containers, it is difficult to ensure the real-time monitoring of goods that are sensitive to storage conditions in traditional transportation systems. Thus, a sensor network should be deployed to monitor the environmental parameters of cargo storage in real time.

The deployment of modern MWCNs can further improve the transport services by combining advanced communication technologies and artificial intelligence. In the first application scenario, sensors on board can send the navigation environment data to the cloud servers, which analyze the data with trained decision models to predict the present situation of the sailing vessel, so as to realize the situational awareness of navigation environment. In case of any emergency predicted by the cloud service, it sends an alert message with detailed information to the onshore rescue center and the vessel itself. In the second application scenario, the MWCNs based on Software Defined Network (SDN) can provide MASS with Enhanced Mobile Broadband (eMBB) or Ultra-reliable and Low Latency Communication (URLLC) services, such as High Definition (HD) surveillance video transmission and remote control of MASS berthing and unberthing. In the third application scenario, intelligent containers equipped with sensors can send monitoring data such as temperature and humidity to a remote server on the vessel. Via MWCNs, the monitoring data are transmitted to the servers onshore, where these data are analyzed, and the storage environment can be evaluated, and control messages can be sent back to the vessel to make adjustment according to the actual needs [12, 13].

1.1.1.2 Marine Environmental Monitoring

Some human activities such as oil spill, industrial wastewater discharge, and overfishing may cause severe damage to the marine environment. The sustainable development of marine resources has gradually become a world consensus. However, it is very challenging to monitor the vast marine areas, especially in the deep ocean. With the recent advanced Internet of Things technologies, it is possible to

collect and forward information with the help of Underwater Wireless Sensor Networks (UWSNs).

The UWSNs are deployed over the different depths in the ocean to monitor the ocean environment and to surveil the marine ecosystem. For vast water bodies like oceans, rivers, and large lakes, data is collected from the different depths of the water levels and then delivered to the surface sinks which are usually installed on the sea surface. Take an example of seawater pollution detection, the sensors nodes that can be deployed on the seafloor or float in the seawater collect and monitor marine environmental parameters, such as water temperature, salinity, pH, and oxygen content. The sensed data are then transmitted to the onshore server via MWCNs [14]. UWSNs can also be applied for underwater pipeline monitoring. In this case, sensor nodes can be divided into two categories: static nodes and floating nodes. The static nodes are attached to the pipelines so that they are able to monitor the critical parameters of the pipelines. The floating nodes pulled by ropes installed on the seabed are arranged in seawater at different depths, which can be used to relay the received underwater acoustic signal transmitted by other nodes to the receivers on the sea surface. The static nodes collect the pressure and velocity of the oil and the acoustic vibration caused by the leakage if there is any, and the sensed data can be forwarded to the floating nodes. Even though these floating nodes may move around in the sea, they are attached to the sea bed or floating buoy with strings to keep them in range. These floating nodes relay the data to the surface sink, which communicate with the control center with radio-frequency communication [15, 16].

1.1.1.3 Entertainment

Marine tourism is one of the largest industries in the world marine economy. Take China as an example. According to the statistics of the National Development and Reform Commission, in 2019, China's value of marine tertiary industry was 5370 billion Yuan, where the marine tourism contributed 1808.6 billion Yuan. In order to meet the continuous development of marine tourism, it is also critical to promote marine communication networks.

In terms of cruise tourism, passengers on board need a broadband communication network to watch live sports events, performances, entertainment programs with High Definition (HD) television, and to have real-time video conferences at sea. In the scenarios of new media game services, the players on board need high-bandwidth and low latency services for immersive gaming experience, such as Virtual Reality (VR), Augmented Reality (AR), ultra-high definition video games. The deployment of MWCNs based on Space-Air-Ground-Sea Integrated Networks (SAGSIN) can extend the coverage and enhance the quality of communication, which will help to realize the entertainment services mentioned above. In some underwater entertainment projects such as scuba dive in the deep sea, diving tourists use underwater acoustic communication networks to communicate with each other, e.g., to exchange position and the equipment status information which are important to ensure their personal safety. It has been pointed out in [17] that the planar Ad Hoc

network based on Very Low Frequency (VLF) or Extremely Low Frequency (ELF) can be used for small underwater formation communication, which makes it possible for a small group of diving tourists to communicate with each other, thus improving their tourism entertainment experience as well as enhancing their ability to deal with emergencies.

1.1.1.4 Emergency Rescue

Emergency rescue is a critical application as various marine natural disasters have caused serious damage to human manufacture and life. It is of critical importance to rescue the crew of the ship when two cruises collide, to evaluate the staff on the drilling platform in case of bad weather, and to tele-medicate injured or sick people on ship. The rescue operation cannot be implemented without the support of communication networks. Different from land emergency communication support, marine emergency communication support usually needs to face adverse conditions such as the difficulties in deployment of communication infrastructures and harsh marine communication environment.

The real-time image and video transmissions of the onsite scene are crucial for the command and coordination of the rescue operation. When a marine accident occurs, the onsite situation of marine search and rescue can be collected by MWCNs in real time, so as to guarantee fast and efficient search and rescue. In addition, underwater emergency communication can also provide communication and positioning services for underwater rescue, wreck positioning, search and rescue as well as salvage. Besides these, MWCNs make telemedicine possible. Maritime telemedicine allows for remote diagnose of patients, monitoring, telemedicine training and surgery, and so on.

In terms of tsunami warning, the USA has implemented a project called Deep-ocean Assessment and Reporting of Tsunamis (DART) [18]. Each DART tsunami buoy includes a seabed pressure recorder anchored on the seabed and an anchored sea buoy. The seabed pressure recorder uses a pressure sensor to detect the sea water pressure change caused by the tsunami and transmit the information to the buoy through the underwater acoustic channel, and the buoy can be used to monitor the sea surface. The data from the seabed and sea surface are transmitted to the ground station through the Geostationary Operational Environmental Satellite (GOES).

1.1.2 Current Marine Wireless Communication Networks

Currently, maritime mobile terminals mainly acquire communication services via maritime satellites or through shore-based communication networks [19]. Specifically, BSs are deployed on the coast line or islands to serve users in the offshore area. In the open sea area where it is very difficult to deploy BSs, maritime satellites are

used to provide effective communications for marine users, which are usually sparsely distributed over the sea and the communication distance is very long.

Traditional maritime satellite communications can provide communication services for aero amphibious users and can be widely used for improving ship safety, disaster rescue, and other maritime services. Compared with territorial network, satellite communications are not limited by geographical locations and thus are suitable for remote stations to communicate with each other [20]. The major issue of satellites communication is the cost as launching a satellite is not an easy task, especially for geostationary satellites where the orbit space is limited. In addition, maritime satellites usually use licensed spectrum, which is precious for wireless users. Due to limited bandwidth of satellites, the data rates of satellites communications are usually on the order of mega bit per second. For example, the maritime communication rates of the Inmarsat and Very Small Aperture Terminal (VSAT) are up to 50 and 46 Mbps, respectively.

In the offshore area, besides maritime satellites communication networks, an alternative networking solution is offshore communication networks where BSs are deployed on the shore area to serve offshore users. For example, Digital Selective Calling (DSC), Navigational Telex (NAVTEX), can provide a communication coverage of several 100 km using MF, HF, and VHF bands. Due to the limited bandwidth in these frequency bands, some killing applications such as HD video and LiDAR may not be fully supported [21, 22].

It has been well recognized that vast unexploited areas lie under water. UWSN is emerging as an enabling technology for underwater explorations, such as monitoring the marine environment for scientific research, commercial exploitation, and coastline protection. Generally speaking, UWSN is a network of a number of autonomous sensor nodes spatially distributed underwater, possibly in different depth, to sense the water temperature, pressure, and other parameters, and transmit the sensed data to a sink node for data analytics. Since radio waves do not propagate well underwater, RF based communications including shore-based maritime wireless communication and maritime satellite communication are not suitable for underwater communications [23]. Instead, underwater sensors use acoustic transceivers to communicate with each other. The acoustic waves are low frequency waves of a small bandwidth but a long wavelength. Thus, acoustic waves can travel long distances, e.g., on the order of kilometers [24].

In the following subsection, we will introduce offshore/open sea communication and UWSNs in MWCNs, respectively. Finally, GMDSS, an application example of MWCNs will be presented.

1.1.2.1 Offshore Wireless Communication

In an offshore wireless communication network, BSs are installed on coasts, islands, or reefs to provide communication coverage to users in the offshore area using MF, HF, and VHF frequency bands. A typical offshore maritime communication system

mainly includes NAVTEX system, PACTOR system, and Automatic Identification System (AIS).

NAVTEX system sends navigational warning, weather warning, weather forecasts, and other maritime safety information to ships from coastal station by using the Narrow Band Direct Printing (NBDP). The information may be relevant to all types and sizes of vessels and the selective message-rejection feature ensures that every mariner can receive the broadcasted safety information relevant to their voyage [25]. It adopts Frequency-Shift Keying (FSK) modulation scheme and mainly uses 518 kHz bands to broadcast information in English and uses 490 kHz band for information in other languages. Basically, it is difficult for NAVTEX to adapt to meet the requirements of modern shipping services as it operates in a direct-printing mode in narrow band, with unitary function and low intelligence.

PACTOR, developed by Special Communications Systems GmbH (SCS), is a digital data protocol combining elements of PACKET and AMTOR Automatic Repeat Request (ARQ). PACTOR I is used by many groups, such as sail-mail for mariners to send and receive e-mails. In order to improve the reception of digital data and achieve robust error control and high data throughput, PACTOR utilizes a combination of simple FSK modulation, and ARQ protocols, and the time division duplex (TDM) is applied for transmitting the digital information in the email form. PACTOR II is up to 8 times faster than PACTOR I, with a bandwidth of 450 Hz. The next version, PACTOR III, introduces 6 speed levels and further improves the achievable throughput and robustness compared to the previous generations of PACTOR I and II, with a maximum bandwidth of 2400 Hz. PACTOR IV is the latest version of the PACTOR series, advancing from PACTOR I-III. It achieves a data rate that is 1.5–3 times faster than PACTOR III and introduces 10 speed levels. Nevertheless, PACTOR systems are not suitable for real-time services due to long time delay.

Telenor, working in the VHF band, aims to providing digital radio services for ships in Norway and the nearby international waters. Its base station is not only distributed in the coastal area of Norway, which is 70 nautical miles away from the coastline, but even on most of Norway's oil facilities in Beihai. According to the ITU-R M.1842-1 protocol, there are four recommendation systems which emphatically describe the data and e-mail exchange for the 18 supplementary channels and equipment characteristics of VHF ocean mobile business. Specifically for the modulation schemes, System 1 mainly adopts $\pi/4$-DQPSK and $\pi/8$-D8PSK, system 2 adopts GMSK, and systems 3 and 4 adopt 16-QAM. TDMA and CSTDMA are employed as the multiple access techniques.

AIS is an automatic tracking system installed on ships, which can realize the automatic exchange of information between ships, such as their position, speed, and navigational status at regular intervals on VHF band, provide collision avoidance measures for ships effectively. In order to ensure that the transmissions of different transceivers do not occur at the same time, the signals are time multiplexed using technology multiple access technique called Self-Organized Time Division Multiple Access (SOTDMA). However, the increasing number of AIS users and the diversification of the demand have brought great load to the AIS channel, which lead to

Table 1.1 Shore-based maritime wireless communication systems

System	Communication method	Modulation mode	Data rate	Communication distance
NAVTEX	MF	FSK	50 bps	460∼740 km
NBDP	HF	FSK	100 bps	>460 km
PACTOR-3	HF	FSK/OFDM	9.6/ 14.4 kbps	4000∼40,000 km
DSC	MF/HF and VHF	–	100/ 1200 bps	Visual range
Telenor	VHF	π/4-DQPSK/GMSK/16-QAM	133 kbps	130 km
AIS	VHF	GMSK	9.6 kbps	Sight distance
VDES	VHF	GSMK/OFDM/QAM	40 kbps	Sight distance

interfering concurrent transmissions that degrade the system performance. To alleviate the interference in the existing VHF frequency band of the AIS system and to ensure effective and efficient system operations, a new system, namely VHF Data Exchange System (VDES), has been emerging.

VDES, as an enhanced and upgraded system of AIS in the field of maritime mobile services, was proposed by the International Telecommunication Union in 2012 after the world radio communication (WRC-12) Conference and was jointly approved by the 162 member countries and 136 international organizations and groups at the 2015 World Radio Communication Conference (WRC-15). It has added the Special Application Message (SAM) and the broadband very high frequency data exchange function to the existing AIS functions, which make it effectively alleviate the pressure of the existing AIS data communication and provide higher data throughput and spectrum utilization.

Generally, the aforementioned offshore maritime wireless communication systems have a relatively low cost and ease of operation, compared with satellites communication systems. It is also worth noting that the offshore systems are dependent on the climate conditions and marine environment. Moreover, the existing systems are narrowband communication systems operating on relatively low frequency bands. Thus, they are not able to provide broadband data services [26]. Table 1.1 summarizes the main system parameters employed in the existing shore-based maritime wireless communication systems.

In some areas, 2G/3G/4G mobile communication networks are also applied for offshore communications, e.g., within 30 km offshore, to support voice and broadband data transmissions [27]. In recent years, a few new systems have been emerging to provide maritime services in a cost-effective way.

The TRI-media Telematic Oceanographic Network (TRITON) was proposed by Singapore for high-rate and low-cost maritime communications in narrow water channels and shipping lanes close to the shore [28, 29]. Figure 1.1 shows the high-level architecture of TRITON. The ships form a mesh network connected to the terrestrial network via shore BSs. Buoys can also form a mesh network with ships. This system is working for Singapore as there are usually a sufficiently large number

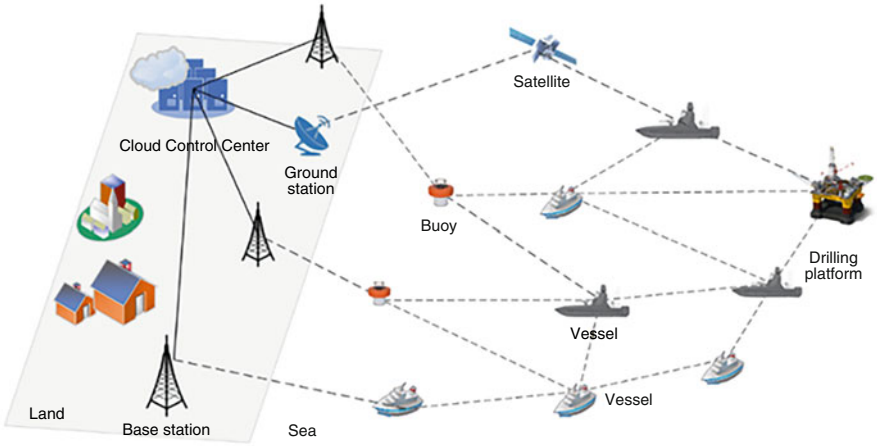

Fig. 1.1 The architecture of TRITON

of ships that provide full network connectivity. In locations where the ships are sparse and the network is not fully connected, then it could be difficult to connect with onshore stations via mesh links. In such case, the mesh node or ship will fall back on a satellite communication link [10, 11].

Singapore's Port Wireless Broadband Access Project (WISEPORT) leverages the mobile World Interoperability for Microwave Access (WiMAX) wireless broadband network to provide data communications with a rate of up to 5 Mbps and a communication distance of 15 km [30]. The network coverage stretches from the southern coast of Singapore to the port water limits. The recent LTE-Maritime project in South Korea [21] aims at developing new MWCNs to enable users at sea to access high-rate data services in coastal areas 100 km from the coast. LTE-Maritime enables near sea ships to directly communicate with BSs in land. Therefore, it is particularly suitable for safety-related maritime services with high reliability and low latency. Another project, namely, Maritime Broadband Communication (MariComm), target to provide two-way high-speed Internet/multimedia services at a rate of 1 Mbps or more on the sea by enabling maritime stations to form maritime heterogeneous relay networks for data forwarding. MariComm is a new marine broadband digital communication system to meet the requirement for the coming e-Navigation era. It provides high quality internet services within 100 km from the shore [31].

Generally, the communication coverage of offshore wireless communication networks is limited. Due to wireless fading channels, maritime stations far away from the shore achieve a low data rate over a long communication distance. Thus, offshore wireless communication networks can support broadband services for maritime stations that are close to the BSs, while faraway maritime stations may still suffer from low communication rate.

1.1.2.2 Open Sea Wireless Communication

Satellite system is suitable for the far ocean navigation as they can provide ships with worldwide Internet access from anywhere. However, the high cost of satellite communications could be a barrier to commercial expansion. According to the altitude, satellites can be classified into three categories: Geostationary Earth Orbit (GEO), Medium Earth Orbit (MEO), and Low Earth Orbit (LEO) satellites. GEO satellites operate at the orbit of 36,000 km high and the propagation delay is around 120 ms; MEO satellites work at an orbit from 10,000 to 20,000 km with a propagation delay on the order of 10 ms; the LEO satellite operates at an orbital altitude from 500 to 1500 km with a propagation delay of less than 1 ms [6, 32].

Inmarsat was the world's first international GEO satellite mobile communication system. It provides data services to users worldwide through 14 geostationary telecommunication satellites. The Inmarsat was originally designed to meet the communications needs of the U.S. Navy and has since evolved to be operated by The International Maritime Satellite Organization, gradually shifting to civilian applications [20]. Inmarsat-3 consists of five L-Band satellites that provide low-bandwidth communications and security services primarily for global shipping. Fleet Xpress, the Global Xpress (GX) service for maritime, delivers seamless connectivity at sea, with high-speed data over Ka-Band, combined with the proven reliability of Inmarsat's flagship Fleet Broadband L-Band service as a back-up [33].

The Iridium satellite constellation project aims at providing voice and data services over the entire surface of the earth. It was first calculated that 77 satellites are needed, hence the name Iridium, after the metal with atomic number 77. It turned out later 66 satellites should be sufficient to complete the coverage of the earth. The first Iridium satellite was launched in 1997 and the first call was made in 1998. The global coverage was complete by 2002. The Iridium constellation continued operation following the bankruptcy of the original Iridium Corporation. The second-generation Iridium-NEXT satellites began to be deployed into the existing constellation without disrupting services in 2017. In 2020, the upgraded Iridium constellation was certified for use in the Global Maritime Distress and Safety System (GMDSS). As the world's only truly global satellite network, Iridium provides reliable communications for maritime stations including unmanned vessels regardless of their geographical locations so that it ensures full network connectivity, improves shipping safety, and communication efficiency [34].

Tiantong-1 satellite communication system was the first satellite of China's satellite mobile communication system launched in 2016. The user link operates in the S band, and the feeder link works in the C band. It supports millions of users at the same time and can provide voice, data, short message, and other communication services for mobile users such as vehicles and ships.

The BeiDou Navigation Satellite System (BDS) is a global navigation satellite system independently constructed and operated by China. The short message communication function is the unique advantage of the BDS that distinguishes it from other global navigation and positioning systems. The BDS has the function of

two-way communication: (1) point-to-point two-way interactive information exchanges and (2) point-to-multipoint one-way transmissions. This function can be used in marine rescue, ocean transportation, and other services. The BDS works in the L-Band. The service area of the BDS includes most areas from 55°S to 55°N, 70°E to 150°E [35].

The satellite-based maritime communication networks can provide low-speed or high-speed data services depending on the spectrum bands they operate, i.e., the narrowband or broadband. Notice that the satellite communication may be highly dependent on the climatic conditions and the marine environment. For example, satellite communications over Ku band are extremely susceptible to attenuation due to rain fade [19]. In addition, compared with GEO and MEO satellite networks, the signal loss of LEO constellation to the ocean would be relatively smaller thanks to a lower orbit.

1.1.2.3 Underwater Wireless Sensor Networks

Underwater communication plays an important role in observation of marine life, water pollution, exploration of oil and gas drilling platforms, monitoring of natural disasters, tactical operations for maritime safety, and observation of changes in the underwater environment. Underwater wireless communication network is usually composed of underwater sensor nodes and sink nodes deployed in the sea surface to jointly complete underwater tasks. Underwater nodes sense the environment and collect data and then transmit the collected data to the sink node in the sea surface which serve as gateway nodes to forward the data to the Internet [24]. Generally, the electromagnetic waves underwater propagate very fast over short distances, yet they significantly attenuate over a long communication distance. Optical communication provides high-bandwidth data rate with a low latency and the minimum spreading delay in aquatic medium. Acoustic waves are the most popular method for underwater communications over long distances with low latency and high spreading delay [36, 37].

In a typical UWSN, as shown in Fig. 1.2, clusters of sensor nodes are deployed underwater. In every cluster, there is an anchor node, or a Cluster Head (CH) node, which collects the information from other nodes in the cluster. Underwater sensor nodes communicate with each other over acoustic communication channels. CH nodes or anchor nodes aggregate and process the data and transmit the processed information to the sink node, e.g., buoyant nodes deployed at the sea surface [38].

In another example, Autonomous Underwater Vehicles (AUVs), Remote Operated Vehicles (ROVs), and underwater gliders are deployed underwater, collecting information from anchor nodes and passing to remote stations. In three-dimension (3D) space, sensors float at different depths to monitor the corresponding objects [39]. Han et al. [40] studied a 3D maritime monitoring network composed of different types of underwater sensor nodes, including the gateway nodes, underwater sensor nodes with buoys, automatic mobile nodes. In a complex underwater environment, the UWSNs face great challenges, which will be discussed in Sect. 1.2.

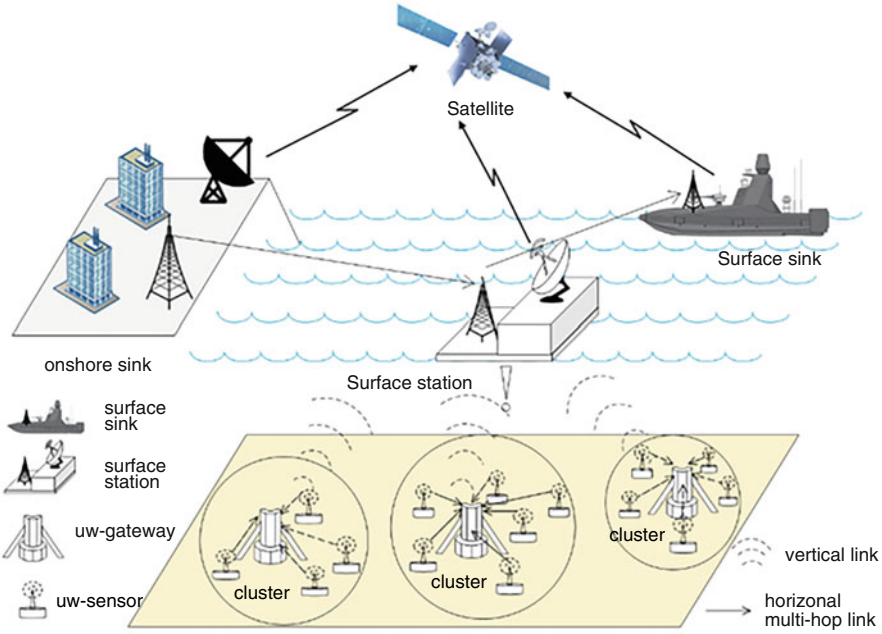

Fig. 1.2 The typical UWSNs

In summary, the current MWCNs include offshore maritime wireless communication networks and satellite communication networks that provide services for offshore stations and mobile users in the open sea, respectively. Generally, a hybrid satellite-terrestrial network provides a good solution to strike a balance between maritime satellite communication system and the offshore maritime communication systems. As a result, the Global Maritime Distress and Safety System (GMDSS), an improved integrated maritime communications system consists of both terrestrial and satellite communications, which will be described below.

1.1.2.4 Global Maritime Distress and Safety System

The GMDSS is a global communication network for maritime distress and rescue operations, safety, and routine communications, which was established in 1988 by IMO. The GMDSS is illustrated in Fig. 1.3. The competent authorities in charge of search and rescue on land and the ships near the one in distress coordinate with each other to perform the rescue tasks. Once the ship is in distress, it first quickly sends out alarm messages to notify the nearby ships or those on the shore. Upon receiving the alarm messages, the nearby ships and the Rescue Coordination Center (RCC) can carry out coordinated search and rescue activities in the shortest possible time to increase the success ratio of search and rescue.

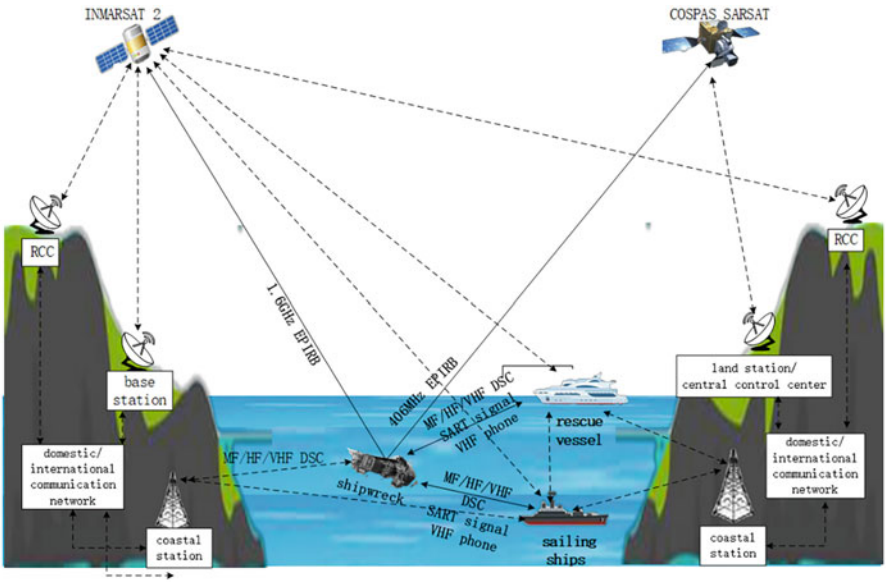

Fig. 1.3 The composition of GMDSS

According to the International Convention for the Safety of Life at Sea, 1974, (SOLAS), governments are requested to provide appropriate shore-based facilities to support space and terrestrial radio communications, as recommended by the IMO. Besides search and rescue services, the GMDSS may also send navigation warning, meteorological warning, meteorological forecast, and other Maritime Safety Information (MSI) to the sailing ships to present them from maritime accidents to the greatest extent. Governments are also requested to provide appropriate shore-based facilities to support space and terrestrial radio communications, as recommended by the IMO. Specifically, every ship equipped with GMDSS at sea shall be able to perform the following nine basic communication functions [41]:

1. Distress alerts. Distress alerts can be transmitted in three directions: ship-to-shore, ship-to-ship, and shore-to-ship.
2. Search and rescue coordinating communications. It is the exchange of distress and safety information about ships in distress by both parties. It has bi-directional communication function.
3. On-scene communications. It refers to the communication between a ship in distress and on-scene commander or coordinator surface search.
4. Signals for positioning. It refers to the process of finding and locating a ship in distress.
5. Transmitting and receiving maritime coordinating messages. Maritime safety information includes navigational warning, meteorological warning, meteorological forecast, and other emergency information related to navigational safety.

6. General communications. GMDSS also should perform some general communications such as pilotage and cargo conditions.
7. Bridge-to-bridge communications. It refers to the radiotelephone communication in a ship's usual steering position for the purpose of safe navigation.

GMDSS utilizes both maritime satellite communication systems and offshore maritime communication systems to perform the above functions, which will be introduced in the following context.

- Maritime Satellite Communication Systems

The two current maritime satellite communication systems are Inmarsat system and COSPAS-SARSAT system. Inmarsat System is an intergovernmental international cooperative organization that operates global maritime satellite communications, providing maritime salvage, secure communications, and commercial communications for maritime users. The Inmarsat system consists of three major components: the space segment, the ground segment, and the mobile station. The space segment includes Inmarsat satellites, the tracking telemetry and control station, and the satellite control center. The ground segment includes ground station (shore station), Network Coordination Station (NCS), and Network Control Center (NCC). The mobile stations are divided into land, maritime, and aero. The system can cover all regions within 76° north and south latitude of the earth and can provide a variety of communication services. It is responsible for most of the current maritime communication services.

COSPAS-SARSAT system is the global search-and-rescue satellite system used to determine the position of three beacons, namely Emergency Locator Transmitter (ELT), EPIRB, and Personal Locator Beacon (PLB). The entire system consists of an emergency beacon, satellite, Local User Terminal (LUT), and Mission Control Center (MCC). The system has two processing modes: (1) real-time mode, which means the signal from the EPIRB is processed and stored by the satellite and immediately sent back to the LUT within the satellite coverage; (2) the global coverage mode, in which data is processed and stored by the satellite, is sent only when the satellite comes over the LUT, so that all operating LUTs in the coverage can receive the data [31, 41].

- Offshore Marine Communication Systems

Offshore marine communication systems consist of ship stations, coastal stations, and domestic/international land public communication network or dedicated communication network connected to the base stations on the shore. Coastal station provides a communication interface between the ship station and the offshore user, as well as plays the role of the transfer between wired communication and wireless communication. The offshore communication systems are responsible for the distress alarm, search and rescue coordination communication, field communication, bridge to bridge communication, and other functions of GMDSS. This system is currently used by ships for business exchanges and ship to shore communications.

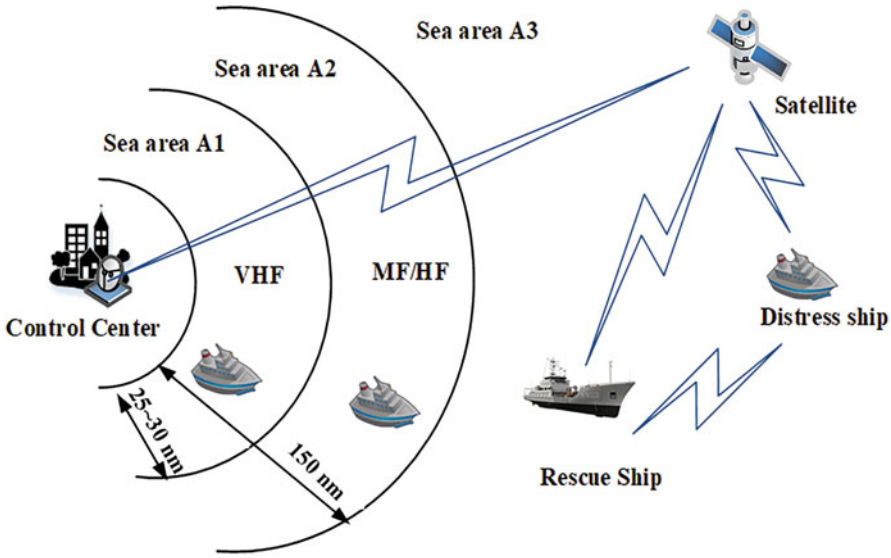

Fig. 1.4 The sea areas

The communication bands of GMDSS should in principle be determined by the navigation sea area of the ships. Basically, the sea area can be divided into four areas, as shown in Fig. 1.4.

Sea Area A1 Sea area A1 refers to the sea area covered by communications over VHF band. In this area, VHF Digital Selective Calling (DSC) alarm can be carried out. Generally, the sea area is 25~30 n mile away from the coast.

Sea Area A2 Sea area A2 refers to the area covered by communications over MF band excluding the sea area A1. In this area, MF DSC alarm can be carried out. Generally, the sea area is 150 n mile away from the coast.

Sea Area A3 Sea area A3 refers to the area covered by synchronous communication satellite excluding the sea area A1 and sea area A2. Generally, the sea area A3 covers an area between 76°S and 76°N.

Sea Area A4 Sea area A4 refers to the remaining area except the sea area A1, sea area A2 and sea area A3, i.e., the sea area beyond 70° north and south latitude to the South Pole or the North Pole.

For ships sailing in the sea area A1, ship-to-ship and ship-to-shore alarm shall be conducted by DSC or VHF Emergency Position Indicating Radio Beacon (EPIRB) on VHF CH70 (156.525 MHz), respectively. The CH70 is designed as the preferred calling channel for ships in distress. For ships sailing in the sea area A2, ship-to-ship and ship-to-shore alarm shall be conducted by DSC and satellite EPIRB on VHF CH70 and/or MF 2187.5 kHz, respectively. For ships sailing in the A3 and A4 areas, ship-to-ship alarm is conducted by DSC on VHE CH70 and/or MF 2187.5 kHz.

Ship-to-shore alarm is carried out using one of the Inmarsat stations and HF DSC or COSPAS-SARSAT ERIRB (1.6 GHz EPIRB is available in A3 sea areas).

In addition to distress and safety communications, GMDSS will fundamentally change the status quo of maritime communications because of its mandatory nature. However, GMDSS may not be able to fulfill all the requirements of the modern maritime applications in the information explosion era. Therefore, IMO is continuously modernizing and improving GMDSS by introducing advanced communication technologies to improve the design and development of the communication systems [5].

1.1.3 The Next Generation Marine Wireless Communication Networks

With the explosive growth of emerging marine services and data, the current MWCNs are facing great challenges to provision seamless signal coverage and high-speed data transmissions at anytime from anywhere. In this subsection, we introduce the next generation marine networks that are adaptive to the complex marine environment. To meet the ubiquitous communication requirements in a cost effectively way, the next generation MWCNs employ a hierarchical network architecture that composed of multi-layer subnetworks including the satellite communication sub-network, the offshore communication sub-network, the air-based communication sub-network, the sea-surface communication sub-network, and the underwater communication sub-network, as illustrated in Fig. 1.5.

- The Satellite Communication Sub-Network

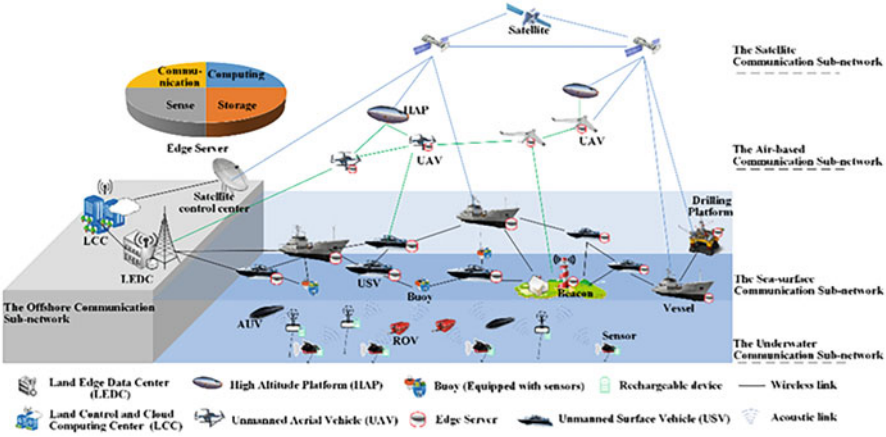

Fig. 1.5 The next generation MWCNs

Satellites can provide communications services in areas beyond the coverage of ground BSs to ensure full coverage of the earth. Compared with GEO and MEO, LEO satellite has the advantages of a low launch cost, a short transmission delay, a small path loss, and a high data transmission rate. The next generation MWCNs will make use of the complementary features of different types of satellites for ubiquitous computing and communications.

- The Air-Based Communication Sub-Network

In the extreme case that it is difficult to guarantee the high reliability and high-speed data services by relying on satellites and terrestrial networks, the air-based communication sub-network can be deployed to relay the data, using stratospheric airships, stratospheric high-altitude balloons, Unmanned Aerial Vehicle (UAVs), helicopters, and other High-Altitude Platforms (HAPs). Notice that high-altitude platforms are vulnerable to bad weather conditions. Since 100 km is the lowest orbit altitude of spacecraft around the earth, people generally take 100 km above the earth's surface (also have 80 km and 120 km and other terms) as the boundary division of "space" and "air." The balloons usually work at a height of 200~1500 m, while the airships usually work at a height of 17~22 km in the stratosphere. The balloons and UAVs controlled remotely by terrestrial base stations and big ships can be equipped with routers or other relaying devices to realize data forwarding between different vessels or between vessels and the shore.

- The Offshore Communication Sub-Network

Coastal BSs, cloud computing center, and edge computing center are deployed in the offshore communication sub-network. Coastal BSs are able to provide communications services to offshore areas. In the offshore with dense users, there may be a great demand for communication and computing resources. Deploying cloud computing centers with powerful computing and storage capabilities on land can help reduce transmission delay and computation delay.

- The Sea-Surface Communication Sub-Network

The sea-surface communication sub-network consists of offshore platforms such as ships, USVs, and buoys, as well as base stations deployed in islands, beacons, drilling platform, and reefs. It can provide broadband communication services for nearby ships and platforms along the coast. Ships, USVs, and buoys equipped with edge servers can provide edge computing and edge caching services. Due to the hostile communication conditions, limited bandwidth, and unstable channel quality, how to make full use of the computing and communication resources for delay-sensitive tasks in the ocean should be further investigated [6].

- The Underwater Communication Sub-Network

The underwater communication sub-network is mainly composed of different sensors and Autonomous Underwater Vehicles (AUVs), which collect sensed data of the ocean, such as salinity, PH, sediment, and so on. Underwater devices are mainly powered by batteries with limited capacity and thus it is difficult to replace batteries

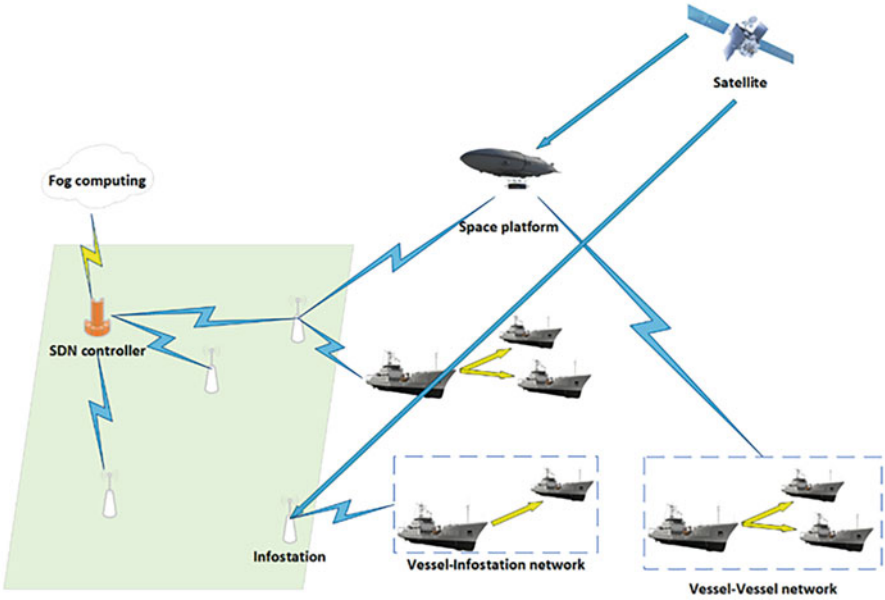

Fig. 1.6 Network architecture of maritime wideband communication system

underwater. Some sensor nodes use renewable energy sources such as tides, to achieve energy sustainable operations. Accordingly, communication and networking protocols for renewable energy powered UWSNs should be further investigated. In addition, different types of sensors may have different capabilities, for example, nodes installed in buoys may have storage space and serve as the edge computing nodes. How to enable edge computing services for UWSNs beckons for further research.

- Enabling Technologies for the Next Generation MWCNs

To further relieve the computing and communication pressure caused by the explosive growth of data and to enhance the security of data transmissions, researchers and engineers are looking for novel enabling technologies for next generation MWCNs. Some key enabling technologies include smart IoT, Cloud/Fog Computing, Mobile Edge Computing (MEC), Software Defined Network (SDN), and Network Functions Virtualization (NFV). With the increasing amount of offshore data, edge computing is an essential solution to reduce the delay of transferring data to the cloud computing. UAVs, USVs, and vessels are equipped with edge servers to achieve efficient sensing, storage, computing, and communication functions.

The network structure of the maritime broadband communication system is shown in Fig. 1.6 [42]. For USVs clusters, a maritime fog-cloud computing architecture is employed. By unloading tasks to distributed USV cluster nodes, underutilized computing resources can be fully utilized to reduce communication

load and processing delay. The USVs cluster and cloud resources are dynamically allocated to achieve the overall optimization of computing performance [43].

SDN can be also combined with edge computing, for the next generation MWCNs. The ship is the communication terminal, and the shore BSs, UAVs, or satellites can be selected to serve the ship based on the location and service requirements. The SDN architecture is adopted to adaptively manage according to the network dynamics [44].

At present, the research on the MWCNs is still in the preliminary stage, and there are still many technical challenges, such as frequency division, routing algorithms, energy replenishment, etc. The next generation of MWCNs will address these challenges to achieve global coverage, ultra-reliable, ultra-low latency maritime services.

1.2 Challenges

In this subsection, we will further discuss the challenging issues in the network deployment, physical layer communications, data link layer resource management, and network layer routing in the development and deployment of next generation MWCNs.

1.2.1 Deployment Challenges

It is a challenging task to design and deploy an efficient and reliable MWCN to provide quality of service for maritime applications discussed in Sect. 1.1.1, mainly because of the deployment constraints resulting from harsh marine environment. First, although the ocean surface is huge, i.e., around 3.62×10^8 km^2 which is about 71% of the earth surface, it is not easy to find a solid area to deploy the network infrastructure. Second, the harsh environment such as high humidity, high salty, and various forms of precipitation may damage network devices, which may affect the performance of spectrum communication. Third, some small satellites have a promising paradigm in marine communication networks. Yet the dense deployment of satellites may result in new research issues in terms of resource allocation and satellites routing, which add a new dimension for multi-hop satellites resource management. So far there is no existing solution to provide full coverage for the open-sea areas. Based on the deployment locations, MWCNs can be deployed in coastline, underwater, water surface, and in high altitude or even via satellites.

- Coastline Networks

In the offshore areas, terrestrial communication infrastructures can be exploited to construct coastline networks. In general, by setting up onshore base stations along the coastline, coastline networks can provide broadband services for nearby offshore

vessels. Currently, the main technologies including wireless access networks, evaporation duct communications, multiple antennas, and free space optical technologies have been proposed for coastal networks to provide dense and long-range network coverage in offshore areas at high speed [1]. Thus, the coastline networks play a key role in extending terrestrial Internet to the offshore areas. However, their coverage is limited due to the short transmission ranges, the limited power supply of some maritime devices, and sea water's absorption to RF signals [45].

- Underwater Networks

Underwater devices are usually powered by batteries. Due to the difficulty in replacing the batteries of underwater devices, it is essential to deploy a reliable underwater network with certain redundancies to ensure sustainable operation of the underwater network in a hostile marine environment. In the case of AUVs, the deployment density can be reduced to some extent as AUVs can move to the desired area to perform tasks. Yet the optimal deployment of AUVs is also critical as moving consumes energy that may reduce the lifetime of the underwater devices. For devices with energy harvesting capabilities, the optimal network deployment ensures that the monitoring area is always covered by an active device with sufficient energy. In a more complicated case of underwater network deployment, different types of energy sources should be jointly considered to ensure long-term energy sustainable underwater network operations.

- Water Surface Networks

On the water surface, base stations can be installed on shipborne, floating platforms, buoys, and beacons that provide wireless communication services in the neighboring area. Big vessels usually have large spaces to install communication infrastructure and have sufficient energy for communication. However, as vessels usually follow routes for safety reasons, ocean areas far away from busy routes may not be covered. Some small vessels such as fishing-boats may not be well equipped with powerful communication devices and sufficient energy supplies due to small loading capacities and shorter antennas for wireless communication [1]. Similarly, buoys and beacons deployed on the water surface to construct shipping lanes for maritime transportation can also be equipped with small antennas and communication modules to provide wireless services. Notice that vessels, floating platforms, buoys, and beacons are low stable facilities as well as the construction and maintenance could be costly. In addition, the hostile marine environment, such as high salty, high humidity, tides, and storm may jeopardize the devices and degrade their performance accordingly. Thus, how to deploy marine communication networks that provide reliable services is a challenging issue.

- Air Networks

High-Altitude Platform (HAP) is a station located on an object at an altitude of 20–50 km and at a specified, nominal, and fixed point relative to the Earth [46]. Deployment cost of HAP is also considerably lower than that of satellites. Compared with BSs on the water surface, the coverage of HAP is much larger, which

is dependent on the altitude and the elevation angle. As the earth is turning around, the HAP needs propulsion and station-keeping against mild wind and turbulence in the stratosphere [47], so that it can provide continuous communication service in one region. Another alternative solution is to use cheap and flexible UAVs to provide communication services occasionally to maritime users. While some UAVs can be powered by green energy, e.g., use replenished energy from solar panels; some other UAVs need to fly back to the coast or big vessels for energy charging. In the latter case, the flight time and energy of the UAV should be considered as constraints in the deployment of UAVs-aided maritime networks.

- Satellite Networks

Last but not the least, satellite communication networks have wide coverage and can provide full-time, stability, and high throughput services. The Inmarsat-5 system, also known as Global Xpress, aims to provide worldwide coverage and the demand of higher bandwidth. However, the cost of ship-borne equipment and the communication charges are very expensive. In view of this, some small satellites become a promising option due to relatively low cost for construction, launching, and operation maintaining. Most satellite systems are not dedicated to the maritime communications but for global network services. Therefore, it is challenging to study how to integrate satellites, along with air networks into water surface networks to provide reliable and efficient marine communication networks.

Given that the ocean is huge that none of aforementioned networks alone can provide satisfactory communication services. Instead, it is more likely that an integration of coastline networks, underwater networks, water surface networks, air networks, and satellite networks is needed to provide efficient and reliable maritime services.

1.2.2 Physical Layer Challenges

To design an efficient maritime communication network, it is essential to understand maritime channel models. In a modern space-air-ground-sea integrated communication network, there are three major types of channels to be investigated, namely the underwater communication channel, the sea-surface communication channel, and the maritime satellite communication channel. Due to the unique features of the maritime propagation environment such as sparse scattering, sea wave movement, and the ducting effect over the sea surface, the modeling of maritime channels differs from that of conventional terrestrial wireless channels in many aspects.

- Underwater Communication

Underwater communication uses acoustic signals to carry information transmitted over a relatively narrow band. Generally, the underwater acoustic channel suffers from severe Doppler shift, multipath fading, and propagation loss compared with Radio Frequency (RF) based wireless communication channels on land. Doppler

shift occurs when transmitters or receivers such as ships, unmanned surface vehicles, and underwater sensors, moves relative to each other, and causes a change in wavelength or frequency. In addition to the relative movement of communication devices, the undulating sea surface, the reflection of the underwater acoustic signal on the uneven seabed, and the refraction of the opposite signal by the turbulence in the water, the ups and downs of sea waves, and turbulence in the sea may also result in a Doppler shift. Due to the low propagation speed of underwater acoustic signals, the Doppler shift in an underwater acoustic communication channel is more severe compared with that of RF communications on land [48].

When acoustic waves propagate in the sea, there may exist multiple paths between the transmitter and the receiver of the acoustic wave due to the refraction of the seawater layered ring and the reflection between the sea surface and the bottom of the sea. As a result, the received signal is the signal superposition of multiple delayed and distorted copy of the transmitted signals over multiple paths. It is well known that the multipath effect will cause inter-symbol interference in the time domain, which may reduce the link capacity.

The propagation process of underwater sound waves is a process of energy radiation. The energy of sound waves attenuates when it travels over distance. The propagation loss of sound waves can be mainly divided into three categories: expansion loss, absorption loss, and boundary loss. The expansion loss is mainly caused by the gradual expansion of the wave front of the sound wave during the transmission process so that the average power density on the wave front is reduced, and accordingly the external manifestation is the attenuation of sound intensity. The absorption loss occurs when part of the sound energy is absorbed by sea water and converted into heat energy during the transmission of sound waves. The boundary loss is mainly caused by energy leakage when sound waves collide with the sea water boundary. Therefore, an accurate underwater channel should characterize the aforementioned Doppler shift, multipath fading effect, and propagation loss.

- Sea-Surface Communication

In maritime wireless communications over the sea surface, the impact of rainfall and cloud needs to be considered in the channel modeling. For frequency band below 10 GHz, the scattering effect of sea humidity on electromagnetic wave is small and can be ignored, but gas components such as oxygen and water vapor in the atmosphere will absorb the energy of electromagnetic wave and cause attenuation of electromagnetic wave energy and field intensity. For radio wave propagation, ducting effects are recognized propagation effect that can significantly increase the strength of the received signal. When the concentration of water vapor decreases or the temperature increases, ducting tends to form rapidly as the height increases. Basically, ducting effects include evaporation duct and elevated duct. Evaporation duct exists almost all the time in the ocean environment as a result of the moisture at sea. When the altitude rises to 600-3000 meters, the pressure and temperature decrease, and the elevated duct begins to appear. Unlike evaporative ducts, the foundation of elevated ducts is above the surface. Figure 1.7 illustrates the two main forms of ducting effects [49].

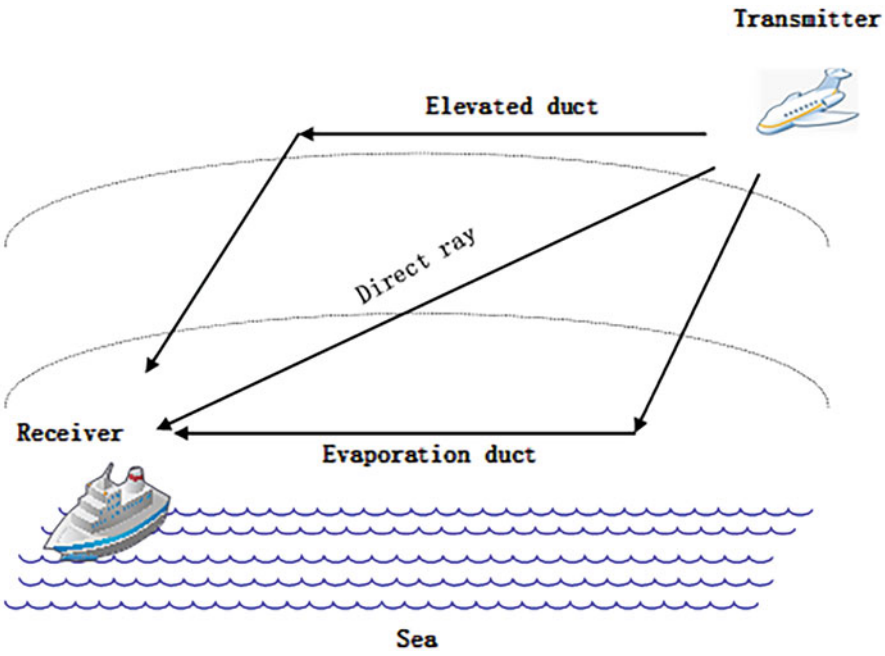

Fig. 1.7 Schematic diagram of evaporation duct and elevated duct

For an air-to-sea channel, the LOS path and the surface reflection path are likely to be the two dominant paths. Considering that the transmitter is in general at high altitude and the transmission distance is large, the so-called curved-Earth two-ray model is usually adopted to take into account the earth curvature. However, in some cases, in addition to the two dominant paths, it is also necessary to consider some scattered paths caused by sea undulations, bubbles, and other factors. The scattering generally happens around the receiver due to the high transmission altitude. Whereas the local scattering could be rich for inland receivers, a maritime user is expected to face much sparser scattering, and hence the over-water setting may simplify the modeling as compared to the inland air-to-ground channels. The channel over the water is described by a three-ray model, which consists of one LOS path and two reflection paths [50]. The stronger reflection path stems from the direct reflection from the sea surface, and the weaker reflection path is formed by many electromagnetic waves from multiple weak sources of reflections [51].

- Maritime Satellite Communication

Currently, mobile terminals on the ocean mainly rely on maritime satellites or BSs on the coast/island to acquire services. Narrow-band satellites, represented by Inmarsat, mainly provide services, such as telephone, telegraph, and fax, at a low communication rate. To provide a practically affordable solution for broadband maritime communications, an efficient hybrid satellite-terrestrial maritime

communication is required to combine the advantage of wide coverage of satellite communications and the high throughput of shore-based communications [52, 53]. However, different from terrestrial cellular networks, the maritime communication still faces many challenges due to the complicated electromagnetic propagation environment, and stringent service requirement of mission-critical applications [19].

Compared with the terrestrial environment, the atmosphere over the sea surface is unevenly distributed due to the large amount of seawater evaporation. Shore-to-ship and ship-to-ship communication are very vulnerable to the sea surface conditions, such as tidal waves, and atmospheric conditions, such as temperature, humidity, and wind speed. In addition, the height and the angle of ship-borne antennas vary greatly with the ocean waves, which results in a great variance in the channel qualities and thus poses great challenges in upper layer resource management.

In summary, maritime communication faces new challenges in the design of communication technologies, compared with terrestrial communications. Accurate and prompt CSI acquisition could be difficult in maritime communications due to long feedback delay caused by long transceiver distances and high variant channel conditions. To address these challenges in the maritime communications, novel adaptive channel coding is required to improve the transmission efficiency over different types of communication channels.

1.2.3 Link Layer Challenges

Link layer resource management plays a critical role in satisfying the demands of diversified maritime applications with Quality of Service (QoS) provision. In the next generation MWCN, rich multimedia information such as voice and video streaming have surged with the rising of various types of vessels including MASS, which poses great challenging for the design and development of maritime communication network. Specifically, in this subsection, we will discuss link layer challenges including limited spectrum resources, spatial uncertainty of maritime communications, and diversified energy constraints of maritime nodes.

1.2.3.1 Limited Spectrum Resources for Maritime Services

Automatic Identification System (AIS) is a worldwide standard that provides information transmission services on VHF Data Links (VDL). AIS consists of two narrow band channels, namely AIS 1 (161.975–162.000 MHz) and AIS 2 (162.025–162.050 MHz) [54]. According to the International Association of Maritime Aids to Navigation and Lighthouse Authorities (IALA), it is not conducive to the smooth transmission of AIS communications when the channel utilization is over 50% [55–57]. A 2012 study in China showed that the traffic load in VDL exceeded 50% in some large ports during the busy periods [57]. Therefore, it is

necessary to develop the next generation system, i.e., the VHF Data Exchange System (VDES) to meet the growing demands of maritime services. According to the recommendation of the International Telecommunication Union (ITU), VDES will consist of four types of channels, i.e., AIS, Application Specific Messages (ASM), VHF data exchange (VDE), and Long-range AIS, with a total of 18 [58]. The standard of VDES is still in its infancy and attracts attention from academia, maritime sectors, and shipping operators. Moreover, given that new channel resources are included such as ASM and VDE channels, new resource management schemes should be updated in the MAC protocol design of the VDES.

1.2.3.2 Spatial Uncertainty of Maritime Communications

For RF communications in a terrestrial network, the propagation delay is usually considered negligible as the light speed is as high as 3×10^8 m/s and the propagation delay is usually on the order of micro-second. Therefore, collision-free transmissions at the sender side will not result in interference at the receiver side. For acoustic underwater communications, the propagation delay is five orders higher than that of RF communications in the air because the propagation speed of sounds is only 1500 m/s [59]. In such case, a collision-free transmission scheduled at the sender side may lead to a collision at the receiver side due to various propagation delays of maritime nodes, which is referred to as a spatial uncertainty problem in underwater communication networks [59]. In other words, the conventional resource management for a terrestrial network schedules the transmission time of senders, assuming that the receivers will receive the data at the same time. This does not apply in an underwater maritime communication network where data transmitted in different time slots may arrive at a receiver in the same time slot, which leads to a collision at the receiver. Therefore, existing resource management for RF communication networks is not applicable for underwater marine communication networks. To achieve high resource utilization while ensuring fair sharing of network resources among multiple nodes, it is essential to consider the spatial uncertainty in the link layer protocol design.

1.2.3.3 Link Dynamics in Hash Maritime Environment

The quality of the link over the sea surface is severely influenced by the harsh maritime environment such as ocean currents, rain, and sea waves. As discussed in Sect. 1.2.2, the path loss characterizes the reflection loss on the sea surface, the diffraction over the sea, and the ducting effects in the air. An efficient link layer resource management should take into consideration the underlying physical layer channel conditions to improve the transmission efficiency. In other words, a PHY/MAC cross layer approach is required for link-aware scheduling to achieve high resource utilization while maintaining the fair resource sharing among multiple maritime nodes, with or without various energy constraints of maritime nodes.

1.2.4 Network Layer Challenges

The complicated ocean environment also brings great challenges to the design of network routing protocols. In the vastness of the ocean, especially in the open ocean, multi-hop routing is usually required to forward the data from nodes to other nodes to the server. In MWCNs, various types of nodes may be equipped with different energy sources that result in different energy constraints, which should also be considered in the routing design. In addition, ocean currents may flow away some marine nodes, and tsunamis may even damage some nodes, coupled with energy exhaustion, the network topology of the MWCNs may be highly dynamic, which calls for reliable and robust routing design. In a short summary, to support the diversified service requirements of the next generation MWCNs, it is essential to design reliable and efficient routing protocols, considering the challenging energy constraints and the highly dynamic network topology.

- Energy Constraints

In MWCNs, how to supply energy to marine nodes either on the sea surface or in the deep ocean is an important issue [60]. Lots of nodes in the MWCNs are powered by batteries which have constrained energy capacity, leading to limited network lifetime [61]. When the energy is exhausted, the nodes on the sea surface, such as USVs and buoys, can be artificially replaced or charged, while underwater, it is highly burdensome to restore the battery factitiously [62]. Wireless charging technology can better solve the energy supply demand of underwater nodes [63]. For example, Inductive-Coupled Resonant technology has high transmission power, and the propagation of near-field electromagnetic field is not affected by seawater medium, it can charge underwater wireless sensors [64]. Using renewable energy such as solar and tides, the energy also can be replenished to sustain the node operations.

To maximize the sustainability of MWCNs, it is critical to balance the energy consumption of the marine nodes across the network. Routing protocols should consider different energy constraints of different types of nodes, as discussed in the link layer. And compared with the dense distribution of nodes in the offshore, the distance between nodes in an open sea is usually much larger, requiring long-distance transmission, which greatly increases the energy consumption.

- Dynamic Ocean Environment

In MWCNs, the network topology may change when marine nodes move in the ocean. For example, the nodes in the MWCNs may float with the ocean currents may flow [65]; and some marine nodes may die due to energy exhaustion, or be damaged by marine organisms and long-term corrosion of seawater. In the case of tsunami, whirlpool may damage multiple nodes in a region, which may result in a network separation. As mentioned above, for nodes with energy exhaustion, we can restore power supply by replacing batteries and continue to provide communication services. However, for those nodes whose hardware is damaged, they can hardly be

repaired or replaced, and the failure of nodes in the region will cause network segmentation. In such cases, moving sensors such as USVs, UAVs can move to the area to connect the network segments. Therefore, in the MWCN, the routing protocol jointly considering the temporary and permanent failure of nodes needs to be further studied.

1.3 Organization of the Book

The book is organized as follows:

In Chap.1, an overview of the current research on MWCNs is first presented, followed by the discussion of research challenges of the next generation MWCNs in terms of network deployment, physical layer communication, link layer resource management, and network layer routing.

In Chap.2, the network deployment is studied for the next generation MWCNs. A three-tier hierarchical network architecture is proposed to support edge computing. Based on hierarchical network architecture, a multi-objective optimization framework is formulated to minimize the network deployment cost while maximizing the network lifetime by determining the deployment locations of network nodes.

In Chap.3, communications between intelligent Internet of Vessels are investigated. A novel OFDM autoencoder and a new channel estimation algorithm for OFDM systems are proposed to adapt to the complex marine environment.

In Chap.4, data link layer protocol design and optimization are studied for the next generation underwater sensor networks with energy harvesting process is modeled and analyzed, and a multi-agent reinforcement learning approach is proposed for underwater sensors to autonomously adapt the random-access parameter based on the interactions with the dynamic network environment.

In Chap.5, routing for underwater wireless sensor networks is analyzed, and an energy-efficient depth-based opportunistic routing algorithm with Q-learning is proposed to guarantee the energy-saving and reliable data transmission.

In Chap.6, we summarize this book and identify some further research issues in the next generation MWCNs.

References

1. S. M. Jiang, Networking in oceans: a survey. ACM Comput. Surv. 54(1), 1-33(2020).
2. UNCTAD, Review of maritime transport 2020 (2020), Review of Maritime Transport 2020 UNCTAD.
3. X. H. Lin, The global ocean economy in 2030: influencing factors, trends and suggestions. Pacific Journal. 28(1), 50-63(2020).
4. X. F. Qi, Analysis of the marine development strategy of the world's major countries. Marine Information. 01, 59-62(2015).

5. B. Lin, Z. Q. Zhang, X. L. Han, L. Liu, Z. Q. Liu, Y. D. Che, Key technologies for space-air-ground-ocean integrated networks towards maritime emergency: an overview. Mob. Commun. 44(9), 19-26(2020).
6. Y. Pang, D. S. Wang, D. D. Wang, L. Y. Guan, C. Y. Zhang, M. Zhang, A space-air-ground integrated network assisted maritime communication network based on mobile edge computing, in 2020 IEEE World Congress on Services (2020), pp. 269-274.
7. J. L. Duan, B. Lin, Y. Wang, R. X. He, Status of maritime wireless broadband network architecture and prospect for related technologies. Telecommunication Engineering. 58(8), 981-988(2018).
8. L Wu, J Yang. The Application of Internet of Things Technology to Water Transport Safety [C]// International Conference on Transportation Information & Safety. 2013:1985-1990.
9. M. Mohaimenuzzaman, S. M. Rahman, M. Alhussein, G. Muhammad, K. A. Al Mamun, "Enhancing safety in water transport system based on Internet of Things for developing countries," Int. J. Distrib. Sensor Netw, vol. 12, no. 2, 2016, Art. no. 2834616.
10. Ø. J. Rødseth, B. Kvamstad, D4.3: Evaluation of ship to shore communication links, MUNIN project, MARINTEK, 2012.
11. A. A. Allal, L. E. Amrani, A. Haidine, et al. Implementation of 5G Communication Network for a Safe Operation of Autonomous and Conventional Ships[J]. International Journal of Engineering Research in Africa, 2020, 51:229-248.
12. W. Lang, R. Jedermann, D. Mrugala, A. Jabbari, B. Krieg-Brückner, K. Schill, "The 'intelligent container'-A cognitive sensor network for transport management," IEEE Sens. J., vol. 11, no. 3, pp. 688-698, Mar. 2011.
13. L. Ruiz-Garcia, P. Barreiro, J. I. Robla, L. Lunadei, "Testing ZigBee motes for monitoring refrigerated vegetable transportation under real conditions," Sensors, vol. 10, no. 5, pp. 4968-4982, 2010.
14. R. Su, D. Zhang, C. Li, et al., Localization and Data Collection in AUV-Aided Underwater Sensor Networks: Challenges and Opportunities[J]. IEEE Network, 2019, 33(6):86-93.
15. N. Mohamed, I. Jawhar, J. Al-Jaroodi, et al., Sensor Network Architectures for Monitoring Underwater Pipelines[J]. Sensors, 2011, 11(11):10738-10764.
16. K. F. Haque, K. H. Kabir, A. Abdelgawad, Advancement of Routing Protocols and Applications of Underwater Wireless Sensor Network (UWSN): A Survey. 2020.
17. H. Zhang, Z. Ren, D. Sun, et al., Research on Underwater Wireless Communication Technology Based on Ad Hoc Network[J]. Audio Engineering, 2015, 39(4): 54-57.
18. J. Dong, S. Z. Tian, W. U. Wen, et al., The development of global tsunami warning systems and their enlightenments to China[J]. Marine Science Bulletin, 2019.
19. T. Wei, W. Feng, Y. Chen, et al., 2021. Hybrid Satellite-Terrestrial Communication Networks for the Maritime Internet of Things: Key Technologies, Opportunities, and Challenges. IEEE Internet of Things Journal, 2021, 8(11): 8910-8934.
20. J. J. Xue, X. L. Zhang, X. S. Wu, Analysis on the development of new maritime satellite communication systems. China Radio, (05), 86-89(2021).
21. S. W. Jo, W. S. Shim, LTE-maritime: high-speed maritime wireless communication based on LTE technology. IEEE Access. 7,53172-53181 (2019).
22. H. J. Zhang, R. W. Su, B. Tang, et al., Future Marine Communication Network Architecture and Key Technologies. Radio Communications Technology. 47(4), 384-391(2021).
23. M. C. Domingo, An overview of the internet of underwater things. Netw. Comput. Appl. 35, 1879-1890 (2012).
24. E. Felemban, F. K. Shaikh, U. M. Qureshi, A. A. Sheikh, S. B. Qaisar, Underwater sensor network applications: a comprehensive survey. International Journal of Distributed Sensor Networks. 11(11), (2015).
25. https://www.navtex.net/
26. M. H. Xia, Y. M. Zhu, E. H. Chen, C. W. Xing, T. T. Yang, W. K. Wen, The state of the art and challenges of marine communications. Sci Sin Inform. 47(5), 677-695 (2017).

27. J. W. Gao, S. A. Xiao, Z. G. Yu, X. G. Lang, D. H. Wang, An Integrated Ocean Communication Perception Service. Journal of CAEIT. 15(4), 343-363(2020).
28. M. T. Zhou, V. D. Hoang, H. Harada, J. S. Pathmasuntharam, H. G. Wang, P. Y. Kong, C. W. Ang, Y. Ge, W. Su, TRITON: high-speed maritime wireless mesh network. IEEE Wirel. Commun. 20(5), 134-142 (2013).
29. J. S. Pathmasuntharam, P. Y. Kong, M. T. Zhou, Y. Ge, H. G. Wang, C. W. Ang, W. Su, H. Harada, TRITON: high speed maritime mesh network. in IEEE 19th International Symposium on Personal, Indoor and Mobile Radio Communications (2008), pp.1-5.
30. T. T. Yang, H. Liang, N. Cheng, R. L. Deng, X. M. Shen, Efficient scheduling for video transmissions in maritime wireless communications networks. IEEE Trans. Veh. Technol. 64(9), 4215-4229 (2015).
31. D. Yoo, H. Kim, J. Choi, B. Jang and S. Ro, "A novel antenna tracking technique for maritime broadband communication (MariComm) system," 2015 17th International Conference on Advanced Communication Technology (ICACT), 2015, pp. 225-229.
32. P. Wang, J. Zhang, X. Zhang, et al. Convergence of Satellite and Terrestrial Networks: A Comprehensive Survey. IEEE Access, 8, 5550-5588(2020).
33. Fleet Xpress - Global Xpress for Maritime (satcomglobal.com).
34. Iridium Satellite Communications | Truly Global Communications.
35. https://www.beidou.gov.cn/
36. M. F. Ali, D. N. K. Jayakody, Y. A. Chursin, S. Affes, S. Dmitry, Recent advances and future directions on underwater wireless communications. Arch Computat Methods Eng. 27, 1379-1412 (2020).
37. S. Khisa, S. Moh, Survey on recent advancements in energy-effcient routing protocols for underwater wireless sensor networks. IEEE Access. 9, 55045-55062 (2021).
38. V. Khajuria, M. Kuar, Underwater wireless sensor network: architecture, applications and challenges. in 2nd International Conference on Trends in Electronics and Informatics (ICOEI) (2018), pp. 939-944.
39. D. Pompili, T. Melodia, I. F. Akyildiz, Three-dimensional and two-dimensional deployment analysis for underwater acoustic sensor networks. Ad Hoc Networks. 7(4), 778-790 (2009).
40. G. J. Han, C. Y. Zhang, L. Shu, J. J. P. C. Rodrigues, Impacts of deployment strategies on localization performance in underwater acoustic sensor networks. IEEE Trans. Ind. Elec-tron. 62(3), 1725-1733 (2015).
41. https://imso.org/gmdss/
42. T. T. Yang, R. Wang, Z. Q. Cui, J. Dong, M. H. Xia, Multi-attribute selection of maritime heterogenous networks based on SDN and fog computing architecture. in 16th International Symposium on Modeling and Optimization in Mobile, Ad Hoc, and Wireless Networks (2018), pp.1-6.
43. K. T. Cui, B. Lin, W. L. Sun, W. Q. Sun, Learning-based task offloading for marine fog-cloud computing networks of USV cluster. Electronics. 8(11), 1287 (2019).
44. F. M. Xu, F. Yang, C. L. Zhao, S. Wu, Deep reinforcement learning based joint edge resource management in maritime network. 17(5), 211-222 (2020).
45. K. A. Yau, A. R. Syed, W. Hashim, el al. Maritime Networking: Bringing Internet to the Sea [J]. IEEE Access, 2019, 7: 48236-48255.
46. D. Zhou, S. Gao, R. Liu, et al. Overview of development and regulatory aspects of high altitude platform system [J]. Intelligent and Converged Networks, 2020, 1(1): 58-78.
47. T. C. Tozer, D. Grace. High-altitude platforms for wireless communications. Electronics & Communication Engineering Journal. 2001, 13(3): 127-137.
48. L. Cai, X. Pan, W. Xu, J. Li, X. Gong, "Underwater acoustic MIMO communication based on active time reversal," 2009 Asia Pacific Conference on Postgraduate Research in Microelectronics & Electronics (PrimeAsia), 2009, pp. 45-48.
49. E. Dinc, O. B. Akan, (2015) Channel model for the surface ducts: large-scale path-loss, delay spread, and AOA. J IEEE Trans, vol. 63, no. 6, pp. 2728-2738.

50. J. Wang et al., "Wireless Channel Models for Maritime Communications," in IEEE Access, vol. 6, pp. 68070-68088, 2018
51. Q. Zhuang, C. Zheng, “Research on INMARSAT based on Ka band and applications,” in Proc. Int. Conf. Inf. Cybern. Comput. Social Syst., Dalian, China, Jul. 2017, pp. 127-129.
52. J. Mashino, K. Tateishi, K. Muraoka, D. Kurita, S. Suyama, Y. Kishiyama, “Maritime 5G experiment in windsurfing World Cup by using 28 GHz band massive MIMO,” in Proc. IEEE Int. Symp. Pers. Indoor Mobile Radio Commun., Bologna, Italy, Sep. 2018, pp. 1134-1135.
53. F. Bekkadal, “Innovative maritime communications technologies,” in Proc. Int. Conf. Microw. Rader Wireless Commun., Vilnius, Lithuania, Jun. 2010, pp. 1-6.
54. S. Bober, “AIS next generation - the development of the VHF Data Exchange System (VDES) for maritime and inland navigation,” in proceedings of Smart Rivers 2015, Buenos Aires, Argentina, 2015.
55. ITU, “Automatic Identification System VHF Data Link Loading,” Report ITU-R M.2287-0, 2013.
56. IALA, “VDL Load Management. Recommendation,”A-124-APPENDIX 18, Edition 1, Saint Germain en Laye, France, 2011.
57. X. Hu, B. Lin, P. Wang, H. Lyu, T. Li, “A collision feedback based multiple access control protocol for very high frequency data exchange system in Enavigation”, Journal of Navi-gation, vol. 74, no. 4, 2021.
58. ITU, “Technical Characteristics for a VHF Data Ex-change System in the VHF Maritime Mobile Band,” ITU-R M.2029-0, 2015.
59. M. Han, J. Duan, S. Khairy, L. X. Cai, “Enabling Sustainable Underwater IoT Networks With Energy Harvesting: A Decentralized Reinforcement Learning Approach,” in IEEE Internet of Things Journal, vol. 7, no. 10, pp. 9953-9964, Oct. 2020.
60. T. T. Xia, M. M. Wang, J. J. Zhang, L. Wang, Maritime Internet of Things: Challenges and Solutions. IEEE Wirel. Commun. 27(2), 188-196 (2020).
61. C. Lin, K. Wang, Z. H. Chu, K. Wang, J. Dong, M. S. Obaidat, G. W. Wu, Hybrid charging scheduling schemes for three-dimensional underwater wireless rechargeable sensor net-works. Journal of Systems and Software. 146, 42-58(2018).
62. S. Khisa, S. Mon, Survey on recent advancements in energy-efficient routing protocols for underwater wireless sensor networks. IEEE Access. 9, 55045-55062(2021).
63. L. J. Feng, C. B. Zhu, J. T. Zhang, L. G. Yu, Research on key technology based on wireless charging technology for unmanned underwater vehicle. SHIP SCIENCE AND TECHNOLOGY. 42(23), 159-162(2020).
64. H. Y. Liu, Research on key technologies of underwater simultaneous wireless information and power transmission in magnetic resonance coupling. Harbin Institute of Technology, (2018).
65. J. H. Luo, Y. P. Chen, M. Wu, Y. Yang, A Survey of Routing Protocols for Underwater Wireless Sensor Networks. IEEE Commun. Surv. Tutor. 23(1), 137-160(2021).

Chapter 2
Topology Optimization of MWCN

The foremost task of the next generation MWCN is network deployment and topology optimization. To this end, we firstly study a hierarchical network architecture of MWCN with support of edge computing which integrates the Underwater Acoustic Network (UAN), the sea-surface wireless network with edge computing, and the air wireless network. Based on the hierarchical network architecture, a multi-objective optimization framework is formulated to minimize the network deployment cost while maximizing the network lifetime by determining the deployment locations of network nodes, including Aerial Relay Nodes (ARNs), Edge Computing Nodes (ECNs), Sea-Surface Nodes (SSNs), and Underwater Relay Nodes (URNs), and the data transmission links between network nodes, subject to various constraints of the network topology, network connectivity, and the battery capacity. As the formulated optimization problem is known to be NP-hard, an Ant Colony based Efficient Topology Optimization (AC-ETO) algorithm is presented to solve the formulated Multi-objective Optimization (MO) problem in various network scenarios of different number of nodes. Extensive simulations are conducted to validate the performance of the proposed algorithm. The results show that the proposed algorithm approaches the optimal solution and outperform some existing solutions.

This chapter is organized as follows: We present a brief research background in Sect. 2.1. The related works about the deployment of MWCN are reviewed in Sect. 2.2. The network model and the problem formulation are described in Sect. 2.3. An AC-ETO algorithm is proposed in Sect. 2.4. The numerical analysis is present in Sect. 2.5. Finally, we close the chapter with conclusions in Sect. 2.6.

2.1 Background

With the deepening of human's understanding of the ocean, as well as the rapid development of science and technology, great attention has been paid to the ocean because of its huge economic potential and strategic importance. The increasing

B. Lin et al., *Next Generation Marine Wireless Communication Networks*, Wireless Networks, https://doi.org/10.1007/978-3-030-97307-0_2

demand for the exploitation and utilization of marine resources calls for the wide deployment of MWCNs, especially marine monitoring networks. For example, a large number of drilling platforms have been built at sea to extract oil from the sea [1]. However, the exploitation of offshore oil resources also brings pollution risk to the marine environment. In 2010, the Gulf of Mexico oil spill accident led to serious harm to the marine ecosystem [2]. In such case, an underwater monitoring network is helpful to detect the oil spill and report the detection results in a timely manner. Another application is real-time monitoring for marine ranching, which is heavily dependent on the quality of marine environment to foster the marine fishery resources [3]. Thus motivated, a real-time MWCN has become an important research topic for both academia and industry. Node deployment is one of the fundamental tasks for MWCN and also is an attractive research topic. During the past decade, many technologies and systems related to marine monitoring have been developed, such as a buoy for marine monitoring [4–6], a prediction model of battery life [7], and a data acquisition and transmission system [8], which build the foundation for the implementation of the real-time MWCN. According to the requirements of marine monitoring, various types of sensors are deployed to monitor and measure different physical and chemical parameters such as water temperature, pressure, water direction and speed, salinity, turbidity, pH, oxygen density, and chlorophyll levels [4], and then the acquired data are transmitted back to the data center on land by relay nodes. The data acquired from the seabed far away from the coast needs to be relayed back to the data center through multi-layer relay. Compared with terrestrial wireless communication networks, deployment of an MWCN is more costly and complex due to the harsh marine environment in three-dimensional space.

Most existing works of the deployment of MWCNs in the literature proposed different algorithms to improve the network coverage. In [9], a distributed node deployment algorithm was proposed to utilize the mobility of the anchor nodes to maximize the coverage of 3D underwater wireless sensor networks in dynamic ocean environments. In [10–13], different algorithms were proposed to deploy sensors, surface gateways in an underwater sensor network. These works mainly focus on the deployment of UAN. To enable marine monitoring service, it is also critical to forward the data of the UAN towards the Base Station (BS) which is usually deployed in the shoreline of ocean. For efficient data communications over the large area of ocean, a multi-tier network that incorporates both underwater acoustic communications, radio communications above the water, and aerial relay over the air is highly desirable. To the best of our knowledge, no existing work on the deployment of marine monitoring network studied the deployment of an integrated multi-tier hierarchical network architecture, which includes underwater acoustic sub-network, sea-surface wireless sub-network, and air wireless sub-network.

In this chapter, we first study an integrated multi-tier hierarchical network architecture of MWCN as shown in Fig. 2.1 for an integrated sea-air-ground monitoring system. In the MWCN, the underwater acoustic sub-network consists of a number of battery-powered sensors with limited energy [14], Autonomous Underwater Vehicles (AUVs) [15] and buoys [16] with acoustic receiving devices

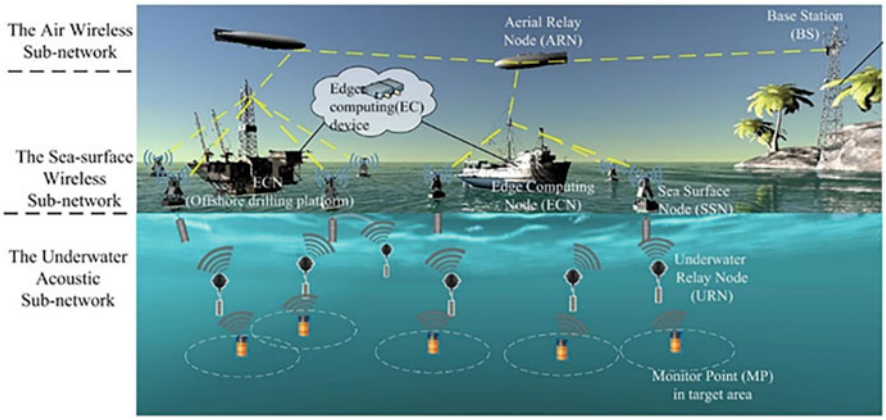

Fig. 2.1 An integrated multi-tier hierarchical network architecture of MWCN

and RF transmitting devices; the sea-surface wireless sub-network consists of unmanned ships which carry RF communication devices; and the air wireless sub-network [17, 18] consists of ARNs, such as Unmanned Air Vehicles (UAVs) with RF communication equipment. Under the proposed network architecture, the node deployment problem is further investigated to achieve the minimum network cost while ensuring the maximum network lifetime. Specifically, an MO problem is formulated to minimize the costs and maximize the network lifetime, by deploying different types of nodes in different tiers of the network, considering the energy and capacity constraints of each node. The formulated optimization problem can be solved by Gurobi. As Gurobi does not work well when the network scale up, we propose a swarm intelligent based optimization approach to find the near-optimal solution of the formulated optimization problem.

2.2 Related Works

Most researches of deployment of MWCN focus on nodes deployment of UAN networks, i.e., sensors and/or surface gateways. Ibrahim S., Cui J., and Ammar R. formulate the optimal gateway deployment problem as an Integer Linear Programming (ILP) problem in [11]. They propose an algorithm to deploy multiple surface-level gateways in [13] and use a greedy algorithm and greed-interchange algorithm to select gateway positions among candidate locations. In these works, they mainly study sensor deployment under 2D space. In [19], Song X., Gong Y. et al. propose a 3D node deployment algorithm for underwater sensor networks. The proposed algorithm can achieve a large coverage area with the minimal number of nodes. In [20], Jiang P., Wang X., and Jiang L. propose a depth adjustment algorithm based on connected tree (CTDA), in which the sink node is used as the first root node of a connected tree, and the whole network is organized as a forest that

comprises many connected sub-trees. To maximize the network coverage, coverage overlaps between the parent node and the child node are reduced within each sub-tree. In addition, in [10, 21, 22], Han G., Pompili D. et al. present 2D and 3D communication architectures and review deployment algorithms and strategies for UASNs from different perspectives. It is found that most existing works focus on the node deployment of underwater sub-network nodes, and few works jointly consider the network deployment of underwater network and network above the water surface. With the popularity of Swarm Intelligence (SI), a number of researches propose to use SI and SI-based algorithms (SIAs) to tackle the optimization problems in node deployment of tradition wireless sensor networks and communication network. Ant Colonies Optimization (ACO) is one of the well-known representative SIAs, where complex collective behavior emerges from the behavior of ants. ACO is effective for solving NP-hard discrete optimization problems and has been successfully applied to a number of scientific and engineering problems, including grid-based deployment for wireless sensor networks [23–25]. ACO is also applied to the topology optimization [26, 27] and routing algorithm [28, 29] for wireless networks. An ACO algorithm coupled with a local search heuristic is proposed in [30] to deploy a WSN under a certain reliability constraint at the minimum deployment cost. However, algorithms for traditional WSN or communication networks cannot be directly applied for MWCNs due to the different characteristics of the deployment environment of ocean in three-dimensional space. To this end, we are motivated to apply ACO for the MWCN deployment under three-tier architecture and formulate a multi-objective optimization problem characterizing the 3D marine environment.

2.3 Network Model and Problem Formulation

2.3.1 Network Model

The hierarchical network model of MWCN is composed of three subnetworks: (1) the underwater acoustic sub-network, (2) the sea-surface wireless sub-network, and (3) the air wireless sub-network, as shown in Fig. 2.1. In an underwater acoustic sub-network, multiple sensors deployed at representative Monitoring Points (MPs) are to monitor the target areas. The MP then transmits the monitoring data to an SSN, typically via one or multiple URNs, when communication distance is beyond the transmission range of sensors at MPs. URN is a buoyancy-driven device which can hover and select a specified position to acquire and transmit data over acoustic communication channels [31–33]. The location of URN should be carefully decided as it is dependent on the influence of ocean flow and undercurrent. SSU is equipped with a wireless communication radio installed on the buoy, an acoustic-electric conversion device, and an underwater acoustic receiver located under the sea surface. After receiving the underwater acoustic signals from URNs, it converts them into radio signals and then transmits radio signals to an ECN or other SSN within its communication distance.

The sea-surface wireless sub-network is comprised of multiple ECNs, which are responsible of receiving radio signals from the underwater acoustic sub-network, processing the data in an edge device, and sending the processed data to the air wireless sub-network. Generally, unmanned ships with communication equipment and small edge server are used as ECNs.

The air wireless sub-network further relays the received data from the sea-surface wireless sub-network to the BS. This sub-network is consisted of multiple ARNs which transmit the received data to the BS over one or multiple hops through other ARNs. Finally, the BS transmit the data from the MWCN network to the data center through the terrestrial wireless networks.

In the MWCN, the BS is the destination node, ARNs, ECNs, SSNs, and URNs are the intermediate nodes and MPs are source nodes. All nodes are organized hierarchically within the communication radius of nodes, and an efficiently tree architecture will be finally formed to achieve an effective communication.

In summary, various nodes involved in the MWCN have a certain communication radius, by using either radio or acoustic communications; and each node only communicate with other nodes of the same sub-network or nodes of the upper sub-network within their communication distance. In addition, the ARN and ECN nodes may have sufficient power supply with no stringent capacity limitation, but battery-powered SSN and URN nodes are typically of small sizes and thus are subject to certain battery constraints, which should be taken into consideration for network deployment.

2.3.2 Energy Model

In the MWCN, ARNs and ECNs usually have sufficient energy supply with no stringent capacity limitation, while battery-powered underwater nodes, i.e., SSNs, URNs, and MPs, are typically of small sizes with limited battery capacity. Thus, to provision quality marine monitoring services of the MWCN, it is of critical importance to improve the operation time of the underwater nodes.

Generally, the states of the battery of a node include sending, receiving, idle, and sleeping. It is reported in [34] that communication module consumes most energy, i.e., around 80% of the total energy consumption. Energy consumption during idle and sleep modes is only related to time. In our system model, energy consumption per unit time during idle and sleep mode is regarded as a constant. Here, a URN communicates to other URNs or SSNs over underwater acoustic channels.

The transmission and receiving energy consumption of node i over a communication channel, i.e., either an acoustic channel [35] or a radio channel [36], are denoted as E_{tr}^{i} and E_{re}^{i}, respectively, which are given by:

$$\mathrm{E}_{tr}^{i}\left(l_{ij}, d_{ij}\right) = \begin{cases} E_0 d_{ij}^{k} 10^{d_{ij}\frac{\alpha(f)}{10}} l_{ij}, & \text{acoustic channel} \\ E_{\text{elec}} l_{ij} + \varepsilon_{\text{amp}} l_{ij} d_{ij}^{2}, & \text{radio channel} \end{cases} \tag{2.1}$$

where E_{elec} is the energy consumption of the transmitter circuit; ε_{amp} is the energy consumption of power amplifier; E_0 is the energy consumption of transmitting one bit of data with a certain communication radius; E_{r} is the energy consumption of receiving one bit of data; k is the energy diffusion factor; l_{ij} is the size of the data packet from node i to node j in bits, and d_{ij} is the transmission distance from node i to node j. $\alpha(f)$ is the Doppler frequency absorption coefficient of signal frequency f, which is given by Throp [35]

$$\alpha(f) = \frac{0.11 f^2}{1+f^2} + \frac{44 f^2}{4100 + f^2} + 2.75 \times 10^{-4} f^2 + 0.003 \tag{2.2}$$

Thus, the communication energy consumption of node i is

$$Ec_i = \sum_{j \in V} E_{tr}^{i}\left(l_{ij}, d_{ij}\right) e_{ij} + \sum_{t \in V} E_{re}^{i}(l_{ti}) e_{ti} \tag{2.3}$$

where $e_{ij} = 1$ indicates that node i can directly communicate with node j and vice versa. And the total energy consumption of node i is

$$E_i = Ec_i + E_{\text{idle}}^{i} + E_{\text{sleep}}^{i} \tag{2.4}$$

where E_{idle}^{i} and E_{sleep}^{i} are the energy consumption of node i during idle and sleep mode, respectively.

2.3.3 Problem Formulation

We model the MWCN as a directed graph $\vec{G} = \left(V, \vec{E}\right)$, where V represents the set of nodes, i.e., BSs, ARNs, ECNs, SSNs, URNs, and MPs, and $\vec{E}$ represents directed edges between two nodes that are within the communication radius. To differentiate nodes, the subsets of BSs, ARNs, ECNs, SSNs, URNs, and MPs are denoted as V_{BS}, V_{ARN}, V_{ECN}, V_{SSN}, V_{URN}, and V_{MP}. Thus, the whole set of nodes $V = V_{\text{BS}} \cup V_{\text{ARN}} \cup V_{\text{ECN}} \cup V_{\text{SSN}} \cup V_{\text{URN}} \cup V_{\text{MP}}$. The edge $e_{ij} \in \vec{\mathrm{E}}$ is a binary variable, $e_{ij} = 1$ indicates there exists a direct communication link from node i to node j and vice versa. The main notations used in the MO problem are listed in Table 2.1.

Table 2.1 Definitions of symbols

Symbols	Definition
g_i	The amount of data of MP_i (per unit time).
R_{MP}	The perceived radius of MPs
D^{ARN}	The communication distance of ARNs
D^{ECN}	The communication distance of ECNs
D^{SSN}	The communication distance of SSNs
D^{URN}	The communication distance of URNs
C^{ARN}	The cost of ARNs
C^{ECN}	The cost of ECNs
C^{SSN}	The cost of SSNs
C^{URN}	The cost of URNs
E_{elec}	Energy consumption for sending and receiving data per bit
P_{UT}	The transmission power of URNs
P_{UR}	The reception power of URNs
EI_i	The initial energy of node i
EC_i	The energy consumption of node i per unit time
K	K-coverage: Each MP must be covered by K URNs
$\vec{E} = \{e_{ij}\}_{\|V\|\times\|V\|}, \forall i,j \in V$	The matrix of edge variables, where $e_{ij} \in \{0,1\}$ is a binary variable and $e_{ij} = 1$ denotes node i can directly communicate with node j and vice versa
$A = \{a_m\}_{1\times\|V_{URN}\|}, \forall m \in V_{URN}$	The location incidence vector of nodes, where $a_m \in \{0,1\}$ is a binary variable and $a_m = 1$ denotes that the candidate location m is selected to deploy a URN and vice versa
$B = \{b_n\}_{1\times\|V_{SSN}\|}, \forall n \in V_{SSN}$	The location incidence vector of nodes, where $b_n \in \{0,1\}$ is a binary variable and $b_n = 1$ denotes that the candidate location m is selected to deploy an SSN and vice versa
$H = \{h_l\}_{1\times\|V_{ECN}\|}, \forall l \in V_{ECN}$	The location incidence vector of nodes, where $h_l \in \{0,1\}$ is a binary variable and $h_l = 1$ denotes that the candidate location m is selected to deploy an ECN and vice versa
$Z = \{z_t\}_{1\times\|V_{ARN}\|}, \forall t \in V_{ARN}$	The location incidence vector of nodes, where $z_t \in \{0,1\}$ is a binary variable and $z_t = 1$ denotes that the candidate location m is selected to deploy an ARN and vice versa
$f_{ij}, \forall\ i,j \in V$	The data flow from node i to node j

As the marine monitoring devices, especially the battery-powered underwater monitoring devices, are expensive, it is desirable to reduce the total number of devices for deployment to minimize the total deployment cost. In the meantime, it is hard if not possible to replace batteries of underwater nodes, and thus it is important to maximize the operation time of network nodes. In this chapter, we will formulate MO problem under the MWCN architecture. The primary objectives are to minimize the total deployment cost while maximizing the network lifetime subjected to the limited node communication radius and battery cdapacities. Here, the network lifetime is defined as the time until the first node runs out of energy [37].

2.3.3.1 Minimization of the Total Network Deployment Cost

The first objective is to minimize C_{net}, the total deployment cost of the network, i.e., the sum deployment cost of ARNs, ECNs, SSNs, and URNs. The MPs are pre-deployed based on the marine areas of interest while other types of nodes are deployed to collect and forward the information from MPs to the Internet servers. Denote the unit deployment cost of ARN, ECN, SSN, and URN as C^{ARN}, C^{ECN}, C^{SSN}, and C^{URN}. Thus, we have

$$C_{\text{net}} = C^{\text{URN}} \sum_{m \in \text{V}_{\text{URN}}} a_m + C^{\text{SSN}} \sum_{n \in \text{V}_{\text{SSN}}} b_n + C^{\text{ECN}} \sum_{l \in \text{V}_{\text{ECN}}} h_l + C^{\text{ARN}} \sum_{t \in \text{V}_{\text{ARN}}} z_t \tag{2.5}$$

where a_m, b_n, h_l, and z_t are binary variables of Candidate Locations (CLs) of URNs, SSNs, ECNs, and ARNs, respectively. The value of 1 indicates that the CL is selected to place a corresponding node and vice versa.

2.3.3.2 Maximization of the Network Lifetime

Besides the network deployment cost, it is also critical to ensure that the MWCN provisions quality marine monitoring services as long as possible. The network lifetime is defined as the operation time of the network until the first battery-powered node exhausts the energy supply and becomes out of service. Given the initial battery of a battery-powered node i, EI_i, and the energy consumption of node i, E_i per unit time, the lifetime of node i is then given by

$$T_i = \frac{\text{EI}_i}{E_i}, \forall i \in V_{\text{URN}} \cup V_{\text{SSN}} \tag{2.6}$$

Therefore, the network lifetime T_{net} is defined as:

$$T_{\text{net}} = \min_{\forall i \in V_{\text{URN}} \cup V_{\text{SSN}}} T_i = \min_{\forall i \in V_{\text{URN}} \cup V_{\text{SSN}}} \frac{\text{EI}_i}{E_i} \tag{2.7}$$

Notice that E_i is dependent on the communication distance and the communication data volume shown as Eqs. (2.1)–(2.4), Thus the network lifetime is determined by Ec_i of the first energy-exhausted node i. Accordingly, to maximize the network lifetime, it is equivalent to minimize the energy consumption of the first energy-exhausted node. According to Eqs. (2.3) and (2.4), the energy consumption of the first energy-exhausted node is given by

$$E_{\max} = \max_{\forall i \in V_{\text{URN}} \cup V_{\text{SSN}}} \left(\sum_{j \in \text{V}} E^i_{tr}(l_{ij}, d_{ij}) e_{ij} + \sum_{t \in \text{V}} E^i_{\text{re}}(l_{ti}) e_{ti} + E^i_{\text{idle}} + E^i_{\text{sleep}} \right) \tag{2.8}$$

Without the loss of generality, the initial energy of node (EI) is regard as 100% in the following formulation.

Thus, the MO problem is formulated as follows:

$$\textbf{minimize} \quad C_{\text{net}} + \omega E_{\max} \tag{2.9}$$

$$\textbf{s.t.} \quad \sum_{j \in V_{\text{URN}}} e_{ij} \geq K, \forall i \in V_{\text{MP}} \tag{2.10}$$

$$\sum_{i \in V_{\text{MP}} \cup V_{\text{URN}}} e_{im} \geq a_m, \forall m \in V_{\text{URN}}, m \neq i \tag{2.11}$$

$$\sum_{j \in V_{\text{URN}} \cup V_{\text{SSN}}} e_{mj} \geq a_m, \forall m \in V_{\text{URN}}, m \neq j \tag{2.12}$$

$$\sum_{j \in V_{\text{SSN}} \cup V_{\text{URN}}} e_{jn} \geq b_n, \forall n \in V_{\text{SSN}}, n \neq j \tag{2.13}$$

$$\sum_{q \in V_{\text{SSN}} \cup V_{\text{ECN}}} e_{nq} \geq b_n, \forall n \in V_{\text{SSN}}, n \neq q \tag{2.14}$$

$$\sum_{q \in V_{\text{SSN}} \cup V_{\text{ECN}}} e_{ql} \geq h_l, \forall l \in V_{\text{ECN}}, l \neq q \tag{2.15}$$

$$\sum_{u \in V_{\text{ECN}} \cup V_{\text{ARN}}} e_{lu} \geq h_l, \forall l \in V_{\text{ECN}}, l \neq u \tag{2.16}$$

$$\sum_{u \in V_{\text{ECN}} \cup V_{\text{ARN}}} e_{ut} \geq z_t, \forall t \in V_{\text{ARN}}, t \neq u \tag{2.17}$$

$$\sum_{s \in V_{\text{BS}} \cup V_{\text{ARN}}} e_{ts} \geq z_t, \forall t \in V_{\text{ARN}}, t \neq s \tag{2.18}$$

$$\sum_{i \in V_{\text{URN}}} f_{ij} + \sum_{k \in V_{\text{MP}}} g_k e_{kj} = \sum_{l \in V_{\text{URN}}} f_{jl} + \sum_{m \in V_{\text{SSN}}} f_{jm}, \forall j \in V_{\text{URN}}, i \neq j, j \neq l \tag{2.19}$$

$$\sum_{i \in V_{\text{SSN}}} f_{ij} + \sum_{k \in V_{\text{URN}}} f_{kj} = \sum_{l \in V_{\text{SSN}}} f_{jl} + \sum_{m \in V_{\text{ECN}}} f_{jm}, \forall j \in V_{\text{SSN}}, i \neq j, j \neq l \tag{2.20}$$

Equation (2.9) is the weighted sum of the two main objectives, where the network cost C_{net} and the energy consumption of the first exhausted node $E_{\max}$ are defined in Eqs. (2.5) and (2.8), respectively, and ω is the weight to strike a balance of the two objectives.

Constraint Eq. (2.10) specifies that each MP must be covered by at least K URNs. Different monitoring tasks have different requirements of K.

Equation (2.11) indicates that if CL j is selected to deploy a URN, then $a_j = 1$, and there exists at least one link of receiving data, e.g., between a MP or URN node i and j. Equation (2.12) indicates that when a URN j is deployed, there exists one link of forwarding data, e.g., between node j to another URN or SSN nodes l.

Similarly, SSNs, ECNs, and ARNs are subject to the constraints Eqs. (2.13)–(2.18), respectively.

Equations (2.13) and (2.14) specify that if a SSU n is deployed, i.e., $b_n = 1$, the SSU n has one link of forwarding data and at least one link of receiving data. Similarly, Eqs. (2.15) and (2.16) specify that if CL l is selected to deploy an ECN, i.e., $h_l = 1$, there exists one link of forwarding data and at least one link of receiving data. Equations (2.17) and (2.18) specify that if CL t is selected to deploy an ARN, i.e., $z_t = 1$, there exists one link of forwarding data and at least one link of receiving data.

Equations (2.19) and (2.20) specify the flow constraints that the output data should be the same as the input data.

2.4 Ant Colony Based Efficient Topology Optimization (AC-ETO)

2.4.1 Algorithm Description

As the formulated optimization problem is an integer linear programming problem, which is known to be NP-hard [38]. The ant colony is widely used to solve various NP-hard problems. Especially [39]. Thus, in this section we propose an Ant Colony based efficient topology optimization algorithm, namely AC-ETO, to solve the proposed problem in P1.

In a traditional ACO algorithm, ants choose the next city through a probabilistic rule and then iteratively construct the best path [40]. The probability for an ant to move from city i to city j is

$$p_{ij} = \frac{\left(\tau_{ij}\right)^{\alpha} \eta_{ij}^{\beta}}{\sum\limits_{j \in V_{\text{allowed}}} \left(\tau_{is} + \tau'_{is}\right)^{\alpha} \eta_{is}^{\beta}} \tag{2.21}$$

where τ_{ij} is the amount of pheromone deposited for a transition from city i to j, α is a parameter to control the influence of τ_{ij}, η_{ij} is a heuristic factor for the transition from city i to j and typically is inversely proportional to the distance between cities i and j, i.e., $\eta_{ij} = 1/d_{ij}$, β is a parameter to control the influence of η_{ij}, and V_{allowed} is the feasible neighborhood of an ant in city i.

In AC-ETO, we select data forwarding paths in the hierarchical MWCN step by step. In each step, a probabilistic transition rule is applied to select a deployment location. For example, at node i, the probability that the deployment location $j\left(\ j = 1, 2, \ldots, |V_{\text{FCL}}^{i}|\right)$ is selected is given by

$$p_{ij} = \frac{\left(\tau'_{ij} + \tau''_{ij}\right)^{\alpha} \eta'^{\beta}_{ij}}{\sum\limits_{j \in V^{i}_{FCL}} \left(\tau'_{ij} + \tau''_{ij}\right)^{\alpha} \eta'^{\beta}_{ij}} \tag{2.22}$$

where τ'_{ij} given in Eq. (2.23) is the global pheromone trail value between node i and node j; τ''_{ij} given in Eq. (2.24) is the local value between the two nodes i and j; η'_{ij} is the heuristic value of adding node j to the connected cover currently being built by the ant, which is defined as Eq. (2.26); and α, β are parameters that control the influence of the pheromone trail values and heuristic information on p_{ij}, respectively; V^{i}_{FCL} is the Feasible Candidate Location (FCL) set of node i, and FCL is defined as CLs within the communication range of a node.

$$\tau'_{ij} = (1 - \rho_1)\tau'_{ij} + \Delta\tau'_{ij} \tag{2.23}$$

$$\tau''_{ij} = (1 - \rho_2)\tau''_{ij} + \Delta\tau''_{ij} \tag{2.24}$$

$$\eta'_{ij} = \begin{cases} \dfrac{1}{E^{i}_{tr}} & i \in V_{URN} \cup V_{SSN} \\ 1 & \text{otherwise} \end{cases} \tag{2.25}$$

where E^{i}_{tr} is given by formula (1). $\Delta\tau'_{ij}$ and $\Delta\tau''_{ij}$ are defined as follows:

$$\Delta\tau'_{ij} = \begin{cases} \dfrac{Q - C^{j}}{C_{bestnet}} & e_{ij} = 1 \\ 0 & \text{otherwise} \end{cases} \tag{2.26}$$

$$\Delta\tau''_{ij} = \begin{cases} \dfrac{Q - C^{j}}{C_{path}} & e_{ij} = 1 \\ 0 & \text{otherwise} \end{cases} \tag{2.27}$$

where C^{j} is the cost of node j, $C_{bestnet}$ is the current minimum network cost, and C_{path} is the cost of the path. Q is a constant greater than 1, ρ_1 and ρ_2 are the rates of global and local pheromone evaporation.

The process of AC-ETO is divided into two phases. The first phase is the initialization phase, which reduces the search space so that only FCLs are selected and stored by certain nodes. The second phase is the planning phase, where the optimization process is iteratively performed to construct the network topology and remove the redundant edges until the desired result is reached.

We first use a small-scale network with 2 MPs as an example to describe the algorithm. In the initialization phase, the distances between nodes are calculated based on the location of nodes. Each node then constructs a FCL table which includes all nodes in its communication coverage. For instance, the FCL table of MP0 includes URN0 and URN1. In the planning phase, a number of iterations are involved. In each iteration, a number of ants are placed on each MP to construct

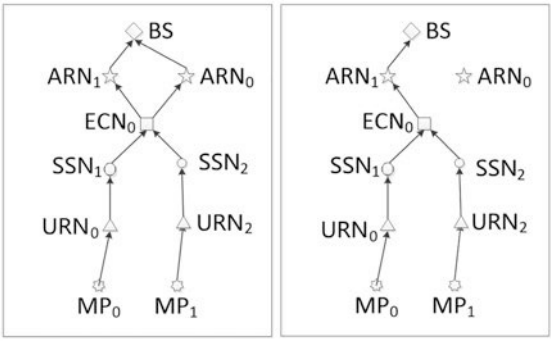

Fig. 2.2 The topology of the network with 2 MPs

paths to the BS by using the probabilistic rule, the local pheromone, and the global pheromone defined in Eqs. (2.23)–(2.25). An ant placed on MP0 moves to the next node, e.g., URN0 in the FCL table according to the pheromones and the transition probability until it arrives at the BS. After the ant reaches the BS, the BS informs all nodes along the path to update the local pheromone and selects the best path from multiple ants, e.g., MP0-URN1-SSN0-ECN0-ARN1-BS0 and MP1-URN2-SSN2-ECN0-ARN0-BS0 in the 2-MP example, as shown in Fig. 2.2a. Notice that the two paths are independently found by ants and there may be multiple links between two nodes, e.g., ECN0-ARN1-BS0 and ECN0-ARN0-BS0. In such case, the two links are compared and the path with higher energy consumption, e.g., ECN0-ARN0-BS0, is removed to obtain a tree with $C_{\text{net}} + \omega E_{\max} = 68.417$, as shown in Fig. 2.2b. The iteration repeats until no better tree with a smaller $C_{\text{net}} + \omega E_{\max}$ can be found.

The pseudo code of the proposed AC-ETO is elaborated in Algorithm 2.1.

Algorithm 2.1: The Pseudo Code of AC-ETO Algorithm

Input: $V_{MP}, V_{URN}, V_{SSN}, V_{ECN}, V_{ARN}, V_{BS}$

/* Phase I: Initialization*/

1: Input positions of nodes and other parameters;
2: $N \leftarrow |V|$;
3: $D_{N \times N} \leftarrow$ the distance between nodes;
4: **for** $i = 1$ to N **do**
5: $T^{i}_{Feable} \leftarrow FCL\_Table\_Bld(i)$;
6: **end for**
/***Phase II: Multi-objective planning*/**
7: $M\_Global_{N \times N} \leftarrow \{1\}$;
8: $V_{start} \leftarrow V_{MP}$, $M \leftarrow |V_{MP}|$;
9: **repeat**
/*Step 1-Network construction*/
10: **for** $i = 1$ to M **do**
11: Take a MPj randomly form V_{start};
12: Place m ants on j; \\ m is a constant integer
13: **for** each ant $r = 1$ to m **do**
14: $M\_Local_{N \times N} \leftarrow \{1\}$;

15: Put j into node_list of r: $V_{list}^{r} \leftarrow V_{list}^{r} \cup \{j\}$;
16: $k \leftarrow j$;
17: $M\_prob_{N \times N} \leftarrow \{0\}$;
18: **while** $(k \notin V_{BS})$ **do**
19: Choose and move to next node k from T_{Feable}^{k};
20: $V_{list}^{r} \leftarrow V_{list}^{r} \cup \{k\}$;
21: **end while**
22: Calculate the cost of V_{list}^{r};
23: Calculate the energy consumption of each node t: EC_t;
24: **end for**
25: Choose the best path for MP_j from $\{V_{list}^{1}, \ldots, V_{list}^{m}\} \rightarrow list_j$;
26: The cost of $list_j \rightarrow C_j$;
27: Calculate the energy consumption of each node t: EC_t;
28: Update $M\_Local_{N \times N}$;
29: **end for**
* **Step 2- Redundant edge removal***\
30: Remove redundant edges from the initial constructed network;
31: Update $M\_Global_{N \times N}$;
32:**Until** iterative number $>\psi$
33:**Output**: the optimal solution, total cost and energy consumption;

2.4.2 Computational Complexity Analysis

In this subsection, we analyze the computational complexity of the proposed (AC-ETO) algorithm.

Phase I—Initialization (Lines 1–6): In the initialization phase, the locations of a number of network nodes, including BS, MPs, CLs of ARNs, ECNs, SSNs, and URNs, are imported. Accordingly, the network parameters such as communication distance, initial energy, transmit and receive power are set as shown in Table 2.3. The complexity of initialization is $O(N)$, where N is the network size; And then the distance matrix between neighboring nodes is calculated first, and the complexity is $O(N^2)$. According to the distance matrix, each node maintains an FCL table that includes the list of nodes that it can directly communicate with. For example, a URN lists a set of other URNs and/or SSNs in its communication coverage. The worst-case complexity is $O((N-1)(N-M))$. Therefore, the complexity of Phase I is $O(2N^2 - MN - N + M)$.

Phase II—Topology planning (Lines 7–31): Based on the FCL tables calculated in phase I, an ant colony based optimal method is used to find the placement of the minimum cost and the energy consumption. The algorithm is interactively performed for network construction and redundant edge removal until a desirable result is reached. In Lines 7–8, the matrix of global pheromone is initialized to 1 by the memset function with a complexity of $O(N)$, and the subset V_{MP}, which has

M elements, is set as the set of starting points V_{start}, and the complexity is $O(M)$, where M is the number of MPs. In Lines 9–31, the iterative optimization process is executed, where Lines 10–29 are for Step 1—Network construction and Lines 30–31 are for Step 2—Redundant edge removal. In Step 1, an ant colony is placed on a MP which is randomly selected from V_{MP} and then move to construct paths towards the BS. By comparing the values of Eq. (2.9) for each feasible path, the best one, the one with the minimum value of Eq. (2.9) is selected and stored. When M ant colonies complete path construction, the sequences of M best paths are selected to construct a network. Step 1 yields the worst-case complexity $O(MN^2 + MN + M^2)$. In Step 2 (Lines 30–31), the result of Step 1 is modified by removing some redundant edges according to the characteristics of the tree structure constraints, and the complexity of this step is $O(N^2 + M^2 + M)$. Figure 2.2 shows an example of Step 2. Figure 2.2a shows the constructed network topology after Step 1. It can be seen that the structure is not a tree topology as the out degree of ECN 0 is 2. In Fig. 2.2b, two redundant edges are removed from the network to form a tree topology. Thus, the complexity of Lines 12–33 is as follows.

$$O(MN^2 + MN + M^2) + O(N^2 + M^2 + M) = O(MN^2 + N^2 + MN + 2M^2 + M)$$

Accordingly, if N is sufficiently large, the complexity of Phase II is $O(\psi MN^2 + \psi MN + \psi M^2 + \psi M)$ approximately, where ψ is the maximum number of iterations.

Therefore, the overall computation complexity of the algorithm is $O(2N^2 - MN - N + M) + O(\psi MN^2 + \psi MN + \psi M^2 + \psi M) \approx O(\psi MN^2 + \psi MN + \psi M^2)$. The AC-ETO is efficient and it achieves a polynomial time complexity.

2.5 Simulations and Discussions

In this section, we validate the performance of the proposed algorithm and compare it with benchmark algorithms in different network scenarios. MPs are predefined carefully in the monitoring sea area according to sea state conditions and needs. Specifically, we first validate the performance in a small-scale network. Then we show the performance of MO problem solved by Gurobi in small-scale networks and compared it with our proposed algorithm. A greedy algorithm is further presented and compared with the proposed AC-ETO algorithm. We setup multiple experiments of 11 network scenarios of different scales, as shown in Table 2.2. The main parameters used in the experiments are listed in Table 2.3. Without loss of generality, the generic cost unit (gcu) and the generic time unit (gtu) are defined to simplify the evaluation of deployment costs and network lifetime in the case studies. The impacts of ω on the results are tested in different scenarios under various network scales, as shown in Fig. 2.3. It can be seen that the deployment cost shows little variance, but the energy consumption may decrease significantly when ω increases. In other experiments, the value of ω is set to 2E+06.

Table 2.2 The setting of simulated scenarios

Scenario index	Number of					
	BS	MP	CLs of ARN	CLs of ECN	CLs of SSN	CLs of URN
0	1	2	2	3	4	6
1	1	2	1	2	10	15
2	1	4	1	2	20	25
3	1	6	2	8	20	30
4	1	8	2	8	25	40
5	1	10	3	5	35	50
6	1	12	3	10	40	60
7	1	15	3	9	50	70
8	1	20	4	12	80	100
9	1	25	5	16	100	120
10	1	35	7	25	125	150
11	1	50	7	25	170	200

Table 2.3 Parameter setting

Parameter	Value
EI_{SSN}, EI_{URN}	2,3(J)
E_r, E_o	10,50(nJ)
E_{elec}	50(nJ)
D^{URN}, D^{SSN}, D^{ECN}, D^{ARN}	5,10,25,30(km)
R_{MP}	0.2(km)
C^{URN}, C^{SSN}, C^{ECN}, C^{ARN}	15,10,9,9(gcu)
ϵ_{amp}	0.84
ω	2E+06

2.5.1 *Performance Validation in Small Scale to Middle Scale Networks*

We first evaluate the network performance of small-scale network scenarios with a few numbers of nodes, i.e., Scenario 0 and Scenario 1. Take Scenario 0 as an example. The results obtained by Gurobi [41], Fig. 2.4 shows the deployment solution of Scenario 0. The deployment cost of this solution is 68, which is the minimum cost in Scenario 0. Similarly, the energy consumption is 8.18E-05, which is also the lowest one among all deployment plans. In this simple case, the optimization solution obtained by Gurobi is optimal, compared with the results obtained from the exhaustive search.

We then compare the solutions of the MO problem P1 with each of the sub-problem of MO, i.e., P2 and P3 under different scenarios from Scenarios 1–7. We then compare the solutions of the MO problem (P1) with each of the sub-problem of MO, i.e., to minimize the cost (P2) or to minimize the energy consumption (P3) under different scenarios from Scenarios 1–7. The results are compared in Fig. 2.5. As shown in Fig. 2.5a, the deployment cost of P1 is slightly

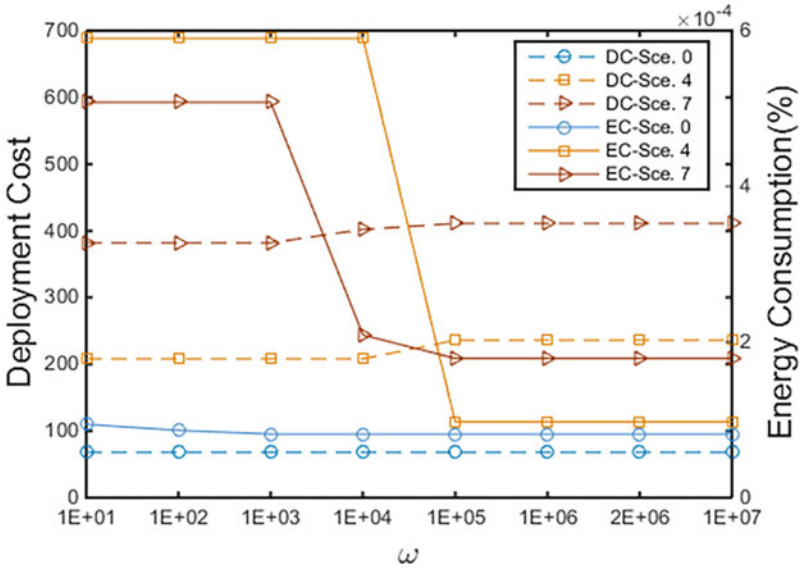

Fig. 2.3 The impacts of DC stands for Deployment Cost, and EC stands for Energy Consumption. Sce. is the abbreviation of Scenario

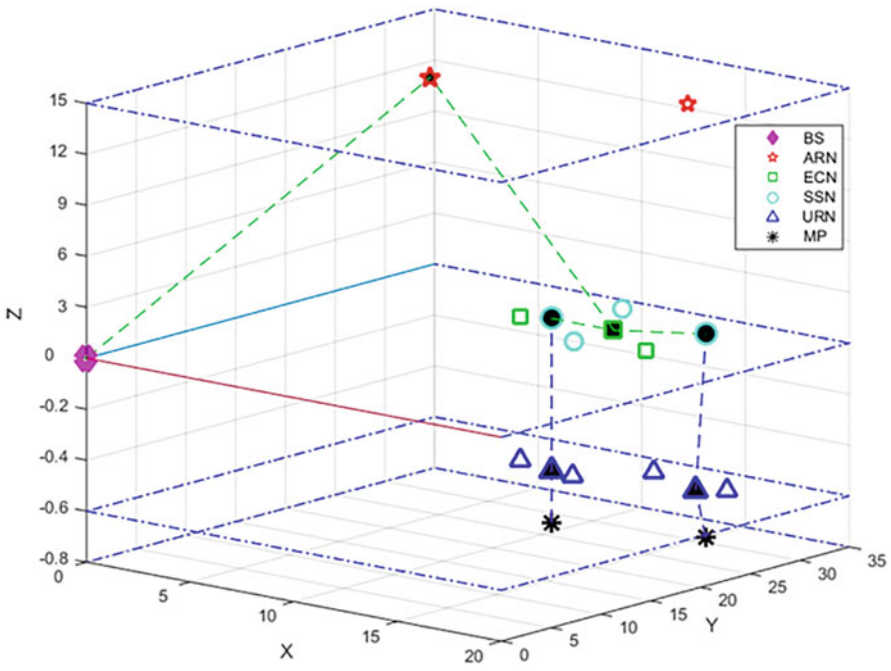

Fig. 2.4 The optimal solution of Scenario ($C_{\text{net}} = 68$ gcu, $E_{\max} = 8.18\text{E} - 0.5\%$)

greater than that of P2, but smaller than that of P3. Figure 2.5b shows that energy consumption of P1 is similar to that of P3 but much smaller than that of P2. Correspondingly, the network lifetime of P1 is much greater than that of P2 while smaller than or equal to that of P3 as shown in Fig. 2.5c. Thus, using P1, a longer network lifetime can be achieved with a lower deployment cost. Again, Gurobi can achieve the optimal solution.

Based on the above process, a series of small-scale network simulation are carried out to verify the performance of the algorithm and compare it with the exhaustive search and Gurobi. As shown in Fig. 2.6, the results of the proposed algorithm in Scenarios 0–2 approaches that of the exhaustive search and Gurobi. For instance, the optimal solution of the AC-ETO in Scenario 0 is 68.818, which equals to that of the exhaustive search. Thus, the solutions of the algorithm in small-scale networks are close to optimal. As the scale of the network increase, it is difficult to obtain the optimal solutions by the exhaustive search. We further compare the solutions of the algorithm with that of the Gurobi in Scenarios 3–5. Figure 2.6 shows that the results of the algorithm are very close to that of Gurobi. Therefore, the optimization solution of the AC-ETO is close to optimal in small scale and medium scale networks.

2.5.2 Performance Analysis of Gurobi and AC-ETO in Different Network Scenarios

We further study the performance of the proposed algorithm AC-ETO under different network scales and compare the results with the solutions of P1 obtained by Guiobi. As shown in Fig. 2.7a, the deployment cost obtained by Gurobi is slightly smaller than that by AC-ETO in Scenarios 5–10. Figure 2.7b, c compares the energy consumption and network lifetime performance obtained by Gurobi and by AC-ETO under different scenarios. Similarly, it can be observed Gurobi slightly outperform AC-ETO in all these metrics. In Fig. 2.7d, when the network scales up with a larger number of nodes, the time complexity of Gurobi increases drastically, while the running time of AC-ETO does not very much. As an example, in Scenario 9 the energy consumption by AC-ETO is 0.69E-4% greater than that by Gurobi, and the deployment cost by AC-ETO is 9.16% higher than that by Gurobi, but the time complexity of Gurobi is 1000 times higher than that of AC-ETO. As the network size increases, Gurobi cannot obtain the results in the last scenario, i.e., Scenario 11, within the set time limit of 300,000 s, yet the proposed AC-ETO algorithm obtains the results efficiently. Thus, the AC-ETO is efficient in dealing with those large-scale network scenarios at the cost of a slight reduction of the optimality.

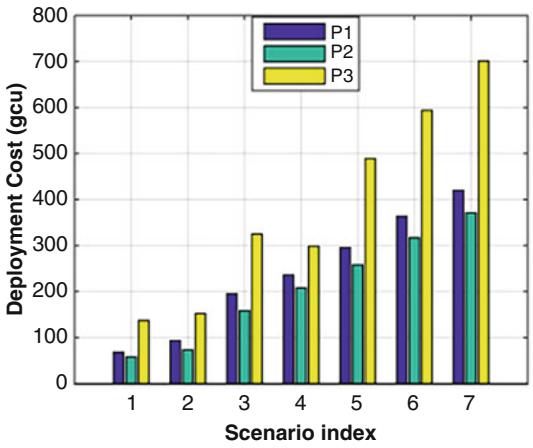

(a)

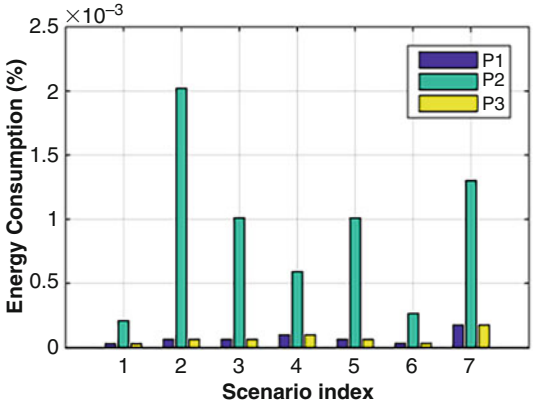

(b)

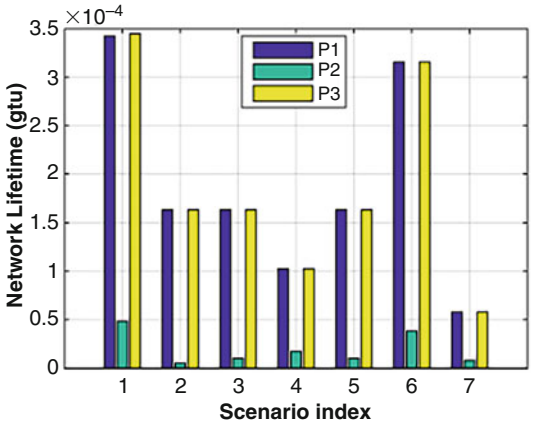

(c)

Fig. 2.5 Comparison of P1, P2, and P3 in terms of the deployment cost, energy consumption, and network lifetime. (**a**) Deployment Cost. (**b**) Energy consumption. (**c**) Network lifetime

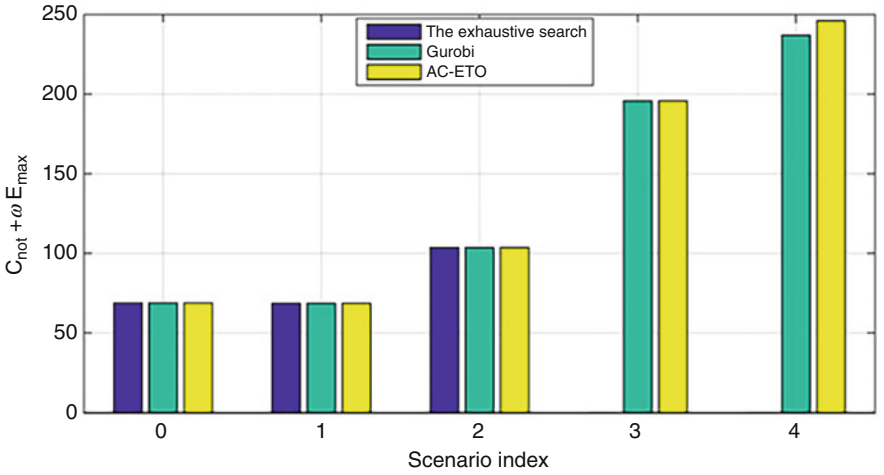

Fig. 2.6 Comparison of the exhaustive search, Gurobi, and the AC-ETO in terms of the optimization objective

2.5.3 Performance Comparison of AC-ETO and a Greedy Algorithm

We further compare the performance of the proposed AC-ETO algorithm with a greedy algorithm shown in Algorithm 2.2. Initially, the feasible table, i.e., FCL table of each node is established to store the CLs within the communication coverage. All CLs in the table are grouped by type in the increasing order of the communication distance. A path is then set to the BS for each MP. To set up a path, each node along the path is selected by checking CLs in FCL_Table of the prior node in an order, until the BS is reached. The network construction completes when all paths are found for any MP.

Algorithm 2.2: A Greedy Algorithm
Input: V_{MP},V_{URN},V_{SSN},V_{ECN},V_{ARN},V_{BS};
Initialization: Input positions of nodes and other parameters;
for each $i \in V$ **do**
Build the feasible table FCL_Table for i;
end for
$M \leftarrow |V_{MP}|$
for i=1 to M **do**
Find a feasible node l from FCL_Table of MPi;
while ($l \notin V_{BS}$) **do**
Find a feasible node k from FCL_Table of l;
$l \leftarrow k$;
path_list of $i \leftarrow k$;
end while

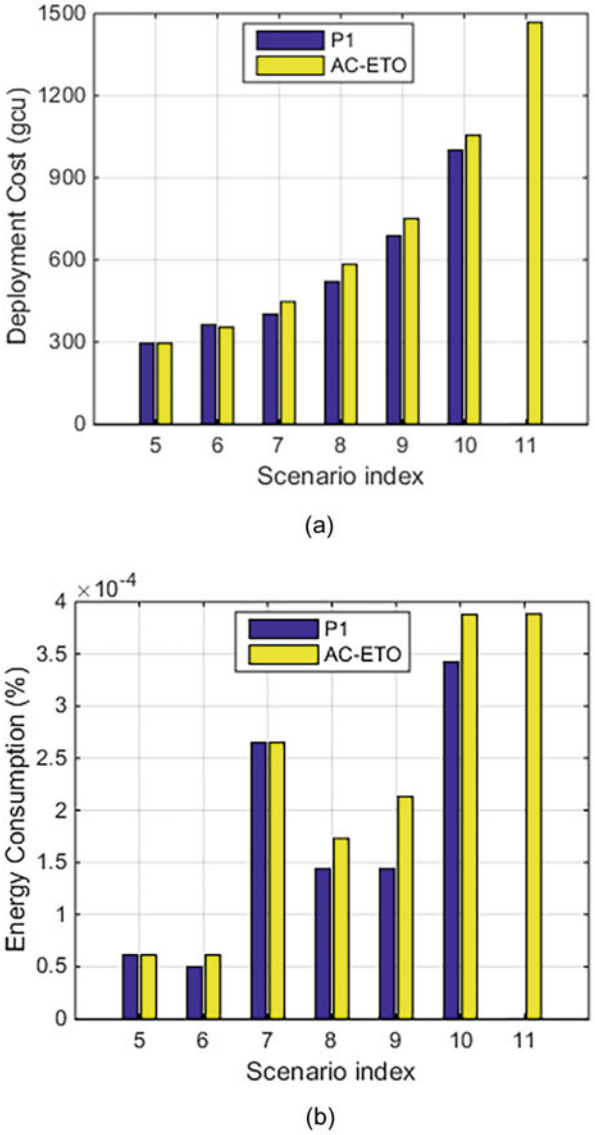

Fig. 2.7 Comparison of Gurobi and AC-ETO in terms of the deployment cost, the energy consumption, the network lifetime, and time complexity under various network scenarios. (**a**) Deployment cost. (**b**) Energy consumption. (**c**) Network lifetime. (**d**) Running time

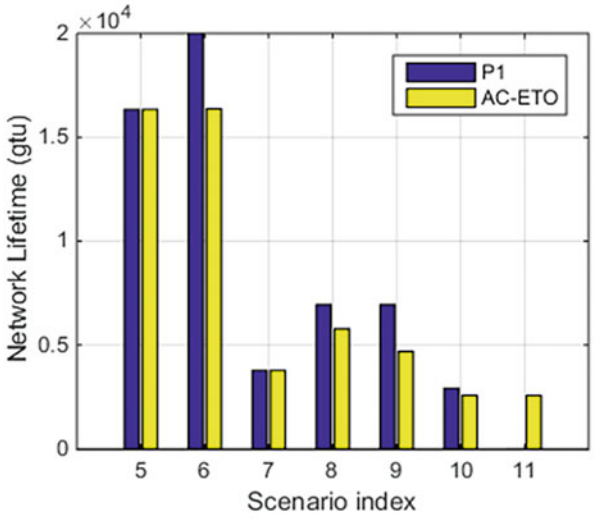

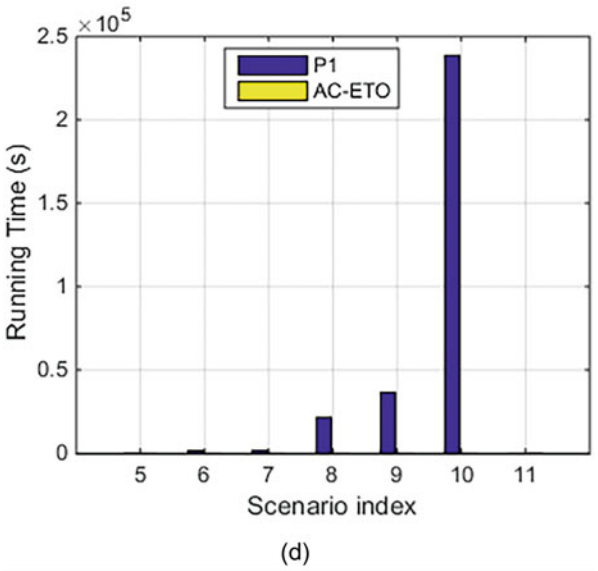

Fig. 2.7 (continued)

end for
for each path **do**
$V_{net} \leftarrow path$;
end for
Calculate the total cost C_{net} and the energy consumption E_{max};
Output: V_{net}, C_{net}, E_{max}

As shown in Fig. 2.8a, the deployment cost of AC-ETO is lower than that of the greedy algorithm. In Fig. 2.8b, it is found that the energy consumption of the greedy algorithm in different scenarios is higher than that of AC-ETO. Accordingly, the network lifetime of AC-ETO is longer than that of the greedy algorithm in

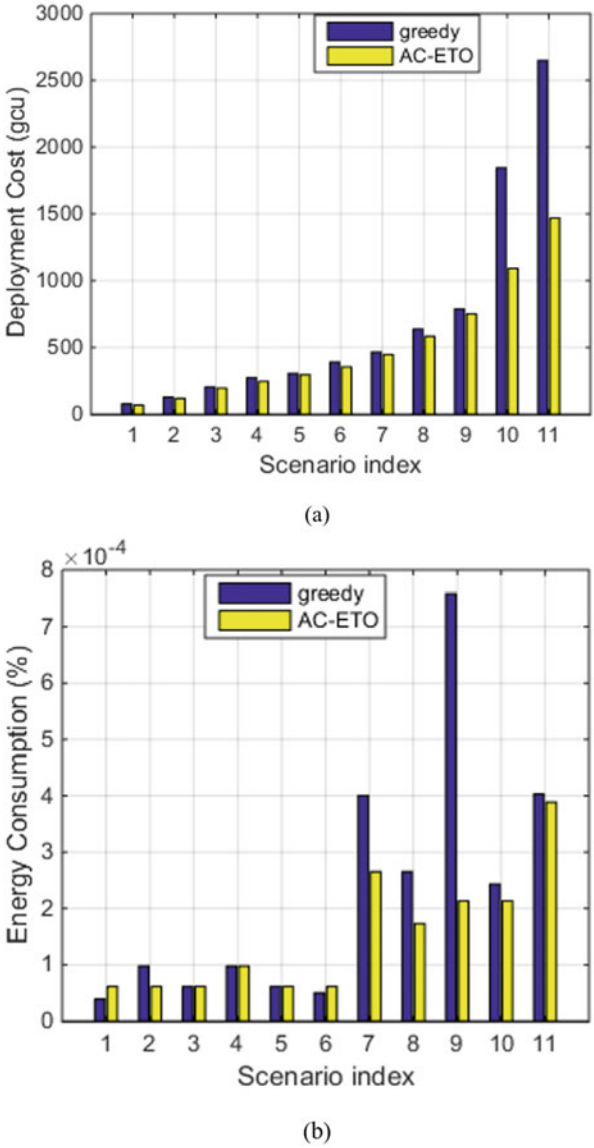

Fig. 2.8 Comparison of AC-ETO and a greedy algorithm in terms of the deployment cost, the energy consumption, the network lifetime, and time complexity under various network scenarios. (**a**) Deployment cost. (**b**) Energy consumption. (**c**) Network lifetime. (**d**) Running time

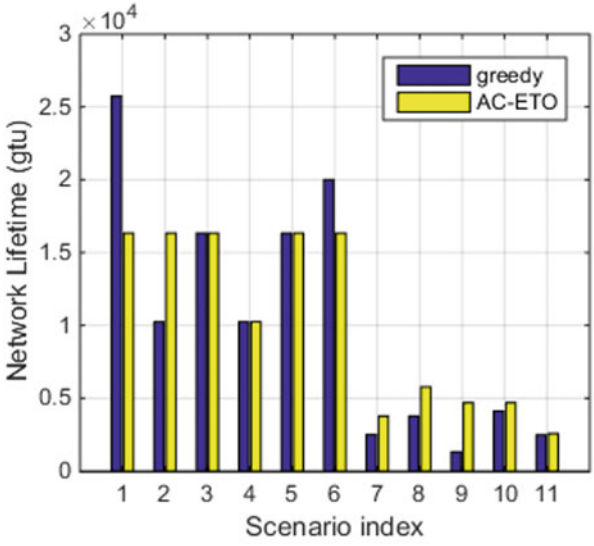

(c)

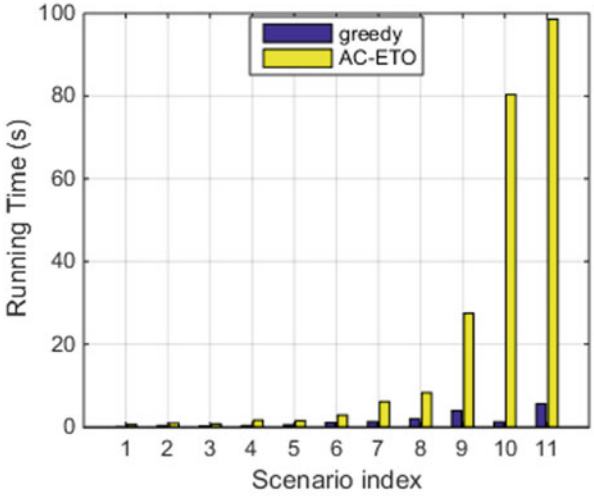

(d)

Fig. 2.8 (continued)

Fig. 2.8c. In the greedy algorithm, it is favorable to select a path with the minimum cost and accordingly the minimum energy consumption, which does not guarantee the cost and energy consumption of the overall network. While AC-ETO guides ants to find the optimal (approximate optimal) solution through two pheromones. Figure 2.8d shows that running time increases with the network size. For instance, in Scenario 7 the deployment cost obtained by AC-ETO is 447 gcu, while the

deployment cost obtained by greedy algorithm is 481 gcu, and the energy consumption obtained by AC-ETO is 5% less than that obtained by greedy algorithm. Thus, AC-ETO achieves better performance than that of the greedy algorithm in different scenarios, at the cost of increased but affordable time complexity.

Based on the above analysis, it is observed that the AC-ETO algorithm outperform greedy algorithm and approaches the optimal solutions in different scenarios, which may be difficult for Gurobi to solve.

2.6 Conclusion

In the chapter, we have investigated a multi-tier hierarchical network architecture with support of edge computing that includes the underwater acoustic sub-network, the sea-surface wireless sub-network, and the air wireless sub-network. Based on the network architecture, we have formulated an MO problem to minimize the total network deployment cost and maximize the network lifetime. To solve the MO problem, we have proposed an efficient algorithm, namely AC-ETO, and analyzed its time complexity. The proposed algorithm approaches the optimal solutions under different network scales with polynomial time. We will jointly study the network deployment of static ocean sensors and trajectory design of mobile ocean vehicles in our future work.

References

1. H. Jiang, J. Pan, K. Shao, T. Han, X. Guan, The state of the world ocean oil and gas resource exploration, China Pet. Ent. 2008,3,77-79.
2. F. Cui, S. Zhang, Ocean exploitation and environmental risk: an analysis of the Gulf of Mexico oil spill in USA. J. Ocean Univ. China (Soc. Sci. Ed.)2011, 5, 6-10.
3. M. Eichhorn, C. Ament, M. Jacob, T. Pfuetzenreuter, D. Karimanzira, K. Bley, M. Boer, H. Wehde, Modular AUV System with Integrated Real-Time Water Quality Analysis. Sensors 2018, 18, 1837.
4. G. Xu, W. Shen, X. Wang, Applications of Wireless Sensor Networks in Marine Environment Monitoring: A Survey. Sensors 2014, 14, 16932-16954.
5. G. Zappalà, G. Caruso, E. Crisafi, The "SAM" integrated system for coastal monitoring. Proc. of the 4th Int. Conf. On Environmental Problems in Coastal Regions, Coastal Environment IV, ed. C.A. Brebbia, WIT Press: Southampton, 2002, 341-350.
6. A. Abramic, N. M. Alzamora, D. R. Gonzalez, P. J. Ferrer, New methodology for analysing and increasing the cost-efficiency of environmental monitoring networks. Marine Pollution Bulletin 2014, 86, 161-173.
7. R. G. Thippa, P. R. M. Swarna, M. Parimala, L. C. Chiranji, K. R. M. Praveen, S. Hakak, W. Z. Khan, A deep neural networks based model for uninterrupted marine environment monitoring. Computer Communications 2020, 157, 64-75.
8. G. Zappalà, A software set for environment monitoring networks. Environ. Studies X 2004, 3-12.
9. C. Liu, Z. Zhao, W. Qu, T. Qiu, A. Sangaiah, A distributed node deployment algorithm for underwater wireless sensor networks based on virtual forces. J. Syst. Architect. 2019, 97, 9-19.

10. D. Pompili, T. Melodia, I. F. Akyildiz, Three-dimensional and two-dimensional deployment analysis for underwater acoustic sensor networks. Ad Hoc Netw. 2009, 7, 778-790.
11. H. Alhumyani, R. Ammar, A. Alharbi, S. Tolba, Efficient surface-level gateway deployment using underwater sensing and processing networks. In OCEANS 2015, Washington, Washington, DC, USA, 1-6.
12. Z. Zheng, L. X. Cai, R. Zhang, X. Shen, RNP-SA: Joint relay placement and sub-carrier allocation in wireless communication networks with sustainable energy. IEEE Trans. on Wireless Commun. 2012, 11, 3818-3828.
13. S. Ibrahim, J. Cui, R. Ammar, Efficient surface gateway deployment for underwater sensor networks. In Proc. ISCC 2008, Marrakech, MAR. 2008, 1177-1182. doi: https://doi.org/10.1109/ISCC.2008.4625609.
14. A. Khan, I. Ali, A. Ghani, N. Khan, M. Alsaqer, A. U. Rahman, Mahmood. H, Routing Protocols for Underwater Wireless Sensor Networks: Taxonomy, Research Challenges, Routing Strategies and Future Directions. Sensors 2018, 18, 1619.
15. I. F. Akyildiz, D. Pompili, T. Melodia, Underwater acoustic sensor networks: research challenges. Ad Hoc Netw. 2005, 3, 257-279.
16. L. Wei, Z. Wang, J. Liu, Z. Peng, J. H. Cui, Power efficient deployment planning for wireless oceanographic systems. IEEE Syst. J. 2016, 1-11.
17. X. Han, J. A. Thomasson, Y. Xiang, H. Gharakhani, P. K. Yadav, W. L. Rooney, Multifunctional Ground Control Points with a Wireless Network for Communication with a UAV. Sensors 2019, 19, 2852.
18. L. Arienzo, Green RF/FSO communications in cognitive relay-based space information networks for Maritime Surveillance. IEEE Trans. Cognitive Commun. and Netw. 2019, 5 1182-1193.
19. X. Song, Y. Gong, D. Jin, Q. Li, Nodes deployment optimization algorithm based on improved evidence theory of underwater wireless sensor networks. Photonic Netw. Commun. 2018, 37, 224-232.
20. P. Jiang, X. Wang, L. Jiang, Node deployment algorithm based on connected tree for underwater sensor networks. Sensors 2015, 15, 16763-16785.
21. N. Celandronietal, E. Ferroet, et al., A survey of architectures and scenarios in satellite based wireless sensor networks: System design aspects. Int. J. Satell. Comm. N. 2013, 31, 1-38.
22. D. Pompili, T. Melodia, I. F. Akyildiz, Deployment analysis in underwater acoustic wireless sensor networks. In Proc. WUWNet'06, Los Angeles, CA, USA, 48-55.
23. D. Martens, M. D. Backe, R. Haesen, J. Vanthienen, B. Baesens, Classification with ant colony optimization. IEEE Trans. Evol. Comput. 2007, 11, 651-665.
24. X. Liu, A deployment strategy for multiple types of requirements in wireless sensor networks. IEEE T. Cybern. 2015, 45, 2364-2376.
25. M. P. López, An ACOR-Based Multi-Objective WSN Deployment Example for Lunar Surveying. Sensors 2016, 16, 209.
26. K. Watcharasitthiwat, P. Wardkein, Reliability optimization of topology communication network design using an improved ant colony optimization. Comput. Electr. Eng. 2009, 35, 730-747.
27. B. Dengiz, F. Altiparmak, O. Belgin, Design of reliable communication networks: A hybrid ant colony optimization algorithm. IIE Transactions 2010, 42, 273-287.
28. J. A. Ren, Y. Q. Tu, Implementation of Ad Hoc Network Routing Protocol Based on Ant Colony Optimization. Comp. Eng. 2012, 38, 114-118,122.
29. N. Kumar, G. D. C. Suresh, ACO-EEOLSR: enhanced energy model based link stability routing protocol in mobile ad hoc networks. J. Chin. Inst. Eng. 2016, 39, 192-200.
30. D. S. Deif, Y. Gadallah, An ant colony optimization approach for the deployment of reliable wireless sensor networks. IEEE Access 2017, 5, 10744-10756.
31. X. Shen, Y. Wang, S. Yang, Y. Liang, H. Li, Development of underwater gliders: an overview and prospect. J. Unmanned Undersea Syst. 2018, 26, 89-106.
32. T. Liu, Y. Xu, Y. Yin, Zh. Hu, X. Zhu, D. Li, Zh. Jiang, Long-term fixed-point vertical-section observation-type underwater robot. CN105644742A. 2016.

33. J. Gu, Zh. Zhang, Ch. Wang, L. Gao, B. Li, Influence of ocean current on motion parameters of underwater glider. J. Naval Univ. Eng. 2018, 30, 1-7.
34. D. Li, W. Chen, R. Huo, D. Liu, Survey on energy efficiency in wireless sensor networks. Comput. Sci. 2008, 35, 8-12. % er Science,} vol.35, no.11, pp.8-12,2008.
35. L. Berkhovskikh, Y. Lysanov, Fundamentals of ocean acoustics. Springer, 1982.
36. W.R. Heinzelman, A. Chandrakasan, Balakrishnan. H, Energy-efficient communication protocol for wireless sensor networks. In Proc. HICSS 2000, IEEE, 4-7.
37. M. Ritesh, L. Sanjay, Distributed algorithms for maximum lifetime routing in wireless sensor networks. IEEE Trans. Wireless commun. 2006, 5, 2185-2193.
38. X. Hou, B. Lin, R. X. He, X. Wang, Infrastructure planning and topology optimization for reliable mobile big data transmission under cloud radio access networks. Eurasip J. Wirel. Comm. 2016, 1, 119-129.
39. H. Duan, D. Wang, J. Zhu, X. Huang, Development on ant colony algorithm theory and its application. Control Decis. 2004, 19, 1321-1320.
40. Y.R. Zhou, Runtime analysis of an ant colony optimization algorithm for TSP instances. IEEE Trans. Evol. Comput. 2009, 13, 1083-1092.
41. Gurobi Optimizer 4.6, Gurobi Optimization Inc., Beaverton, Oregon, USA, 2012.

Chapter 3
Autoencoder with Channel Estimation for Marine Communications

Due to the special characteristics of the underwater environment such as pressure and temperature, many wireless communication technologies that can be implemented in a terrestrial environment cannot be implemented well in underwater environments. Therefore, it is very important to study the new generation of MWCNs. To solve the challenges mentioned in Sect. 1.2.2, this chapter proposes a novel Orthogonal Frequency Division Multiplexing (OFDM) autoencoder featuring CNN-based channel estimation for marine communications with complex and fast-changing environments. We demonstrate that the proposed OFDM autoencoder system can be generalized to work under various channel environments, different throughputs, while outperform the traditional OFDM counterparts, especially when working at high throughputs. In addition, since OFDM systems require accurate channel estimations to function properly, this chapter also proposes a new channel estimation algorithm for OFDM systems that combine the power of deep learning with the philosophy of super-resolution reconstruction, which uses Dense convolutional neural Networks (Dense-Net) to reconstruct low-resolution pilot information images into high-resolution full Channel Impulse Responses (CIRs). The Dense-Net structure has the characteristics of dense connections and feature multiplexing. Simulation results show that under slow fading, the proposed channel estimator can estimate the CIRs perfectly. Under fast fading, the proposed channel estimator outperforms existing learning-based algorithms with fewer neural network parameters. Therefore, the proposed novel autoencoder scheme and the powerful channel estimator are potentially attractive approaches for MWCNs.

This chapter is organized as follows: We present a brief research background in Sect.3.1. The related works about typical OFDM communication systems in Sect. 3.2. The proposed OFDM autoencoder is described in Sect.3.3. The simulation results are presented in Sect.3.4. Finally, we close the chapter with conclusions in Sect. 3.5.

B. Lin et al., *Next Generation Marine Wireless Communication Networks*, Wireless Networks, https://doi.org/10.1007/978-3-030-97307-0_3

3.1 Background

Emerging Internet of Vessels (IoV) [1] is expected to play an important role in the realm of the next generation marine wireless communication networks. Specifically, Maritime Autonomous Surface Ship (MASS) is widely recognized as the development trend of future shipping industry. IoV invokes a large amount of information exchange among vessels and land-shore facilities, such as position, speed, and route. As a result, IoV has the ability to realize the refinement of shipping management, the comprehensiveness of industry services, and the humanization of user experiences by providing an intelligent and safer navigating environment [1, 2]. Thus, high throughputs and reliability are essential for IoV communications and networking, which can employ Orthogonal Frequency Division Multiplexing (OFDM) techniques [3, 4] as the information-bearing signaling. Furthermore, marine wireless communication systems are required to accommodate complex and fast-changing channel environments, as compared with their terrestrial counterparts. In the first chapter of this book, the maritime channel challenge part is introduced, and the analysis is focused on underwater communication, on the sea-surface communication and the maritime satellite communication. In order to realize intelligent communication at maritime, this chapter combines the idea of Deep Learning (DL) to solve the problem of maritime communication.

Therefore, the effort of introducing DL into the field of wireless communications [5, 6] grows significantly with the breakthrough of DL in image processing, speech recognition, natural language processing, etc. The resultant DL-based wireless transceivers have already demonstrated promising system performance and provided inspirations in many aspects of communication system designs. In particular, the pioneering work of [7, 8] proposed a communication system based on the concept of autoencoder optimized through end-to-end learning. In contrast to conventional communications systems, this single-carrier autoencoder architecture employs neural networks to jointly optimize the transmitter and receiver, conditioned on the surrounding channel environments. Since then, researchers around the globe have relentlessly pushed the boundary of deep learning into higher OSI layers, such as hatching the idea of deep learning in resource allocation [9, 10], routing [11], and multiple access protocols [12].

As for multi-carrier modulations, OFDM technologies are often used to combat the effect of frequency-selective fading, since it can transform a frequency-selective fading channel into parallel flat-fading subchannels [13]. Naturally, the challenge of fusing DL with OFDM motives researchers to design innovative frameworks for Internet of Vessels, where an increasing number of vessels are required to be connected. Among them, [14], [15], and [16] used Full Connected (FC) neural network layers to implement an OFDM system based on autoencoder structures. However, FC layers require a large amount of network parameters, and the vanish of gradients during training becomes problematic, when building deep neural networks.

Conversely, OFDM systems demand high accuracy channel estimations in order to recover information correctly, where pilot-based channel estimation algorithms

such as Least Squares (LS) and Linear Minimum Mean Square Error (LMMSE) algorithms are often used [17]. More explicitly, [18] implemented a channel estimation module based on LS algorithm using Deep Complex Convolutional Networks, whereas authors in [19] proposed an OFDM channel estimation module using FC neural networks. [20] proposed a model approach that combined DL with the expert knowledge to replace the existing channel estimation module. In addition, the channel estimation problem can also be formulated as the issue of super-resolution reconstruction in the field of image processing [21]. The pilot data across the time and frequency domain are treated as a low-resolution image and the full channel responses that need to be estimated are considered to be the corresponding high-resolution image [22], where vanilla Convolutional Neural Networks (CNNs) were used. However, this shallow CNNs structure prevented the channel estimation algorithm to achieve higher accuracy.

A novel autoencoder based OFDM system using CNNs layers to facilitate end-to-end learning designed for IoV is proposed. Compared with FC layers, our CNN-based systems can learn intricate signal representations with fast convergence during training while using fewer network parameters. Moreover, Long Short-Term Memory (LSTM) network layers [23] are also used to exploit the dependency of time sequence, so that the channel coding gain becomes achievable. Furthermore, in order to handle complex marine communication environments, we propose a novel channel estimation algorithm for OFDM systems combining the power of DL with super-resolution reconstruction, where the low-resolution pilot information image is reconstructed into a full channel response high-resolution image using Dense-Net [24]. The Dense-Net structure allows us to effectively solve the vanishing gradient problem caused by the excessive network layers of typical CNN networks. In addition, Dense-Net has fewer network parameters than the Residual Network (Res-Net) [25] architecture. We will demonstrate that the proposed algorithm's channel estimation performance is better than the state-of-the-art DL-based algorithm [18]. Apart from the performance gain, the proposed algorithm has a deeper network structure to learn high-level features with fewer total parameters than that of [18]. Our main contributions in this chapter can be summarized as follows:

- The carefully designed CNN layers allow the learned OFDM autoencoder to have generalization capability while achieving optimal Block Error Rate (BLER) performance, namely support flexible data rates, suitable for AWGN and Rayleigh as well as non-AWGN channels.
- Furthermore, LSTM layers are introduced on top of CNN layers to achieve the channel coding gain, which is essential to combat hostile marine communication environments. Namely, the entire transmitted sequence is encoded using LSTM layers before transmission, while the LSTM layers at the receiver are responsible for extracting adequate correlated information for detection.
- To the best of our knowledge, this is the first study in the literature to propose a novel Dense-Net channel estimation scheme based on the idea of image super-resolution, which not only achieves state-of-the-art estimation accuracy, but also

solves conventional CNN's problem of gradient vanishing and excessive parameters through dense connections and feature multiplexing.
- The proposed OFDM autoencoder and the novel Dense-Net based channel estimator can be trained jointly with fast convergence, hence becomes an appealing solution to dynamic IoV communications.

3.2 Typical OFDM Communication Systems

In this section, a conventional OFDM communication system is briefly described, which is used as the bench-marker for the proposed DL-based OFDM autoencoder.

The block diagram of a conventional OFDM communication system is shown in Fig. 3.1. Firstly, the input bits are mapped to QAM constellation points, which consist of In-Phase and Quadrature components (IQ) in the constellation plane. Then, the IQ signals are mapped to N (equals to the number of subcarriers used to transmit data) sets of parallel data streams via Serial to Parallel (S/P) conversion. Later, pilot data is inserted in each frequency domain OFDM symbol. The insertion pattern of the pilot signals is chosen to be comb mode in order to combat the effect of fast fading [26], which is shown in Fig. 3.2. Hence, the resultant frequency domain OFDM symbols are converted to their time domain representations using Inverse Discrete Fourier Transform (IDFT) operations, followed by adding Cyclic Prefix (CP) to deal with Inter-Symbol Interference (ISI). The CP's length depends on the size of the multipath delay.

The multipath fading channel is modeled as:

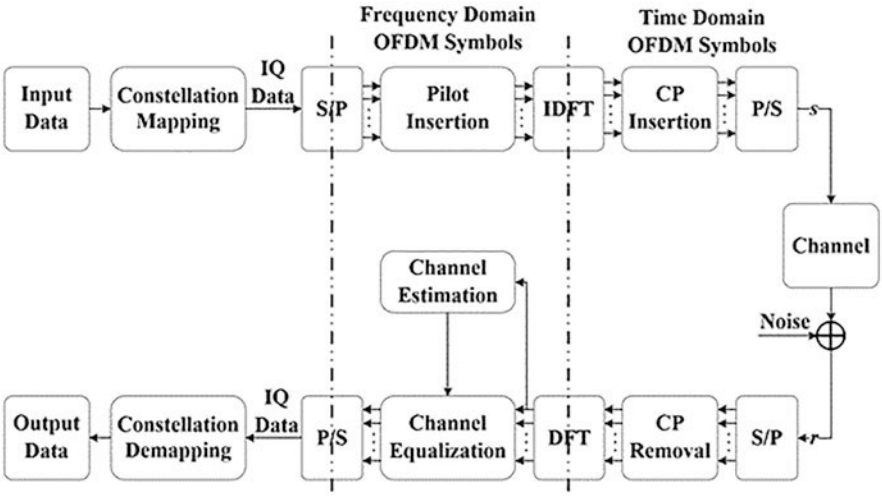

Fig. 3.1 The block diagram of a conventional OFDM communication system

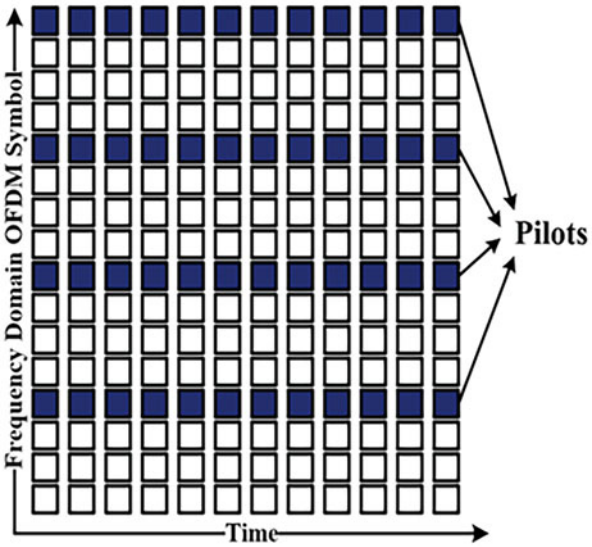

Fig. 3.2 The insertion of pilot data in a frequency domain OFDM symbol

$$r = s \otimes h + n \tag{3.1}$$

where vectors s and r represent the transmitted and received signals in the time domain, respectively. And n represents the white noise. h is the Channel Impulse Responses (CIRs) of the multipath channel and $\otimes$ denotes the convolution operation. Assuming that the channel response remains static within one OFDM symbol while changing between difference OFDM symbols, the tapped delay line model [27] of h is given by

$$h(\tau, t) = \sum\nolimits_{k=1}^{K} a_k(t)\delta(\tau - \tau_k) \tag{3.2}$$

where $a_k(t)$ is the gain of the signal on the kth path and τ_k is the delay of the kth path, K is the total number of paths.

At the receiver, after removing the CPs, the received time domain OFDM symbols r of Eq. (3.1) will be converted to its frequency domain representations via Discrete Fourier Transform (DFT) operations. Then, the channel estimation module of Fig. 3.1 estimates the full CIRs using the received pilot data, which assist the channel equalization module to equalize the received frequency domain symbols. Finally, the output signal is demodulated into binary data streams after the P/S operation.

3.3 Proposed OFDM Autoencoder

In this section, the design and training methods of the proposed OFDM autoencoder for IoV are introduced, where the system diagram is illustrated in Fig. 3.3. The purpose of the end-to-end structure is to find appropriate signal representations for the transmitter that can adapt to the surrounding marine channels, such that the receiver can recover the information with minimum error probability. More explicitly, two autoencoder structures are proposed. One uses CNN layers to facilitate the task of modulation, the other is designed using both CNN and LSTM layers to perform "joint" channel coding and modulation.

Besides, the problem of channel estimation is tackled using the idea from imagine super-resolution [28, 29], where pilot data are the low-resolution signals and neural networks are used to reconstruct full CIRs.

3.3.1 CNN-Based OFDM Autoencoder

The proposed OFDM autoencoder based on CNN is shown in Fig. 3.3. Firstly, a group of $N \times \log_2 m$ information bits are converted into one-hot matrix format $\boldsymbol{X} \in \mathbb{C}^{N \times m}$, which corresponds to N number of conventional m-array QAM symbols in conventional OFDM systems. The one-hot data format can assist the transmitter to

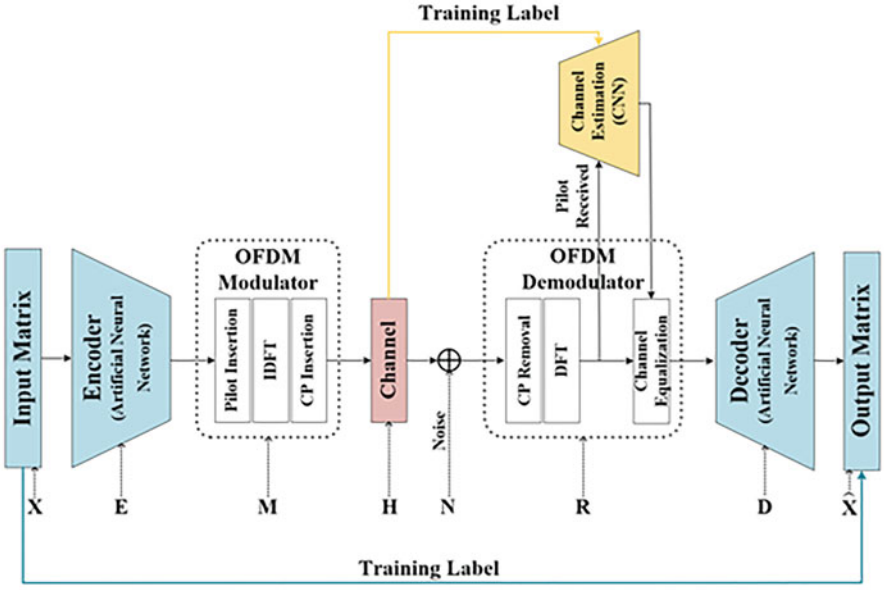

Fig. 3.3 The block diagram of the proposed OFDM autoencoder with a novel CNN-based channel estimator

converge to the optimal solution quickly. Then, the CNN-based autoencoder $\boldsymbol{E} \in \mathbb{C}^{m \times 2}$ transforms input matrix X into $\boldsymbol{XE} \in \mathbb{C}^{N \times 2}$, where the real and imaginary parts of the signal are represented as two real numbers. Furthermore, information signal $\boldsymbol{XE}$ is protected by adding P number of pilot signals and C number of CPs, before modulated to multiply carriers using IDFT operations, as seen in Fig. 3.3. This process is characterized using a matrix operation denoted as $\boldsymbol{M} \in \mathbb{C}^{S \times N}$, where $S = N + P + C$. Hence, the learned signal $\boldsymbol{MXE} \in \mathbb{C}^{S \times 2}$ propagates through the channel $\boldsymbol{H} \in \mathbb{C}^{S \times S}$ and $\boldsymbol{MXE}$ is corrupted by AWGN $\boldsymbol{N} \in \mathbb{C}^{S \times 2}$ before arriving at the receiver.

Next, the OFDM demodulator at the receiver of Fig. 3.3 performs an inverse matrix operation denoted as $\boldsymbol{R} \in \mathbb{C}^{N \times S}$ to the received signal, where CP removal, DFT calculations, and channel equalizations are processed. More importantly, a novel CNN-based channel estimator of Fig. 3.3 is used in order to accurately estimate the CIRs based on the pilot signals. Then, the CNN-based decoder transforms the received baseband signal into suitable representations using $\boldsymbol{D} \in \mathbb{C}^{2 \times m}$ of Fig. 3.3, so that the recovery of data $\widehat{\boldsymbol{X}} \in \mathbb{C}^{N \times m}$ using supervised learning becomes feasible.

Finally, the whole OFDM autoencoder of Fig. 3.3 can be expressed using matrix operations as:

$$\widehat{X} = (R(H(MXE) + N))D \tag{3.3}$$

Unlike traditional OFDM communication systems of Fig. 3.1 that are designed block by block, the proposed end-to-end learning architecture can globally find the optimal solution for the OFDM signaling representation and detection in the overparametrized neural network space while subject to challenging channel conditions.

Compared to FC neural networks, the employed convolutional layers of Fig. 3.3 can significantly reduce the number of trained parameters through weights sharing. From the communication perspective, this means the information are processed locally or in block manner. In addition, the convolutional layers are capable of mapping bit streams to higher dimensions by increasing the number of kernels. The detailed parameters of CNN layers used in Fig. 3.3 are shown in Table 3.1. More explicitly, one-dimensional convolutional (Conv-1D) layers are used for both encoding and decoding, where B in the first dimension of the output shape is the mini-batch size, and the second output dimension N in Table 3.1 is the number of OFDM symbols, and the last dimension is the number of kernels.

Note that since the kernel size of all the Conv-1D layers of Table 3.1 is set to one, hence, each information vector is processed individually rather than jointly, which means that there is no correlation between the information vectors. In the language of traditional communications, the proposed autoencoder of Table 3.1 replaces traditional QAM modulation/demodulation using Conv-1D layers, which enable the autoencoder system to search for the optimal modulation solution in an over-parameterized space for different channel conditions.

Table 3.1 The Proposed CNN-based autoencoder

Layer name	Type	Output shape
Input	One-hot vector	(B, N, m)
Encoder1	Conv1D, kernel size: 1	(B, N, 256)
Encoder2	Conv1D, kernel size: 1	(B, N, 256)
Encoder3	Conv1D, kernel size: 1	(B, N, 2)
Modulator	Non-trainable	(B, $N + P + C$, 2)
Channel	Non-trainable	(B, $N + P + C$, 2)
Demodulator	Non-trainable	(B, $N + P$, 2)
Equalization	Non-trainable	(B, N, 2)
Decoder1	Conv1D, kernel size: 1	(B, N, 256)
Decoder2	Conv1D, kernel size: 1	(B, N, 256)
Output	Conv1D, activation: softmax	(B, N, m)

Table 3.2 The Proposed Coded CNN-based autoencoder using LSTM

Layer name	Type	Output shape
Input	One-hot vector	(B, N*e, m)
Encoder1	Conv-1D, kernel size: 1	(B, N*e, 32)
Encoder2	Conv-1D, kernel size: 3	(B, N*e, 32)
Encoder3	Conv-1D, kernel size: 1	(B, N*e, 32)
Encoder4	LSTM, units: 128	(B, N*e, 128)
Encoder5	Time distributed	(B, N*e, 2/e)
Reshape I	Reshape	(B, N, 2)
Modulator	Non-trainable	(B, $N + P + C$, 2)
Channel	Non-trainable	(B, $N + P + C$, 2)
Demodulator	Non-trainable	(B, $N + P$, 2)
Equalization	Non-trainable	(B, N, 2)
Reshape II	Reshape	(B, N*e, 2/e)
Decoder1	LSTM, units: 64	(B, N*e, 64)
Decoder2	LSTM, units: 32	(B, N*e, 32)
Decoder3	Conv-1D, kernel size: 1	(B, N*e, 32)
Decoder4	Conv-1D, kernel size: 3	(B, N*e, 32)
Output	Time distributed	(B, N*e, m)

3.3.2 Coded CNN-Based OFDM Autoencoder Using LSTM

Furthermore, it is well known that channel coding can improve the system's performance by correlating the information bits to adjacent bits using Convolutional Codes (CC), turbo codes, etc. In this section, we propose an OFDM autoencoder empowered by LSTM layers, so that the architecture has the capacity of achieving channel coding gain, where the specific neural network structure is given in Table 3.2 and illustrated in Fig. 3.4.

At the transmitter side, three Conv-1D layers are employed to facilitate signal transformation; however, the second Conv-1D layer's kernel size is set to 3 to

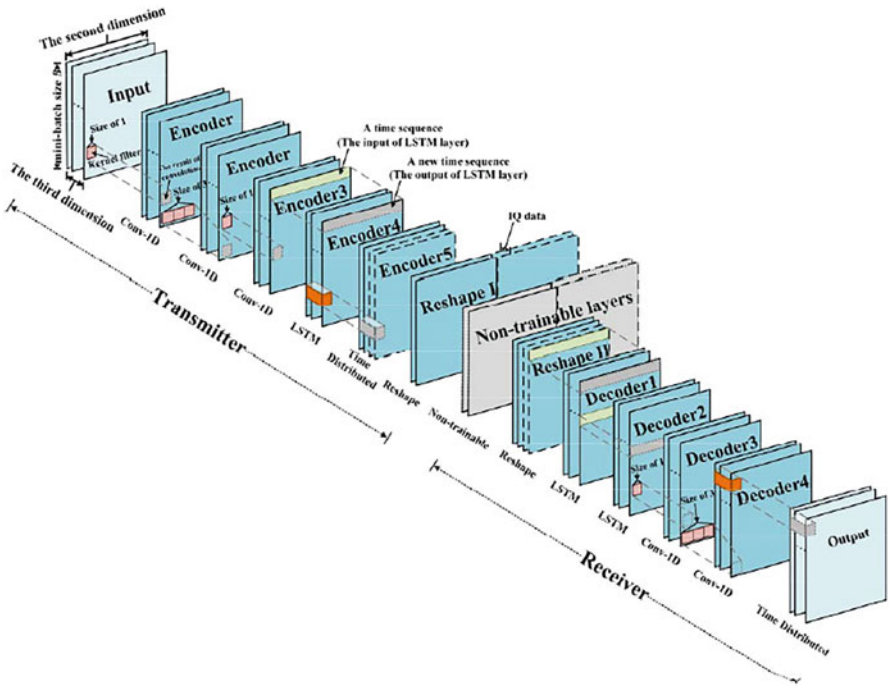

Fig. 3.4 Illustration of the proposed coded CNN-based autoencoder using LSTM, as listed in Table 3.2

correlate the information symbols, as seen in Table 3.2. Later, an LSTM layer having 128 units is added after the Conv-1D layers in order to further spread information vector to adjacent transmit sequence, so that having CC like channel coding becomes possible. More specifically, the output data sequence of the last Conv-1D layer is feed into the LSTM cell to recurrently encode current information to all the past time-steps through LSTM's input, output, and forget gates. In addition, 128 units are used to ensure that adequate features are encoded into the whole sequence. In other words, it is the CNN layers together with the additional LSTM layer jointly carry out the task of modulation and channel coding for the autoencoder system. In addition, Time Distributed and Reshape layers of Table 3.2 are used to conform the transmit signals to the appropriate OFDM frame structure.

At the receiver, compared with the pure CNN-based autoencoder of Table 3.1, two LSTM layers are added to extract the correlated information from the received sequence, followed by two Conv-1D layers, so that the channel decoding and demodulation are carried out jointly. Finally, the Time Distributed layer is used to reconstruct the extracted features at each time step into one-hot vector to complete the task of data recovery.

Unlike the traditional communication system, where channel coding and modulation are optimized separately, the proposed coded CNN-based OFDM autoencoder

using LSTM of Table 3.2 uses a stack of Conv-1D and LSTM layers to encode and correlate the data jointly. Furthermore, Conv-1D layers have limited correlation capability of time sequence, since the kernel size is small. Conversely, increasing the kernel size makes the neural network difficult to converge. Therefore, the additional LSTM layers are necessary to complement the Conv-1D layers in terms of correlating long-time sequence signals, given that the LSTM layer has broader data receptive and processing field than Conv-1D layers.

Besides, the autoencoder system's code rate e can be controlled by changing the number of input bits, that is, each group of $(N * e) \times \log_2 m$ m information bits is converted into a one-hot matrix as the input.

3.3.3 CNN-Based Channel Estimation

We also propose a novel CNN-based channel estimator for dynamic marine channel environments as shown in Fig. 3.3, where the specific network structure is given in Table 3.3 and illustrated in Fig. 3.5. The received pilot signals are served as the input of the channel estimator. Then, the data are reshaped through the reshape layer of Table 3.3, based on which the following two-dimensional convolutional (Conv-2D) layers can infer full CIRs. The pilot data is further up-sampled using a FC layer; therefore, the pilot signals' dimension is expanded to $2(N + P)$. Furthermore, 12 consecutive Conv-2D layers together with the shortcuts of the learned features of the previous layers are used, namely the concatenation layers in Table 3.3. This

Table 3.3 The proposed Dense-Net channel estimation in Fig. 3.3

Layer name	Type	Output Shape
Input	Received Pilot signals	$(B, P, 2)$
Reshape1	Reshape	$(B, 2P, 1)$
Up-Sampling	FC, activation: linear	$(B, 2(N + P), 1)$
DN1	Conv-2D, 1×1, activation: elu	$(B, 2(N + P), 8)$
Concat1	Concat [DN1, Up-Sampling]	$(B, 2(N + P), 9)$
DN2	Conv-2D, 3×3, activation: elu	$(B, 2(N + P), 8)$
Concat2	Concat [DN2, Concat1]	$(B, 2(N + P), 17)$
DN3	Conv-2D, 1×1, activation: elu	$(B, 2(N + P), 8)$
⋮	⋮	⋮
DN11	Conv-2D, 1×1, activation: elu	$(B, 2(N + P), 8)$
Concat11	Concat [DN11, Concat10]	$(B, 2(N + P), 89)$
DN12	Conv-2D, 3×3, activation: linear	$(B, 2(N + P), 1)$
Reshape2	Reshape	$(B, N + P, 2)$
Denoise1	Lambda (IDFT)	$(B, N + P, 2)$
Denoise2	Lambda (Zero-Setting)	$(B, N + P, 2)$
Output	Lambda (DFT)	$(B, N + P, 2)$

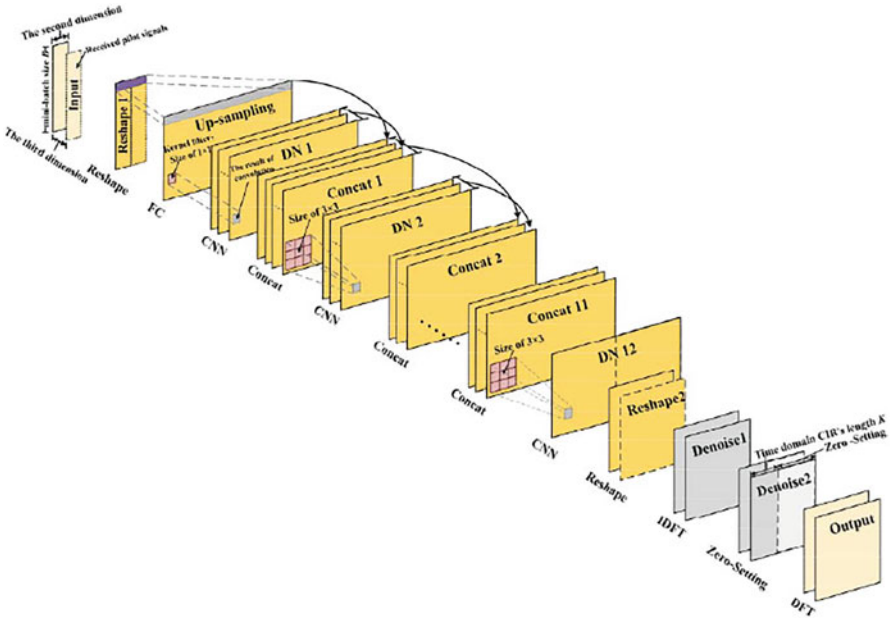

Fig. 3.5 Illustration of the proposed Dense-Net channel estimation network, as listed in Table.3.3

Dense-Net type structure allows the proposed channel estimator to accurately reconstruct the full channel frequency responses from the Up-Sampled pilot data.

Furthermore, the effect of pilot signal's AWGN is minimized by three specially designed denoising layers in Table 3.3. More specifically, Denoise1 layer of Table 3.3 converts the estimated frequency channel response to time domain CIRs through IDFT. Then, the last $(N + P)$-K samples are set to zero, since the full CIR's length is restricted to K. Finally, time domain CIRs are converted back to frequency domain through DFT, which will be used in the channel equalizer.

The design philosophy of the proposed CNN-based channel estimator originates from image super-resolution in image processing. That is, treating the pilot data having a size of $B \times 2P$ as a low-resolution two-dimensional image, and the full channel frequency response as the corresponding high-resolution image having a size of $B \times 2(N + P)$. Then, we innovatively design a Dense-Net network structure to facilitate the super-resolution process, where the input of each Conv-2D layer is the concatenation of all the previous layers, which means the features learned by each layer are directly passed to all the latter layers. In contrast, shallow CNN networks are unable to deliver the precision of the estimation required by the CE module, even though they are adequate for the autoencoder itself. In other words, the channel perturbation is more complex to learn than the encoding/decoding of the information sequence, hence deeper and powerful Dense-Net architecture is necessary. Additionally, the proposed Dense-Net CE has the ability of fast convergence, owing to inherited shortcut connections. This structure allows the channel estimator to piece

together all the learned features to solve the "puzzle." Also, through feature multiplexing, the parameters required by the Dense-Net are greatly reduced. For example, only 8 filters using kernel of size 1×1 or 3×3 are used in each Conv-2D layer in the DN layers of Table 3.3. In addition, the dense connections alleviate the vanishing gradient phenomenon usually seen during the training of deep CNN networks.

3.3.4 Model Training

For the proposed CNN-based OFDM autoencoder system and the coded CNN-based OFDM autoencoder system using LSTM of Fig. 3.3, random one-hot data are generated as training data. And cross entropy of Eq. (3.4) is used as the loss function, which is given by

$$L_{\text{Cross-Entropy}} = -\sum_{i=1}^{U}\sum_{j=1}^{g} y_{ij} \log x_{ij} \tag{3.4}$$

where x and y are training and label datasets and g is the number of categories, U is the number of samples.

The training data of the CNN-based channel estimation of Fig. 3.3 is obtained after the pilot signals propagate through multipath fading channels, and the perfect CIRs are used as the label data. Besides, Mean Square Error (MSE) is used as the loss function:

$$L_{\text{MSE}} = \frac{1}{U}\sum\nolimits_{i=1}^{U}(y_i - x_i)^2 \tag{3.5}$$

The *elu* and linear activation functions are used in Tables 3.1, 3.2, and 3.3 to perform nonlinear and linear transformations, respectively, and the SoftMax activation function is used at the decoder. We found that *elu* activation is more suitable to solve the problem of vanishing gradient and cell "dying" for the proposed autoencoder and CE networks, compared with *tanh*, *relu,* and other commonly used activation functions. We also find that using early stopping and dropout mechanism with a rate of 0.05 are useful to prevent overfitting. ADAM optimizer [30] is used to optimize the back-propagation process and to control the step and direction of the gradient during training. In order to speed up the training process and facilitate neural network convergence, the initial learning rate is set to be 0.01 and the learning rate will be reduced by a factor of ten, whenever the loss function of Eqs. (3.4) or (3.5) is saturated for 5 consecutive epochs. In addition, the Mini-batch Gradient Descent algorithm is used to speed up the training process, which is set to $B = 64$.

Besides, the training E_b/N_0 is also an important factor to converge to optimal solutions. When training at low E_b/N_0, neural networks have difficulty to learn intricate data structure because of high noise power. Conversely, if the training E_b/N_0 is too high, neural networks lose the generalization ability to cope with noise contaminated data. In this paper, the CNN-based OFDM system of Table 3.1 was trained in the range of 4 to 10 dB, the coded CNN-based OFDM autoencoder system using LSTM of Table 3.2 was trained in the range of 10 to 20 dB which higher than un-coded system, while the CNN-based channel estimator of Table 3.3 was trained at 20 dB.

3.4 Simulation Results

After the detailed OFDM parameters are given in Table 3.4, the BLER performance of the proposed CNN-based OFDM autoencoder under AWGN and multipath fading channels is provided, when the receiver has perfect CIRs. The CNN-based OFDM autoencoder of Fig. 3.3 is benchmarked by the conventional OFDM systems of Fig. 3.1 having corresponding m-array QAM modulations. The performance of the coded autoencoder using LSTM is compared with the traditional half-rate convolutional coded OFDM system. Furthermore, the OFDM autoencoder's BLER performance using the proposed Channel Estimator (CE) of Table 3.3 is also provided under slow or fast fading channels. Our source codes are implemented in Keras and will be available on GitHub upon publication.

For the marine communication channel, since the relatively low onboard antenna's height on a vessel and local scatters around the user introduce multiple paths in wireless channels [31], multipath Rayleigh fading models are used with flat fading or having a Doppler frequency of 8.73 Hz for fast fading [32], which corresponds to the maximum relative speed between ships of 60 km/h. We will show that, firstly, the OFDM autoencoders of Tables 3.1 and 3.2 can adapt to marine channel

Table 3.4 OFDM parameters of the proposed OFDM autoencoder

Carrier frequency	157.2 MHz (International VHF Marine Radio Channel 24)
DFT Size	64
Pilots per OFDM symbol	8
Number of used subcarriers	56
CP duration	0.1 ms
Data symbol duration	0.4 ms
Total symbol duration	0.5 ms
Pilot pattern	Comb of Fig. 3.2
Pilot value	$1 + 1i$
Channel model	AWGN, multipath fading
Channel coherence	Taps updated per OFDM symbol
Doppler frequency	Flat or 8.73 Hz

environments through learning, secondly, the proposed CE scheme is capable of outperforming existing deep learning-based channel estimations [18] for marine channels.

3.4.1 AWGN and Fading Channels

Figure 3.6 demonstrates the BLER performance of the CNN-based OFDM autoencoder of Fig. 3.3 under AWGN channels. In the case of $m = 2$ and 4, the proposed CNN-based OFDM system achieves nearly identical BLER performance compared with conventional expert OFDM systems of Fig. 3.1 having the same throughput, when using BPSK and QPSK. However, when the system throughput increases as $m = 16$ and 64, the CNN-based OFDM achieves slightly better BLER performance than that of the expert OFDM systems using 16-QAM and 64-QAM. That is because the CNN structure can optimize the data symbols jointly in higher dimensions. In addition, the CNN operations inheritably enable hamming-type block coding to the information bits [7], which becomes more transparent when the increase of m.

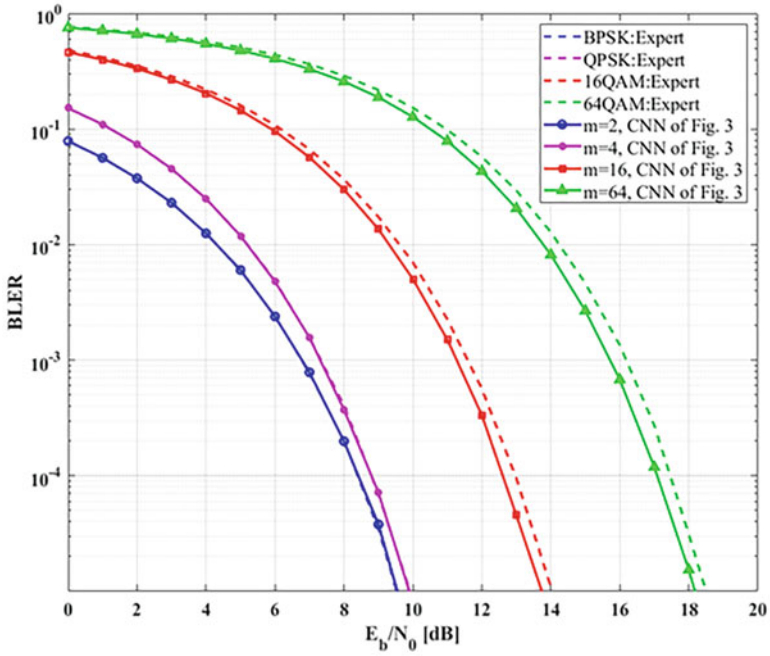

Fig. 3.6 The BLER performance of the proposed CNN-based OFDM autoencoder under AWGN channels, when compared with corresponding expert OFDM systems

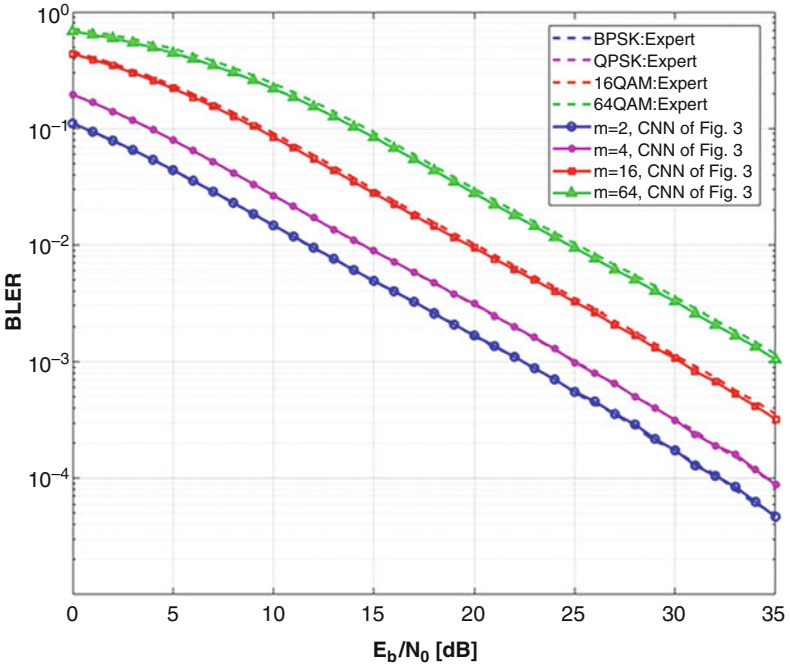

Fig. 3.7 The BLER performance of the CNN-based OFDM autoencoder of Fig. 3.3 under multipath Rayleigh fading channels of Doppler frequency 8.73 Hz, when having perfect CIRs and compared with corresponding expert OFDM systems

Figure 3.7 shows the BLER performance of the CNN-based OFDM autoencoder of Fig. 3.3 under multipath Rayleigh fading channels of Doppler frequency 8.73 Hz, when having perfect CIRs. Again, we observe that for $m = 2$ and 4, the BLER performance of the CNN-based OFDM is in agreement with the baseline systems. At $m = 16$ and 64, the CNN system's BLER performance is slightly better than their conventional counterparts. This phenomenon indicates that the CNN-based autoencoder architecture can converge quickly subject to not only simple AWGN conditions, but also to more dynamic multipath fading environments. In other words, CNNs are flexible enough to learn useful signal representations under different channel variations at the transmitter while distinguishing different symbols at the receiver after channel impairment.

In order to further illustrate on CNN structure's quick convergence, Figs. 3.8 and 3.9 plot the training loss and validation loss of the proposed CNN-based OFDM autoencoder under AWGN and multipath fading channels with Doppler frequency of 8.73 Hz. CNN's learning process is further complicated by setting $m = 64$. However, despite high data rate and dynamic channel environments, we observe in Figs. 3.8 and 3.9 that the convergence happens around training over 25 and 50 epochs. Observe that the autoencoder working under fading channels of Fig. 3.9 converges slower than under AWGN channels of Fig. 3.8. That is because the fading channels

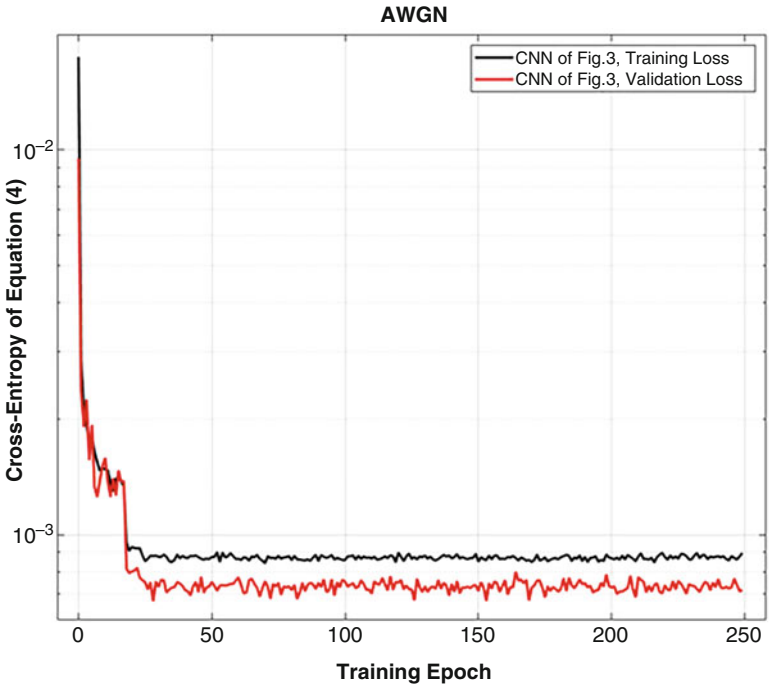

Fig. 3.8 Training loss and validation loss of the CNN-based OFDM autoencoder of Fig. 3.3 under AWGN channels with $m = 64$

are more complicated than the AWGN channels, the proposed autoencoder requires more data to gain comprehensive knowledge of the surrounding environments. Besides, the training loss and validation loss match quite well, which means the issue of overfitting can be alleviated by proper design of the CNN model.

Figure 3.10 shows the BLER performance of the coded CNN-based OFDM autoencoder using LSTM of Table 3.2 under AWGN channels. In the case of $m = 16$ and $m = 64$, it can be clearly seen that the BLER performance of coded OFDM autoencoder having a rate of $e = 1/2$ is greatly improved over the un-coded OFDM autoencoder of Table 3.1 having a rate of $e = 1$. This means the proposed LSTM-aided model can achieve the coding gain. Even better, when compared with the corresponding expert OFDM system using CC of $e = 1/2$, the proposed half-rate coded OFDM autoencoder archives a better BLER performance in the whole range of E_b/N_0. This is because the proposed combination of CNN and LSTM layers can better exploit and extract the features of the entire transmission sequence than the individually designed convolutional coded expert systems. That is, the autoencoder carries out the search for optimal transmission sequence in a much larger over-parameterized space, compared with the traditional hand-crafted constellation points. Also, the constraint length of a CC is limited to 7, whereas the LSTM layer can correlate current input information to the whole vector having a length of $N*e$,

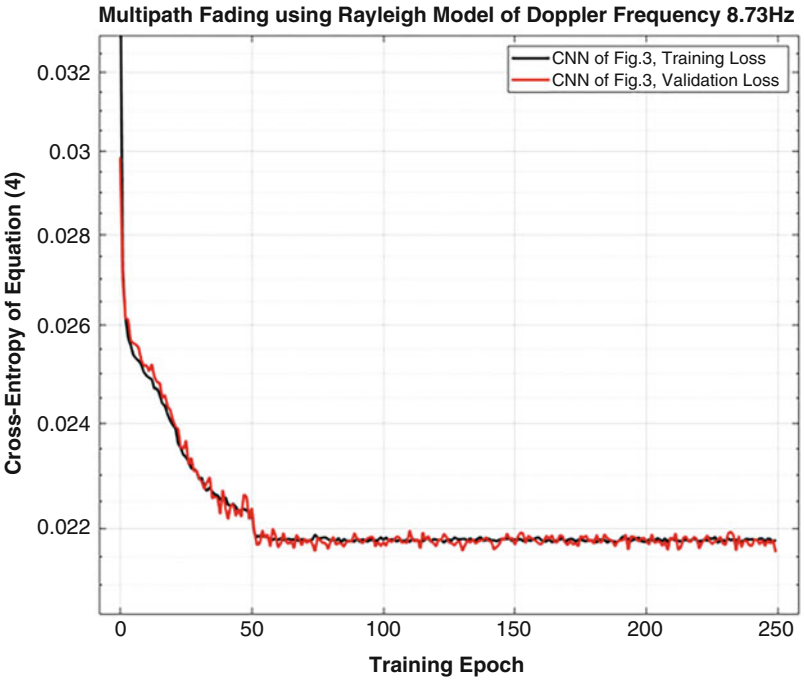

Fig. 3.9 Training loss and validation loss of the CNN-based OFDM autoencoder of Fig. 3.3 with $m = 64$ under multipath Rayleigh fading channels with Doppler frequency of 8.73 Hz

which also assists the LSTM layer at the receiver to observe and extract information from the entire received signals. So, the LSTM layers at the transmitter are able to correlate each information vector much further in a transmission sequence than a simple CC, and the LSTM layers at the receiver can exact more information than a Viterbi decoder.

Then, Fig. 3.11 shows the BLER performance of three half-rate ($e = 1/2$) systems under AWGN channels, which are the proposed CNN-based OFDM autoencoder of Table 3.1, the coded CNN-based OFDM autoencoder of Table 3.2 and the corresponding CC-coded expert OFDM system. It can be clearly seen that the coded OFDM autoencoder outperforms both its expert OFDM counterpart and the un-coded OFDM autoencoder significantly, which exemplifies LSTM's ability of properly encoding and decoding information across a total number of one-thousand time-steps through learning [23], whereas the CC has a limited constraint length of 7. Conversely, we also note that the un-coded CNN-based OFDM autoencoder beats the BLER performance of CC-coded expert OFDM system in the low SNR range, before the power of CC kicks in for high SNRs. Again, this proves that the key to approach Shannon capacity is to correlate the transmitting sequence through coding.

Furthermore, the BLER performance of coded CNN-based OFDM autoencoder using the LSTM of Table 3.2 having a rate of $e = 1, 1/2, 1/4$ is shown in Fig. 3.12

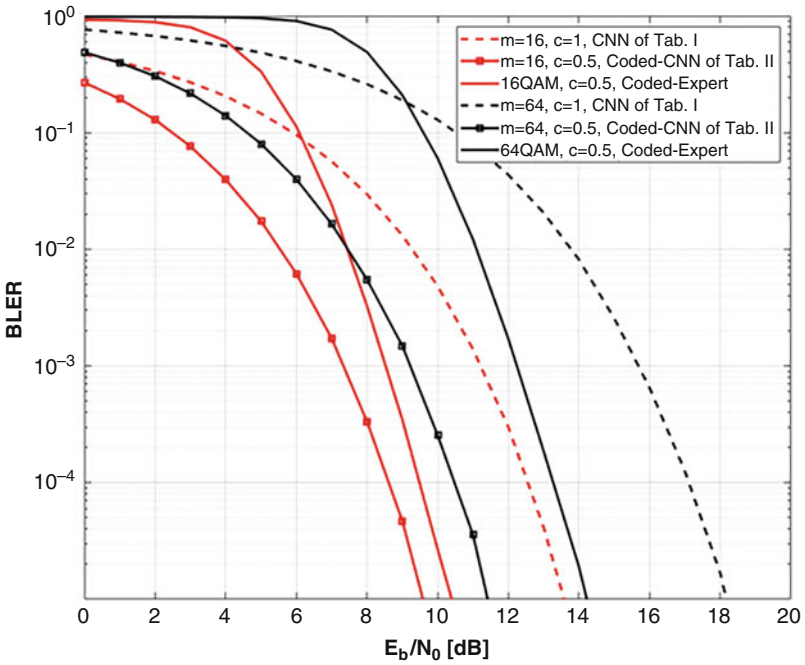

Fig. 3.10 The BLER performance of the proposed CNN-based OFDM autoencoder of rate $e = 1$ and coded CNN-based OFDM autoencoder using LSTM of $e = 1/2$ under AWGN channels, when compared with corresponding expert OFDM systems using CC of $e = 1/2$

when transmitting over multipath Rayleigh fading channels of Doppler frequency 8.73 Hz. It is obvious that our proposed autoencoder can indeed function under multipath fading channels and working with various rates, owing to the learning ability of neural networks. What's more, the BLER performance keeps improving significantly, with the help of increasing redundancy from $e = 1$ to 1/4. This means that the proposed coded CNN-based OFDM autoencoder using LSTM can exploit the redundancy efficiently through sufficient training.

3.4.2 Channel Estimation

There are two factors that contribute to the accuracy of the CE, namely the noise level in the pilot data and the fast-changing nature of the marine wireless channel, characterized by Doppler frequency.

Figure 3.13 shows the BLER performance of the proposed CNN-based OFDM autoencoder of Fig. 3.3 using CNN-based CE of Table 3.3 when communicating over flat multipath Rayleigh fading channels. In order to demonstrate the proposed CE's learning ability, the OFDM system's BLER performance using perfect CIRs

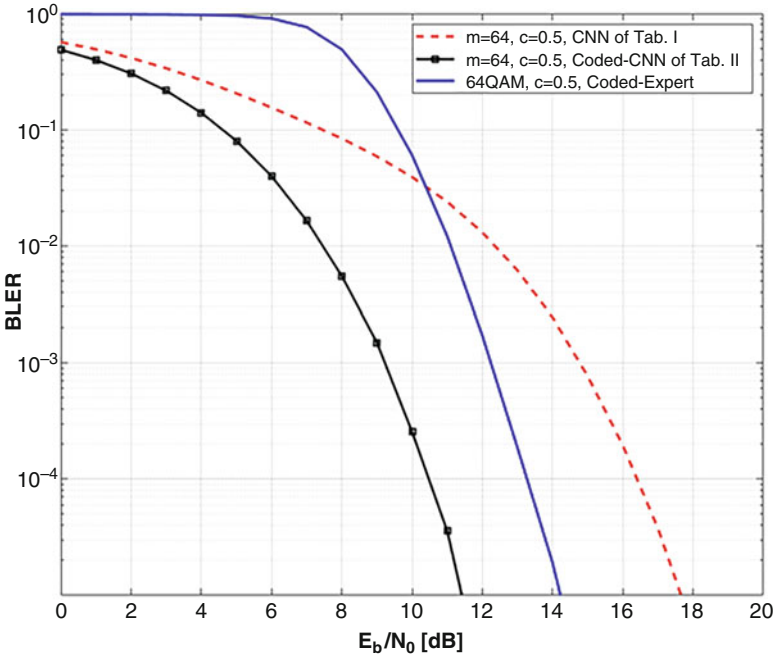

Fig. 3.11 The BLER performance of the proposed CNN-based OFDM autoencoder of rate $e = 1/2$ and coded CNN-based OFDM autoencoder using LSTM of $e = 1/2$ under AWGN channels, when compared with corresponding expert OFDM systems using CC of $e = 1/2$

and using state-of-the-art deep learning-based channel estimation [18] is also given as the bench markers. When $m = 2$ and 4, we observed that both reference [18] and the proposed CE can achieve the same performance as that of using the perfect CIRs.

Also observe in Fig. 3.13 that, in the case of $m = 16$ and 64, there exists an error floor for CE of [18] at high E_b/N_0 region. However, our proposed CNN-based CE of Table 3.3 remains capable of accurately reconstructing CIRs, which results in close BLER performance with the case of using perfect CIRs. This improvement over [18] comes from Dense-Net structure's deepened layers and multiple shortcut connections, which allow the proposed CE to infer better based on the pilot data.

For fast multipath Rayleigh fading channels having a Doppler frequency of 8.73 Hz, Fig. 3.14 plots the BLER performance of the CNN-based OFDM system of Fig. 3.3 using CNN-based CE of Table 3.3, when compared with using perfect CIRs and reference [18]. Firstly, observe in Fig. 3.14 that all the BLER performance under fast fading environments are worse than that of flat-fading channels in Fig. 3.13, owing to the increasing unpredictability of the channel. In this case, the comb pattern pilot signals of Fig. 3.2 are insufficient to capture the change in the environment. Secondly, all the CE algorithms in Fig. 3.14 exhibit error floors at high SNR regions, and the error floors become more apparent for large m. However, the proposed CE algorithm of Table 3.3 still manages to beat the performance of [18].

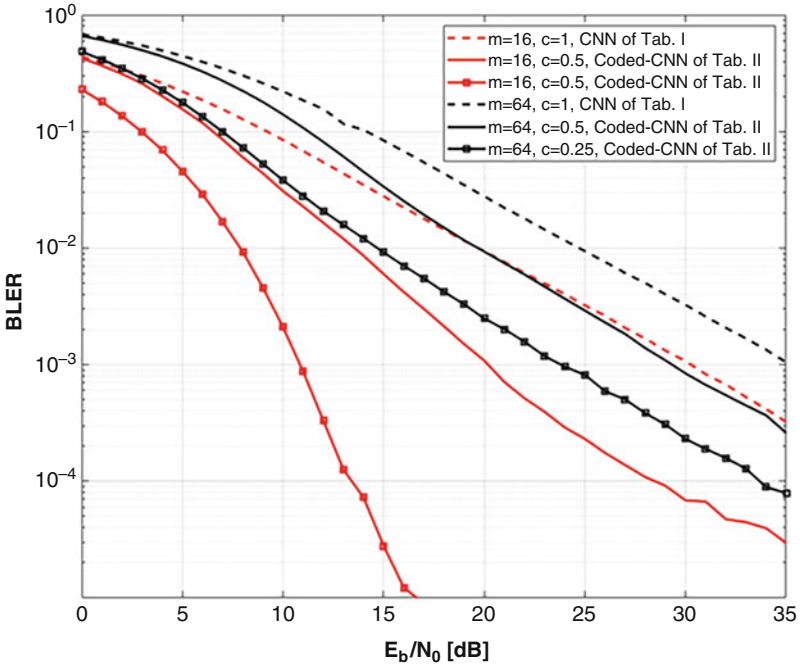

Fig. 3.12 The BLER performance of coded CNN-based OFDM autoencoder using the LSTM of Table 3.2 having a rate of $e = 1, 1/2, 1/4$, when transmitting over multipath Rayleigh fading channels of Doppler frequency 8.73 Hz, while having perfect CIRs

Again, this means that the proposed Dense-Net structure can estimate the CIRs better than that of [18]. In addition, the proposed CNN-based CE uses fewer neural network parameters (total number of parameters = 19,192) than [18] (total number of parameters = 64,292). In other words, the proposed CNN-based CE invokes less computational cost.

3.5 Conclusion

In order to design an intelligent communication system for challenging maritime channel environment, a novel OFDM autoencoder is proposed, which employs CNN and LSTM layers to facilitate end-to-end learning. Furthermore, the proposed learning-based autoencoder is best suitable for communication systems that having a precise channel model is either impractical or impossible, which is not limited to maritime communications. Our OFDM autoencoder consists of multiple CNN layers in order to learn intricate signal representations for optimal transmissions while using fewer parameters than using FC layers. In addition, the proposed CNN architecture is able to converge to optimal solutions easily during training as of

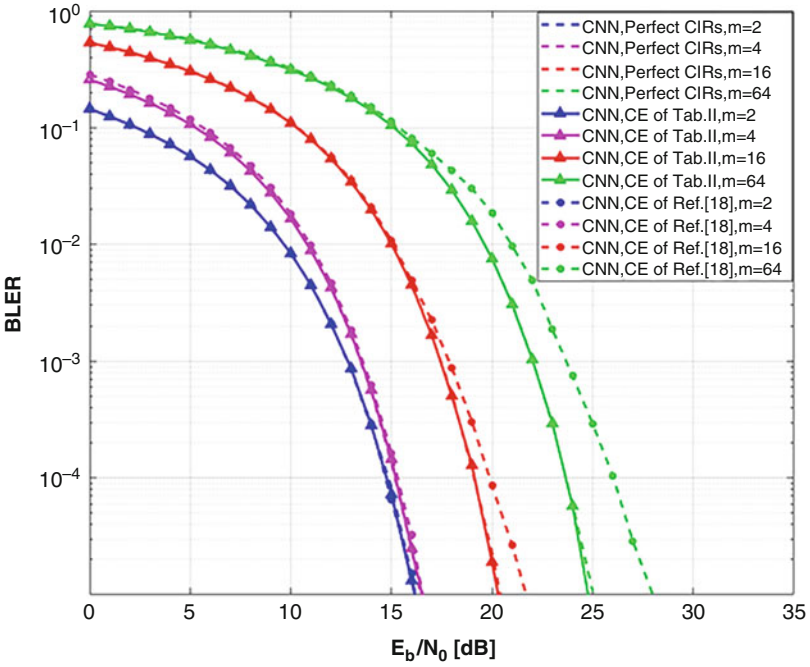

Fig. 3.13 The BLER performance of the CNN-based OFDM autoencoder of Fig. 3.3 with CNN-based Channel Estimation (CE) of Table III, when communicating over flat multipath Rayleigh fading channels, while compared with OFDM systems having perfect CIRs and using CE of reference [18]

Figs. 3.8 and 3.9. When operating at low throughput, the proposed autoencoder exhibits similar BLER performance comparable to conventional QAM-assisted OFDM systems. And the proposed system is able to outperform traditional OFDM systems in high throughput settings as seen in Figs. 3.6 and 3.7. Furthermore, we also propose an LSTM-aided OFDM autoencoder of Table 3.2, which has the capacity of achieving a better channel coding gain than the convolutional coded counterparts, which is shown in Figs. 3.10 and 3.12.

In the meantime, we also propose a new channel estimation algorithm for OFDM systems that marries the power of DL with the idea of super-resolution reconstruction, where a specially designed Dense-Net architecture is used to reconstruct low-resolution pilot information image into a high-resolution image. The Dense-Net architecture solves traditional CNN's problem of vanishing gradient and excessive parameters through dense connections and feature multiplexing. Under slow fading channels, the proposed channel estimator can estimate the CIRs near perfection. In the case of fast fading channels, the proposed channel estimator achieves better performance than that of the existing DL-based algorithms with lower computational complexity. Finally, the proposed coded OFDM autoencoder and the proposed CNN-based CE require significant amount of computation power to train

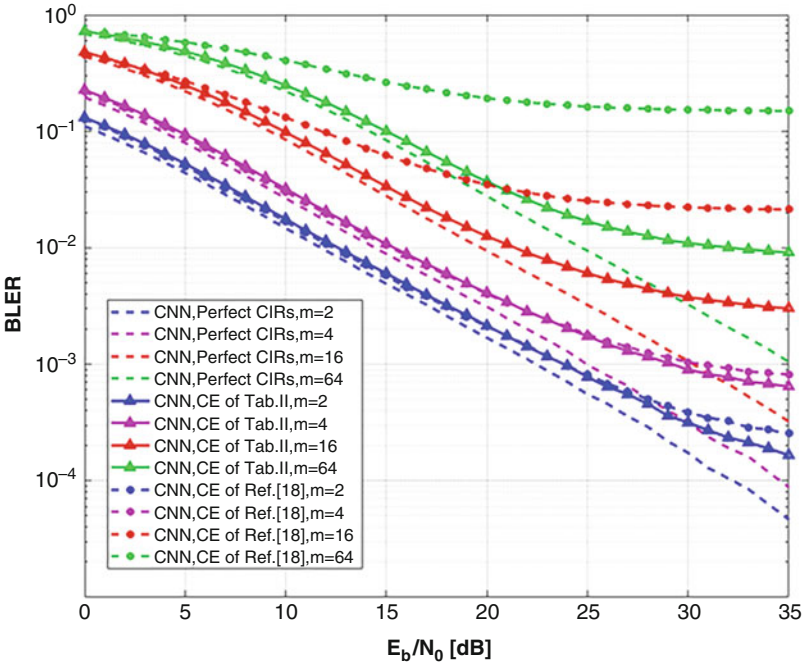

Fig. 3.14 The BLER performance of the CNN-based OFDM autoencoder of Fig. 3.3 with CNN-based Channel Estimation (CE) of Table 3.3, when communicating over fast multipath Rayleigh fading channels of Doppler frequency 8.73 Hz, while compared with OFDM systems having perfect CIRs and using CE of reference [18]

offline; however, once the training is complete, the proposed autoencoders enjoy simple deployment by loading trained parameters and readily online training update.

In summary, we believe that the proposed OFDM autoencoder's generalization ability married with superior BLER performance and adaptability to complex marine environments, which are blessed by LSTM-aided CNNs, hold to key to the evolution of MWCNs.

References

1. W. Zhen, B. Lin, "Maritime Internet of Vessels," in Encyclopedia of Wireless Networks, X. Shen, X. Lin, and K. Zhang, Eds. Berlin, Germany: Springer, Cham, 2019, pp. 1-9. [Online]. Available: https://link.springer.com/referencework/10.1007/978-3-319-32903-1
2. L. Jiang, G. Huang, C. Huang, W. Wang, "Data Mining and Optimization of a Port Vessel Behavior Behavioral Model Under the Internet of Things," IEEE Access, vol. 7, pp. 139970-139983, Sep, 2019, DOI:https://doi.org/10.1109/ACCESS.2019.2943654.
3. D. Chen, Y. Tian, D. Qu, T. Jiang, "OQAM-OFDM for wireless communications in future Internet of Things: A survey on key technologies and challenges," IEEE Internet of Things

Journal, vol. 5, no. 5, pp. 3788-3809, Oct,2018, DOI:https://doi.org/10.1109/JIOT.2018.2869677.
4. S. Gao, M. Zhang, X. Cheng, "Precoded index modulation for multi-input multi-output OFDM," IEEE Transactions on Wireless Communications, vol. 17, no. 1, pp. 17-28, Jan, 2017, DOI: https://doi.org/10.1109/TWC.2017.2760823.
5. C. Jiang, H. Zhang, Y. Ren, Z. Han, K.C. Chen, L. Hanzo, "Machine learning paradigms for next-generation wireless networks," IEEE Wireless Communications, vol. 24, no. 2, pp. 98-105, Apr, 2017, DOI:https://doi.org/10.1109/MWC.2016.1500356WC.
6. C. Zhang, P. Patras, H. Haddadi, "Deep learning in mobile and wireless networking: A survey," IEEE Communications Surveys, vol. 21, no. 3, pp. 2224-2287, Mar, 2019, DOI:https://doi.org/10.1109/COMST.2019.2904897.
7. T. O. Shea, J. Hoydis, "An Introduction to Deep Learning for the Physical Layer," IEEE Transactions on Cognitive Communications and Networking, vol. 3, no. 4, pp. 563-575, Dec, 2017, DOI:https://doi.org/10.1109/TCCN.2017.2758370.
8. T. O. Shea, K. Karra, and T. C. Clancy, "Learning to communicate: Channel auto-encoders, domain specific regularizers, and attention," in 2016 IEEE International Symposium on Signal Processing and Information Technology (ISSPIT), Limassol, Cyprus, 2016, pp. 223-228.
9. Q. Z. Li, L. W. Zhao, J. Gao, H. B. Liang, L. Zhao, X. H. Tang, "SMDP-based coordinated virtual machine allocations in cloud-fog computing systems", IEEE Internet of Things Journal, vol. 5, no. 3, pp. 1977-1988, Jun, 2018, DOI:https://doi.org/10.1109/JIOT.2018.2818680.
10. H. B. Liang, X. Zhang, J. Zhang, Q. Z. Li, S. Zhou, L. Zhao, "A novel adaptive resource allocation model based on SMDP and reinforcement learning algorithm in vehicular cloud system", IEEE Transactions on Vehicular Technology, vol. 68, no. 10, pp. 10018-10029, Oct, 2019, DOI:https://doi.org/10.1109/TVT.2019.2937842.
11. B. Mao, Z. M. Fadlullah, F. Tang, N. Kato, et al., "Routing or computing? The paradigm shift towards intelligent computer network packet transmission based on deep learning," IEEE Transactions on Computers, vol. 66, no. 11, pp. 1946-1960, Nov, 2017, DOI:https://doi.org/10.1109/TC.2017.2709742.
12. N. Ye, X. M. Li, H. Yu, L. Zhao, W. Liu, X. Hou, "Deep NOMA: A unified framework for NOMA using deep multi-task learning" IEEE Transactions on Wireless Communications, Jan, 2020, DOI: 10.1109/TWC.2019.2963185, early access.
13. L. Cimini, "Analysis and simulation of a digital mobile channel using orthogonal frequency division multiplexing," IEEE transactions on communications, vol. 33, no. 7, pp. 665-675, Jul, 1985, DOI: https://doi.org/10.1109/TCOM.1985.1096357.
14. E. Balevi, J. G. Andrews, "One-bit OFDM receivers via deep learning," IEEE Transactions on Communications, vol. 67, no. 6, pp. 4326-4336, Jun, 2019, DOI: https://doi.org/10.1109/TCOMM.2019.2903811.
15. A. Felix, S. Cammerer, S. Dörner, J. Hoydis, S. T. Brink, "OFDM-Autoencoder for End-to-End Learning of Communications Systems," in 2018 IEEE 19th International Workshop on Signal Processing Advances in Wireless Communications (SPAWC), Kalamata, Greece, 2018, pp. 1-5.
16. M. Kim, W. Lee, D. H. Cho, "A Novel PAPR Reduction Scheme for OFDM System Based on Deep Learning," IEEE Communications Letters, vol. 22, no. 3, pp. 510-513, Mar, 2018, DOI: https://doi.org/10.1109/LCOMM.2017.2787646.
17. M. Morelli, U. Mengali, "A comparison of pilot-aided channel estimation methods for OFDM systems," IEEE Transactions on signal processing, vol. 49, no. 12, pp. 3065-3073, Dec, 2001, DOI: https://doi.org/10.1109/78.969514.
18. Z. Zhao, M. C. Vuran, F. Guo, S. Scott, "Deep-waveform: A learned OFDM receiver based on deep complex convolutional networks," 2018, arXiv:1810.07181. [Online]. Available: https://arxiv.org/abs/1810.07181
19. H. Ye, G. Y. Li, B. H. Juang, "Power of deep learning for channel estimation and signal detection in OFDM systems," IEEE Wireless Communications Letters, vol. 7, no. 1, pp. 114-117, Feb, 2017, DOI: https://doi.org/10.1109/LWC.2017.2757490.

20. X. Gao, S. Jin, C. K. Wen, G. Y. Li, "ComNet: Combination of deep learning and expert knowledge in OFDM receivers," IEEE Communications Letters, vol. 22, no. 12, pp. 2627-2630, Dec, 2018, DOI: https://doi.org/10.1109/LCOMM.2018.2877965.
21. A. Brifman, Y. Romano, M. Elad, "Unified Single-Image and Video Super-Resolution via Denoising Algorithms," IEEE Transactions on Image Processing, vol. 28, no. 12, pp. 6063-6076, Dec, 2019, DOI: https://doi.org/10.1109/TIP.2019.2924173.
22. M. Soltani, V. Pourahmadi, A. Mirzaei, H. Sheikhzadeh, "Deep learning-based channel estimation," IEEE Communications Letters, vol. 23, no. 4, pp. 652-655, Apr, 2019, DOI: https://doi.org/10.1109/LCOMM.2019.2898944.
23. S. Hochreiter, J. Schmidhuber, "Long short-term memory," Neural computation, vol. 9, no. 8, pp. 1735-1780, Nov, 1997, ISSN: 0899-7667. [Online]. Available: https://doi.org/10.1162/neco.1997.9.8.1735
24. G. Huang, Z. Liu, L. V. D. Maaten, K. Q. Weinberger, "Densely connected convolutional networks," in Proceedings of the IEEE conference on computer vision and pattern recognition (CVPR), Honolulu, HI, USA, 2017, pp. 4700-4708.
25. K. He, X. Zhang, S. Ren, J. Sun, "Deep residual learning for image recognition," in Proceedings of the IEEE conference on computer vision and pattern recognition (CVPR), Las Vegas, NV, USA, 2016, pp. 770-778.
26. M. H. Hsieh, C. H. Wei, "Channel estimation for OFDM systems based on comb-type pilot arrangement in frequency selective fading channels," IEEE Transactions on Consumer Electronics, vol. 44, no. 1, pp. 217-225, Feb, 1998, DOI: https://doi.org/10.1109/30.663750.
27. M. Patzold, A. Szczepanski, N. Youssef, "Methods for modeling of specified and measured multipath power-delay profiles," IEEE Transactions on Vehicular Technology, vol. 51, no. 5, pp. 978-988, Sep, 2002, DOI: https://doi.org/10.1109/TVT.2002.801747.
28. J. Yu, X. Gao, D. Tao, X. Li, K. Zhang, "A unified learning framework for single image super-resolution," IEEE Transactions on Neural networks Learning systems, vol. 25, no. 4, pp. 780-792, Apr, 2014, DOI: https://doi.org/10.1109/TNNLS.2013.2281313.
29. H. S. Mousavi, V. Monga, "Sparsity-based color image super resolution via exploiting cross channel constraints," IEEE Transactions on Image Processing, vol. 26, no. 11, pp. 5094-5106, Nov, 2017, DOI: https://doi.org/10.1109/TIP.2017.2704443.
30. Z. M. Fadlullah, F. Tang, B. Mao, N. Kato, et al., "State-of-the-art deep learning: Evolving machine intelligence toward tomorrow's intelligent network traffic control systems," IEEE Communications Surveys Tutorials, vol. 19, no. 4, pp. 2432-2455, May, 2017, DOI: https://doi.org/10.1109/COMST.2017.2707140.
31. J. Wang, H. Zhou, Y. Li, Q. Sun, et al., "Wireless channel models for maritime communications," IEEE Access, vol. 6, pp. 68070-68088, Nov, 2018, DOI: https://doi.org/10.1109/ACCESS.2018.2879902.
32. J. I. Smith, "A computer generated multipath fading simulation for mobile radio," IEEE Transactions on Vehicular Technology, vol. 24, no. 3, pp. 39-40, Aug, 1975, DOI: https://doi.org/10.1109/T-VT.1975.23600.

Chapter 4
Decentralized Reinforcement Learning-Based Access Control for Energy Sustainable Underwater Acoustic Sub-Network of MWCN

Due to energy limitations, inadequate frequency band, mobility of underwater nodes, the most challenging issue of the next generation MWCN is the access control of the underwater acoustic sub-network. In this chapter, we focus on an Energy Sustainable Underwater acoustic sub-network of MWCN with tidal energy harvesting. For simplicity, we use the term ESUN for the energy sustainable underwater sub-network of MWCN in the later sections. Specifically, an analytical model is first developed to analyze the network performance of ESUN, characterizing the stochastic nature of energy harvesting and traffic demands of ESUN nodes, and the salient features of acoustic communication channels. It is found that the spatial uncertainty resulting from underwater acoustic communication may cause severe fairness issue. As such, an optimization problem is formulated to maximize the network throughput under fairness constraints by tuning the random-access parameters of each node. Given the global network information, including the number of nodes, energy harvesting rates, communication distances, etc., the optimization problem can be efficiently solved using the Branch and Bound (BnB) method. Considering a realistic network where the full network information may not be available at the ESUN nodes, we further propose a multi-agent reinforcement learning approach for each node to autonomously adapt the random-access parameter based on the interactions with the dynamic network environment. Numerical results show that the proposed learning algorithm outperforms the existing solutions in terms of the network throughput and approaches the derived theoretical bound.

The remainder of this chapter is organized as follows: Sect. 4.1 studies the background. Section 4.2 discusses the related works. Section 4.3 describes the system model and the analytical framework to investigate the throughput performance of an ESUN. In Sect. 4.4, a multi-agent reinforcement learning algorithm is presented. Numerical results are provided in Sect. 4.5, followed by concluding remarks in Sect. 4.6.

B. Lin et al., *Next Generation Marine Wireless Communication Networks*, Wireless Networks, https://doi.org/10.1007/978-3-030-97307-0_4

4.1 Background

The expansion of marine industries to the far and deep ocean puts forward higher requirements for the next generation MWCNs. However, the marine environment is harsh and complex, and the traditional network access method is difficult to be directly applied to the marine environment. The MWCN faces many problems, such as power supply, balanced access to the network of underwater nodes, and so on. In the last decade, we have witnessed the rapid development of the wireless sensor network technology. Billions of wireless sensors and other communication devices have been deployed to provide numerous intelligent services such as smart home, smart city, and smart ocean [1–4]. Compared with smart home and smart city, the service of smart ocean is relatively under-explored; yet it has attracted increasing attentions from both industry and academia to exploit the abundant marine resources including marine life, oil and gas, minerals, and tidal energy [5]. To build a smart underwater MWCN, an extension of wireless sensor network in the underwater environment has been proposed in 2012 [6]. In such a network, underwater sensor nodes are deployed in the ocean to track the cycles of marine life and monitor ocean environment like the water temperature and pressure in certain areas, direction and speed of ocean current, salinity, turbidity, oxygen density, and chlorophyll levels of water [7]. Generally, wireless sensor nodes are considered to be powered only by battery with limited capacity. One obvious downside of the battery-powered nodes is the need of frequent battery replacement. But in the underwater environment, the battery replacement for underwater node can be challenging, costly, and inconvenient [8]. To tackle this issue, energy harvesting is considered as a promising solution to provide a sustainable network. Fortunately, the tidal current can be considered as a good source for energy harvesting. Since, recent researches find that the energy density of tidal current is much higher compared with other renewable sources such as wind and solar [9–11]. This is because tides are more predictable than wind energy and solar energy. Therefore, tidal energy can be further exploited to provide an ESUN.

Compared with nodes of terrestrial wireless communication network, ESUN nodes in the underwater environment use acoustic wave to communicate instead of Radio Frequency (RF) signals. This is because, in underwater environment, acoustic waves attenuate less compared to radio waves and optical waves. Therefore, it is of great importance to consider both the features of the acoustic waves and marine environment in designing the MAC protocols for ESUN. For example, the propagation speed of sound in water is only about 1500 m/s, which causes long propagation delay that is five orders higher than that in terrestrial communication network. Therefore, while the propagation delay can be ignored for RF communication, the propagation delay is vital for acoustic communication. For ESUN nodes distributed in different locations, a collision-free transmission at the transmitter side may still result in a collision at the receiver side due to various propagation delays over the acoustic channels. As a result, this issue is referred as spatial uncertainty problem. In addition to the spatial uncertainty problem, the underwater acoustic communication

system usually has limited bandwidth and low data rate. Last but not least, the importance of different ESUN nodes should be considered. Since different ESUN nodes may have quite different responsibilities, some nodes are used to monitor the underwater environment, while other nodes are used to build disaster prevention systems such as earthquake warning system. Thus, it is crucial to consider such salient features of acoustic communications in the design of ESUN.

Most existing works of underwater communications in the literature propose different scheduling-based algorithms and protocols to address the spatial uncertainty problem. In [12], a receiver-based schedule scheme is proposed to ensure data are received in order at the receiver side, assuming the propagation delay of each node can be perfectly known. But the locations of underwater sensor nodes may change over time due to water current which leads to varying propagation delays. Such network dynamics make it difficult to have an efficient transmission schedule of underwater sensor nodes. A few papers propose to use random-access protocols for underwater sub-network of MWCNs. In [13], three protocols are evaluated in terms of delay and throughput, by simulations. In [14, 15], it is shown that slotted ALOHA achieves similar performance as pure ALOHA due to the location-dependent propagation delay. To improve the throughput, an enhanced slotted ALOHA protocol is proposed in [16] where the frame arrival time is aligned in slots at the receiver side. These works are either based on only simulations or on an over-simplified model, e.g., Poisson data arrival in the network. In addition, these aforementioned works consider conventional battery-powered underwater sensor nodes that have sufficient energy to operate in the network. For an ESUN powered by tidal energy harvesting, the number of nodes ready for data communications may change from time to time, which makes it challenging for the protocol design and optimization. To the best of our knowledge, no prior work investigates the design and development of ESUNs with energy harvesting.

In this chapter, we study a random access based ESUN with tidal energy harvesting. Specifically, an analytical framework is developed to analyze the throughput of ESUN nodes, characterizing the stochastic nature of energy harvesting, traffic demands of ESUN nodes, and the acoustic communication channels. Based on the analysis, the impact of long propagation delay of acoustic communication channel and the spatial uncertainty on the network performance is investigated. According to our analysis, we find that spatial uncertainty may cause severe fairness issue in an ESUN, as a closer node may access the channel more frequently than a faraway node. To achieve the maximum network throughput while ensuring fair sharing of network bandwidth, an optimization problem is formulated. By adapting the random-access window of each node, the maximum throughput can be achieved under the fairness constraint. Given the global network information, i.e., the total number of network nodes, the traffic demands of ESUN nodes, and the communication distance between the ESUN nodes and the Access Point (AP), the optimization problem can be efficiently solved using the Branch and Bound (BnB) optimization method. In a realistic network setting, the information of ESUN may not be available at ESUN nodes. Thus, we further propose a multi-agent reinforcement learning approach for each ESUN node to distributively adapt the access

parameters based on the dynamic network environment. The main contributions of this chapter can be summarized into fourfold.

- A generic mathematical model is developed to analyze the performance of an ESUN with energy harvesting, capturing the salient features of underwater communication channel and the stochastic energy harvesting process.
- An optimization problem is formulated to maximize the weighted sum throughput of ESUN nodes under the fairness constraint. Given the global network information, the optimization problem can be solved with BnB method to find the optimal setting of random-access parameters of ESUN nodes.
- In a fully distributed ESUN where the global network information is not available, a multi-agent reinforcement learning approach is further introduced for each ESUN node to adapt the access parameter in a distributive manner.
- Extensive simulations are conducted to demonstrate that the proposed learning algorithm approaches the derived theoretical bound and significantly outperforms some existing solutions.

4.2 Related Works

The existing MAC protocols proposed for underwater sub-network of MWCNs can be classified into two categories: scheduling-based and contention-based protocols [17]. For scheduling-based protocols, the communication channel is usually divided into multiple subchannels in the time domain, which are allocated for contention-free data transmissions of underwater nodes. Due to the scarcity of the available bandwidth, Frequency Division Multiple Access (FDMA) is not suitable for underwater networks. Most existing scheduling-based protocols aim to optimize the transmission schedule to improve the throughput performance of an underwater acoustic network. In [18], a MAC protocol proposed for underwater sensor network applies graph coloring to schedule as many conflict-free concurrent transmissions as possible to achieve high throughput, based on the global network topology. In [19], a distributed scheduling scheme is proposed without the full information of the network topology but using a distributed clustering approach coordinating neighboring nodes. The proposed solutions in [18, 19] involve large signaling overheads to obtain the network topology or form distributive clusters, which may not be suitable for energy constrained underwater nodes. In [20], a load-based slot allocation scheme is proposed for underwater wireless sensor networks, which combines TDMA and Carrier-Sense Multiple Access with Collision Avoidance (CSMA/CA). However, the scheme in [20] ignores the impact of long propagation delay of underwater communications by simply adopting a long slot duration which comprises the data transmission time and the maximum propagation delay. In [21], a delay and queue aware adaptive scheduling-based MAC protocol is proposed, taking into consideration the data queue length of nodes and various propagation delays of different nodes at different locations. This paper considers a static network with a

fixed number of nodes which are well synchronized with the central scheduler. In [22], the performance of sender-based scheduling and receiver-based scheduling where the schedule is decided by the sender and receiver, respectively, are compared. To improve the energy efficiency, a depth-based protocol named ED-MAC is proposed in [23] by scheduling duty cycles of underwater sensors. In all these aforementioned works, it is assumed that all nodes always have sufficient energy to transmit. For ESUN nodes with energy harvesting, the nodes may not always have sufficient energy to operate in the network and they become inactive for data transmissions from time to time. In such case, the number of active ESUN nodes in the network may vary over time. Thus, it is difficult for the central scheduler to decide the transmission schedule for ESUN nodes.

Besides the scheduling-based protocols, some papers propose contention-based protocols for underwater wireless networks. To address the spatial uncertainty problem, an enhanced slotted ALOHA protocol is presented in [15], where guard bands are added with respect to the maximum propagation delay in each slot. Similarly, a reservation-based protocol is proposed in [24], where competing users contend to send short busy-tone signals to reserve the channel. However, the proposed protocol requires that each node keeps sensing the channel for each contention round when competing for channel access, which is not energy-efficient and thus not suitable for ESUN nodes. In [25], two variants of ALOHA-based protocols are proposed to improve the throughput by exploiting the long propagation delay. The performance of the enhanced ALOHA protocol proposed in [15] is analytically studied in [26]. It is found that the bandwidth waste resulting from the guard time is proportional to the propagation delay.

With the popularity of machine learning, some related works incorporate the learning algorithm on the protocol design of traditional wireless network [27–31]. However, there is no work considering the unique feature of ESUN. To sum up, these aforementioned works mainly aim at improving the network throughput or energy efficiency of conventional battery-powered underwater sensor networks, without considering the spatial fairness issue in an ESUN. It is well known that fairness is an important performance metric of MAC protocol design. In addition, tidal energy harvesting poses new challenges in the design and development of an energy sustainable ESUN, which should be taken into consideration. Thus motivated, in this chapter, we investigate the protocol design and optimization of an ESUN with tidal energy harvesting, characterizing the stochastic nature of energy harvesting and data arrivals of ESUN nodes. However, when the network information is not available.

By applying reinforcement learning, each ESUN node can intelligently utilize its harvested energy and adapt their protocol parameters to attain the maximal sustainable network throughput.

4.3 Performance Analysis of ESUN with Energy Harvesting

In this section, we will first introduce the system model considered in this chapter. Then, based on whether the data requires acknowledgement from the AP, we will mathematically analyze the performance of ESUN nodes for both cases.

4.3.1 System Model

In the system, we consider an ESUN consisting of one AP and M ESUN nodes. These M ESUN nodes are randomly deployed in a 3-D space which is shown in Fig. 4.1. The propagation delay of ESUN node i is assumed to be dependent only on the distance to the AP which is denoted as D_{iA}. Based on the numerical results in [16], we can find that the ESUN nodes with different propagation delays may introduce random collisions at the receiver sides caused by the spatial uncertainty problem. Thus, slotted ALOHA performs similarly to pure ALOHA algorithm. To tackle the spatial uncertainty problem, in this chapter, we postpone the transmissions according to the propagation delay to ensure that the data can be received at the start of a slot. The postpone process is shown in Fig. 4.2. In Fig. 4.2, one ESUN node with propagation delay 1.2 slot supposes to transmit a data packet at time $t = 1$. To ensure that the data can be received at the beginning of one slot, the ESUN node will postpone the transmission time to $t = 1.8$.

It is assumed that ESUN nodes are only powered by tidal energy generated from periodic flow of water. In each time slot, the probability that node i harvests one unit of energy is denoted as $P_e(i)$. The power capacity of each ESUN node is assumed to

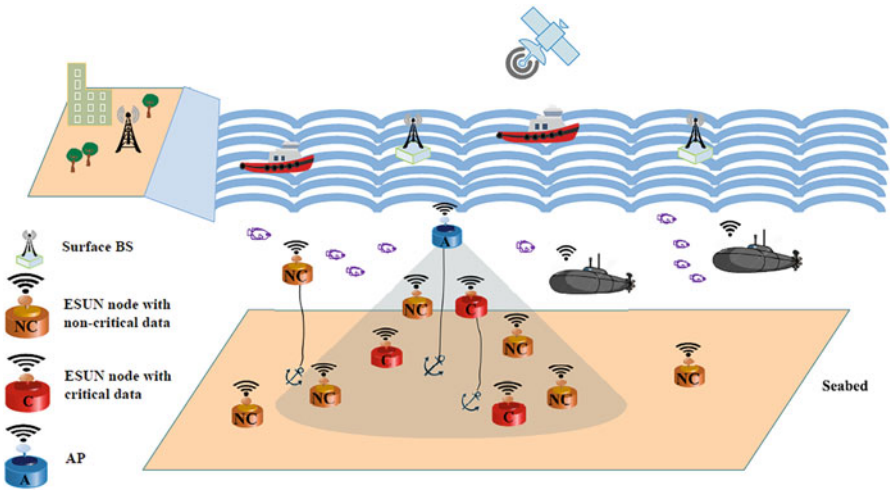

Fig. 4.1 The ESUN model

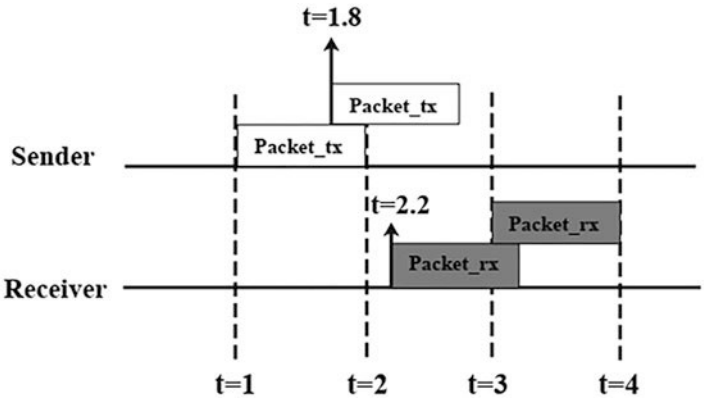

Fig. 4.2 Receiver synchronization

be W units. When one ESUN node has W unit of energy, it can be ready to transmit. Thus, each IoT node will keep harvesting the tidal energy until it reaches the capacity of W energy units. After transmitting the data, no matter successful or failure, a node depletes the energy buffer and needs to take some time to recharge for the next transmission.

Each ESUN node monitors the ocean environment for certain duration and randomly generates data for transmission. For data of ESUN nodes, we consider the following two cases: (1) In the first case when a critical event is detected, an ESUN node generates a critical data that require reliable transmission to the AP. Thus, unicast transmission with immediate acknowledgement (ACK) is required. (2) In the second case, an ESUN node may also report some non-critical data to the AP and no mandatory immediate ACK is required. It is worth noting that due to the long propagation delay, the ACK cannot be protected by using a Shortest Interframe Space (SIFS) as in conventional random-access protocols. Thus, the AP transmits ACK at a high-power mode to ensure successful reception of ACK. We assume data arrival follows Bernoulli distribution with mean value $Pd(i)$ for node i. When a node has charged sufficient energy W and has a data in the queue, the ESUN node is then ready for data transmission. In what follows, the term ready nodes refer to the nodes that have both data and enough energy. Due to stochastic nature of the data generation and energy harvesting, the AP may not able to accurately predict the set of ready nodes and then schedule the transmissions efficiently. Therefore, in this work, we consider that each node adopts the slotted ALOHA-based random-access protocol to access the channel when it is ready. Specifically, in the beginning of each slot, a ready node randomly selects random-access parameter, i.e., a backoff counter, from $[0, CWi - 1]$. The backoff counter decrements by one in each slot. When the backoff counter reaches zero, the node is able to transmit. The channel is assumed to be ideal such that the transmission will be successful if there is no collision at the receiver side.

4.3.2 Analysis of ESUN Nodes

In this section, we develop the analytical model to study the performance of ESUN network with energy harvesting. Based on whether the data requires acknowledgement from the AP, the nodes can be divided into two categories, i.e., nodes carrying critical data and nodes carrying non-critical data. Firstly, the ready probability along with the access rate of the nodes with non-critical data is derived in Sect. 4.3.2.1. Then, the access rate of nodes carrying critical data is derived in Sect. 4.3.2.2. Based on the access rate and the ready probability, the system throughput can be obtained.

4.3.2.1 Analysis of ESUN Nodes with Non-critical Data

In this subsection, we analyze the average ready probability for the ESUN nodes who carry the data without the requirements of reliability. We define the ready probability as the probability that the ESUN node has enough energy and non-empty data at a random slot. The main parameters used in the analytical part are listed in Table.4.1. Let $Da^i(t)$ denote the data state for ESUN node i in slot t. This discrete time scale is directly related to the system time. Similarly, the unit of energy stored at time t for a given ESUN node is denoted as $E^i(t)$. As mentioned previously, W denotes both the power storage capacity and the energy required to transmit data. The bi-dimensional process $\{Da^i(t), E^i(t)\}$ with Markov chain of node i is illustrated in Fig. 4.3. The non-null one step transition probabilities are:

$$\begin{cases} P\{1,k+1|1,k\} = P_e(i), k \neq W \\ P\{1,k+1|0,k\} = P_e(i)P_d(i), k \neq W \\ P\{0,k+1|0,k\} = (1-P_d(i))P_e(i), k \neq W \\ P\{0,0|1,W\} = p(i)(1-P_d(i)) \\ P\{1,0|1,W\} = p(i)P_d(i) \\ P\{1,W|1,W\} = 1-P(i) \end{cases} \quad (4.1a-f)$$

The first three equations in Eq. (4.1) show the transition probabilities when the ESUN node is not ready in the previous slot. Eq. (4.1a) shows that given the ESUN

Table 4.1 List of Notations

Description	Notation
The number of ESUN nodes	M
The distance between node i and AP	DiA
Prob. of arriving of n unit energy in one slot for node i	$Pe(i)$
Prob. of arriving of one packet in one slot for node i	$Pd(i)$
Window size of node i	$CW(i)$
Energy capacity of a node	W

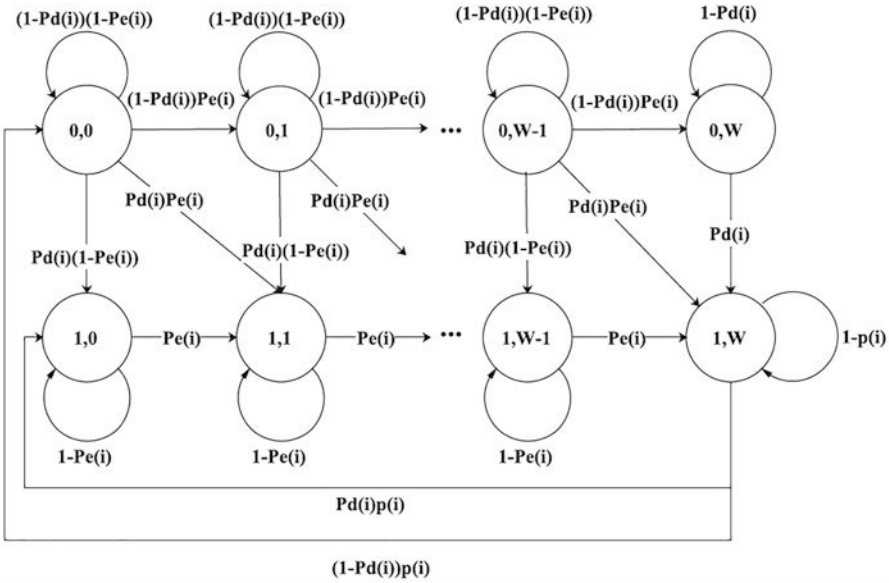

Fig. 4.3 Markov chain

node has k units of energy and the data queue is not empty in the previous slot, the probability that it harvests one unit of energy is *Pe(i).* Since the data state is one in the previous slot and the data queue is one, the data state will still be one in the next slot regardless of the data arrival in the following slot. Since each node only transmits the most updated data. In Eq. (4.1b), node i with no data and k units of energy changes to state $(1, k+1)$ with probability $Pd(i)Pe(i)$. If the data state remains zero in the next slot, the probability is $(1 - Pd(i))$ which is shown in Eq. (4.1c). Equation (4.1d–f) account for the fact that when the node is ready in the previous slot, the state in the next slot depends on the data arrival. If a new data arrives when node i is transmitting, the next state is (1,0). *p(i)* is the average transmission probability of node i. Given the window size of node i is *CWi,* the average transmission probability is

$$\pi^i_{\{0,k\}} = \begin{cases} p(i)(1-p_d(i))\pi^i_{\{1,W\}} + \pi^i_{\{0,0\}}(1-p_e(i))P_d(i), k=0 \\ (1-p_d(i))\pi^i_{\{0,k-1\}}p_e(i), k \in [1, W-1] \\ (1-p_d)\left(\pi^i_{\{0,W-1\}}P_e + \pi^i_{\{0,W\}}\right), k=W \end{cases} \quad (4.2\text{a}-\text{c})$$

Let $\pi^i_{\{d,e\}} = \lim_{t\to\infty} P\{Da^i(t) = d, E^i(t) = e\}, d \in (0,1), e \in (0,W)$ denote the steady state probability when the data state is d and energy state is e for the ESUN node i. The steady state probabilities when the data state is zero are given in Eq. (4.2).

Equation (4.2a–c) are the steady state probabilities when $k = 0$, $k \in [1,W\text{-}1]$, and $k = W$. Similarly, we can obtain the steady possibilities when the data state is one which are shown in Eq. (4.3). Equation (4.3a) is the steady probability of $\pi^i_{\{1,k\}}$ when $k \in [0, W\text{-}1]$. While Eq. (4.3) is the steady probability when k is W.

$$\pi^i_{\{1,k\}} = \begin{cases} \pi^{k-1}_{\{1,x\}} P_e(i) + P_d(i)\pi^i_{\{0,k-1\}} P_e(i) \\ \pi^i_{\{1,W-1\}} P_e(i) + \pi^i_{\{1,W\}}(1 - p(i)) \\ +P_d(i)\pi^i_{\{0,W\}} + P_d(i)\pi^i_{\{0,W-1\}} P_e(i) \end{cases} \quad (4.3a - b)$$

According to the total probabilities rule, we have

$$\sum_{x=0}^{W} \pi^i_{\{0,x\}} + \sum_{x=0}^{W} \pi^i_{\{1,x\}} = 1 \quad (4.4)$$

After solving Eqs. (4.1)–(4.4), the steady state probabilities $\pi^i_{\{1,k\}}$ for each state can be derived using *CWi*. Among all steady state probabilities, $\pi^i_{\{1,W\}}$ denotes the ready probability that the device has enough energy and non-empty data queue in a random slot. In a special case when all ESUN nodes carry non-critical data. Given the ready probability and the total number of ESUN nodes, the average number of ready ESUN nodes in each slot can be written as:

$$N_r = \sum_{i=1}^{M} \pi^i_{\{1,W\}} \quad (4.5)$$

Given that node i is ready with probability $\pi^i_{\{1,W\}}$, the average waiting time until the node is ready is $\frac{1}{\pi^i_{\{1,W\}}}$. A ready node attempts to transmit on the channel with probability $p(i)$. Thus, the access rate is given by

$$\mu(i) = \frac{1}{\frac{1}{\pi^i_{\{1,W\}}} + \frac{1}{p(i)}} \quad (4.6)$$

When the ESUN node gets the opportunity to transmit over the channel, a collision occurs when at least one of the remaining ESUN nodes is transmitting. Thus, the conditional collision probability given the tagged ESUN node i is transmitting is given by

$$P^i_{cc} = 1 - \prod_{k \neq i, k \in [1,M]} (1 - \mu(k)) \quad (4.7)$$

The average throughput of node i is given by

$$Th_i = \mu(i)\left(1 - P_{cc}^{i}\right)R \tag{4.8}$$

where R is the transmission rate.

4.3.2.2 Performance Analysis of ESUN Nodes with Critical Data

In this subsection, we analyze the performance of ESUN nodes with critical data. Specifically, AP transmits an acknowledgement (ACK) message which informs the sender whether the packet has been received or not to the transmitters immediately after the reception of a packet. Therefore, the ACK message can reach the transmitter side after a round-trip time which is two times the propagation delay between the transmitter and the receiver. Meanwhile, in the transmitter side, the ESUN node keeps sensing the channel until it receives the ACK or the expiration of the ACK timeout. We consider that each ESUN node can only update the data queue when it receives the ACK or the expiration of ACK timeout. Note that each node can still harvest the energy while waiting for the ACK.

Now, we analyze the possible events could happen during two successive transmissions for a tagged node *i*. The possible events that could occur between two successful transmissions of a tagged node are illustrated in Fig. 4.4. As shown in Fig. 4.4, the possible events that could happen between two successive transmissions are dependent on whether the previous transmission is successful or not. If the previous transmission is successful, the data queue of the tagged node is cleared, the node waits for the new data arrival and energy arrival. In contrast, if the previous transmission is collided, the ESUN node waits only for the energy after the ACK. Denote $P_e(i)$ and $Pd(i)$ as the probability that the node i has a data or energy arrival in a random slot. The time instant of the end of last transmission is denoted as m. The probability that the data arrives after time + 1) can be expressed as:

$$P_{(T_d>t)}(i) = 1 - \sum_{j=1}^{t} (1 - P_d(i))^{j-1} P_d(i) \tag{4.9}$$

Similarly, the probability that the energy is sufficient after time $(t0 + t)$ is given by

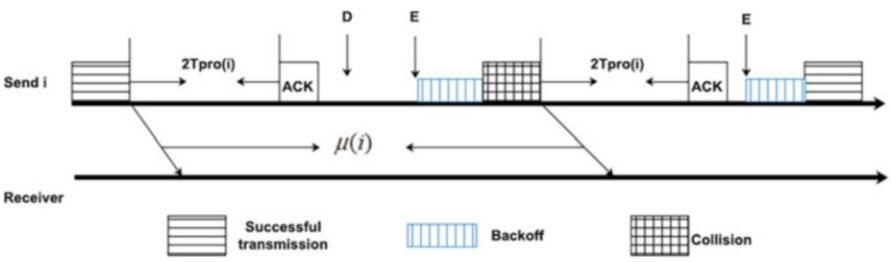

Fig. 4.4 Channel access of reliable node *i*

$$P_{(T_e>t)}(i) = 1 - \sum_{j=W}^{t} \mathrm{C}_W^t (1 - P_d(i))^{t-W} P_e(i)^W \tag{4.10}$$

Given the previous transmission is successful, the average waiting time is dependent on whether energy arrives before data or not. Denote the propagation delay of the node is $T_{\mathrm{pro}}(i)$. Each node keeps harvesting the energy while waiting for the ACK, the probability that the energy arrives before the ACK is $1 - P(t > 2T\mathrm{p}_{\mathrm{ro}}(i)')$. Given the energy arrives after the ACK, the probability that the data arrives first is given by

$$P_{df} = \frac{\sum_{j=W}^{\infty} C_W^j (1 - P_e(i))^{j-W} P_e(i)^W \left(1 - P_{(T_d>j)}(i)\right)}{P_{\left(T_d>2T_{\mathrm{pro}}(i)\right)}} \tag{4.11}$$

Then, the probability that energy arrives no earlier than the data can be written as $1 - pdf$. Given data arrives first, the average waiting time after ACK can be written as:

$$E\left[T_{df}\right] = \frac{\sum_{j=W}^{\infty} C_W^j (1 - P_e(i))^{j-W} P_e(i)^W \left(1 - P_{(T_d>j)}(i)\right) j}{P_{\left(T_d>2T_{\mathrm{pro}}(i)\right)}} \tag{4.12}$$

If data arrives earlier than the time that the energy is sufficient, the average waiting time after ACK is

$$E\left[T_{ef}\right] = 1/P_d(i) \tag{4.13}$$

Using Eqs. (4.11)–(4.13), the average waiting time after ACK can be written as:

$$\begin{aligned} E[T_r(i)] = {} & P_{\left(T_e>2T_{\mathrm{pro}}\right)}(i)\left(E\left[T_{df}\right]p_{df} + E\left[T_{ef}\right]\left(1 - p_{df}\right)\right) \\ & + \left(1 - P_{\left(T_e>2T_{\mathrm{pro}}\right)}(i)\right)\left(\frac{1}{P_d(i)}\right) \end{aligned} \tag{4.14}$$

where the first line represents the average duration between the time that the packet has been sent and the time that the node is ready given the condition that energy is sufficient after the ACK. Meanwhile, the second line is the average waiting time when the energy is sufficient after the ACK. The average waiting time between a successful transmission and the first transmission is given by

$$T_{\mathrm{st}}(i) = E[T_r(i)] + 2T_{\mathrm{pro}}(i) + T_{\mathrm{ACK}} + \frac{\mathrm{CW}_i}{2} \tag{4.15}$$

When the previous transmission is not successful, after the ACK timeout, the ESUN node only needs to wait for the energy arrival. The average duration between a collision and a transmission is

$$T_{ct}(i) = (1 - P(T_e > t)(i))2T_{\text{pro}}(i) + P(T_e > t)(i) \times \frac{\sum_{j=W}^{\infty} C_W^j (1 - P_e(i))^{j-\text{W}} P_e(i)^W \left(j + 2T_{\text{pro}}(i) \right)}{P_{\left(T_d > 2T_{\text{pro}}(i)\right)}} \tag{4.16}$$

Denote the probability that the transmission of the tagged node i is collided in the receiver side with $p_c(i)$. Therefore, the average time between two successive successful transmissions is

$$T_{ss}(i) = T_{st}(i) + (1/p_c(i) - 1)T_{ct}(i) \tag{4.17}$$

Then, the access probability that the node transmits a packet to the central node in a random slot can be expressed as:

$$\mu(i) = \frac{1/(1 - p_c(i))}{T_{ss}} \tag{4.18}$$

Node i accesses the channel with probability $\mu(i)$ in each slot. Denote CR and NC as the set of ESUN nodes carrying critical data and non-critical data, respectively. Thus, the system throughput can be written as:

$$\text{Th}_{tot} = \sum_{i \in \text{RE}} \mu(i) \prod_{c \neq i,\, c \in \text{CR}} (1 - \mu(c))R + \sum_{i \in UR} \mu(j) \prod_{d \neq j,\, j \in \text{NC}} (1 - \mu(d))R \tag{4.19}$$

4.3.3 Optimization Problem

In this section, we first formulate the optimization problem and then show how to solve it using the proposed analytical model. Denote *CR* and *NC* as the set of ESUN nodes carrying critical data and non-critical data, respectively. Jain's index is used to quantify the fairness of the system and is defined as:

$$J((\text{Th}_1, \text{Th}_2 .. \text{Th}_N)) = \frac{\left(\sum_{i=1}^{N} \text{Th}_i\right)^2}{N \sum_{i=1}^{N} \text{Th}_i^2} \tag{4.20}$$

The goal is to maximize the weighted throughput by the optimal selection of the window size. A tolerance parameter y is used to ensure the fairness due to the different locations.

$$\begin{aligned} \text{maximize}_{\text{CW}_{i,j}} \quad & \alpha_1 \sum_{i \in \text{CR}} \text{Th}_i + \alpha_2 \sum_{j \in NC} \text{Th}_j \\ \text{s.t.} \quad & \text{CW}_{\min} \leq \text{CW}_i \leq CW_{\max}, \\ & J((\text{Th}_1, \text{Th}_2..\text{Th}_N)) \geq \gamma, \end{aligned} \tag{4.21}$$

where the first constraint represents the constraints on the selections on the window size and the second constraint specifies the fairness requirement. For non-convex problems, Branch and Bound (BnB) optimization method [32] can be used to find the optimal solution. Thus, BnB algorithm is adopted to find the optimal solution. In BnB algorithm, the searching space is divided into different subsets which is called branching or splitting. The algorithm keeps track of both lower bound and upper bound of each branch. These bounds are used to prune the search space. Because the bound on the branch may prove that candidate solutions in this branch do not contain an optimal solution. Therefore, many branches can be terminated.

4.4 Learning-Based Random Access for ESUN Nodes

Using the analytical model proposed in Sect. 4.3, the optimal window size can be determined when the full network information, i.e., the number of ESUN nodes, energy harvesting rate P_e, traffic parameter P_e can be obtained.

In practice, network information from every individual node may not be able to obtain accurately and timely at the AP side. Additionally, the stochastic nature in energy harvesting and data generation results the number of ready nodes in the network contending for channel access may vary from time to time, which is very difficult to track at the AP. Thus motivated, the powerful reinforcement learning algorithm which can allow each node to autonomously adapt their action, i.e., selecting a random window for channel access, based on its own interactions with the network environment.

Specifically, we propose a distributed learning algorithm based on multi-armed bandit learning for each node. Different from some other learning algorithms like Q-learning or SARSA learning, multi-armed bandit learning is stateless, which means that there is no state nor state transitions and the reward is only dependent on the action space. In the original multi-armed bandit problem, there is a slot machine with n arms with each arm having its own rigged probability distribution of success. Since the true probability distributions of n arms are not known, the ultimate target is to find the optimal arm regardless of the state. The multi-armed bandit learning is carried out via the means of trial-and-error and value estimation. In our problem, all ESUN nodes have different selections of random-access parameter, i.e., contention window CW which can be modeled as different arms (action).

Denote as the instant reward received when action a is chosen for the k-th time slot. And $Qk(a)$ denotes the estimation of action a after it has been selected for k — 1 times, which can be written as [33]:

$$Q_k(a) = \frac{R_1(a) + R_2(a) + \ldots + R_{k-1}(a)}{k-1} \tag{4.22}$$

According to (22), a record of all previous rewards is needed to obtain the estimated Q-value. However, the problem is that the memory and computational requirements would grow over time as more rewards are obtained. For simplicity, we can devise incremental formulas for updating averages with small, constant computation required to process each new reward. Equation (4.22) can be rewritten as:

$$Q_k(a) = Q_{k-1} + \frac{1}{k-1}(R_{k-1}(a) - Q_{k-1}(a)) \tag{4.23}$$

In reinforcement learning, there is a classic explore-exploit dilemma need to be addressed. More specifically, the agents have to choose between exploring new actions which may potentially yield higher rewards in the future and exploiting the state that yields the highest reward based on the existing knowledge. To strike a balance between the exploration and the exploitation, we adopt the £-greedy policy as the exploration strategy. In ε-greedy policy, the probability that an agent selects a random action is ε and the probability that the action with the highest Q-value is chosen is (1- ε) [34]. Instead of using a constant ε, a decayed ε is adopted. A high value of ε—1 is used in the beginning to ensure that more explorations are performed and the ε decays when agent has already investigated some actions and built confidence in selecting a good action. Specifically, in this algorithm, we decrement the value of ε by a p_ε (e.g., $p_\varepsilon = 0.1$) after a number of N_ε iterations until ε reaches the minimum value $\varepsilon_{\min}$.

The definitions of each element in the learning algorithm are listed as follows:

- Agent:
  Each ESUN node is an agent.
- Action:
  The action of each agent is to select a window size that can maximize the weighted throughput while satisfying fairness constraint. Let CW_{min} and CW_{max} denote the minimum and the maximum window sizes that can be selected, respectively. The window size that can be selected is from *[CWmin, CW + CWstep, CWmax],* where *CWstep* is the step size of the window size. Each node only selects the action when it has data and sufficient energy for transmission.
- Reward:
  We define the reward of action a as,

$$R(a) = \begin{cases} \alpha_1 \sum_{i \in CN} \mathrm{Th}_i + \alpha_2 \sum_{j \in NC} \mathrm{Th}_j, J \geq \gamma \\ 0. J < \gamma \end{cases}$$

In one observation window, the AP monitors the successful transmissions and calculates the weighted sum throughput. Then, the AP sends this information to all nodes through ACK frames or broadcast beacon frames.

Algorithm 4.1: Cooperative Learning Algorithm for Optimal Contention Window Selection

Input:

CW_{min}, the minimum value of CW; CW_{max}, the maximum value of CW;
£, the exploration policy parameter; N_e, the number of iterations before reducing £;
Emin, the minimum value of of ε;γ, the tolerance rate;
Te, the time of one episode.

Output:

CW*, the optimal CW; For each node ;

while *convergence is not reached* **do**

if N_ε *has been reached* **then**

$\varepsilon = \max(\varepsilon_{\min}, \varepsilon - p_\varepsilon)$

Randomly choose $p_e \in [0, 1]$**;**

if $p_e < \varepsilon$ **then**

Enter exploration;
Select the next action randomly

else

Enter exploitation;
Select the next action with maximum Q value

Receive a reward;

if $J \geq \gamma$ **then**

Receive the reward: $a_1 \sum_{i \in \mathrm{RE}} \mathrm{Th}_i + a_2 \sum_{j \in \mathrm{UR}} \mathrm{Th}_j$

else

Receive the reward:
0

Update the Q table;

In the learning process, we consider the ESUN nodes take an action and keep the action during an observation window. For example, given the observation window is 200 slots, each ready node keeps to use the same window during $\{200\ k\ 200(k + 1)\}$. Each node can select a new action in the following observation window. The detailed procedure of the learning algorithm is described in Algorithm 4.1.

The detailed proof of convergence of the cooperative learning algorithm can be found in [35]. It has been proven that the convergence can be guaranteed for multi-agent system if one state Q-learning algorithm is used and all agents have a common interest. In our cooperative learning algorithm, the updating rule of Q matrix is the

same as one state Q-learning in [35]. In addition, the agents in our proposed learning algorithm have the same throughput-related reward, which is the common interest of all agents. Therefore, the convergence of the cooperative learning algorithm is guaranteed.

4.5 Performance Evaluation

To validate the proposed analytical model and to evaluate the performance of the proposed learning algorithm, extensive simulations have been performed using MATLAB. We set up the experiments as described in Sect. 4.3. The minimum and maximum backoff window sizes are 8 and 64, and the step size of window change is 2. If not otherwise specified, we set up $N = 40$ nodes, and $P_e(i) = P(i) = 0.1$.

The throughput performance of ESUN nodes with critical data (with immediate ACK in case 1) and non-critical data (with no immediate ACK in case 2) are shown in Fig. 4.5. To illustrate the impact of distance uncertainty on the throughput performance, two groups of ESUN nodes are randomly distributed with mean distance of 75 m and 750 m to the AP. As shown in Fig. 4.5, the throughput of the two groups of nodes with non-critical data in case 2 are the same regardless of the distance; however, in case 1, the nodes with shorter communication distances achieve a much larger throughput than those with longer communication distances.

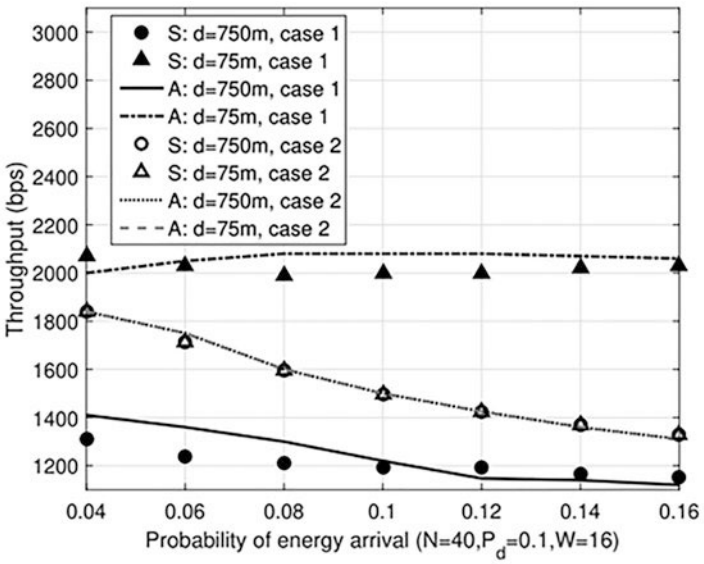

Fig. 4.5 Throughput performance under different P_e

The throughput gap increases with p_e. This is because, in case 1 when critical data is transmitted, an ESUN node needs to wait for an ACK which takes a long round-trip time. Nodes with a smaller communication distance complete a transmission in a shorter round-trip time and thus achieve a higher throughput. For nodes at 75 m, when ACK is used in case 1, ESUN nodes need to wait for an ACK before initiating the next transmission, thus the contention level is reduced. In case 2 when no ACK is required, nodes will not wait for ACK but becomes ready for transmission when energy and data buffer are non-empty. The high contention level in case 2 degrades the throughput performance. When p_e increases, ESUN nodes are more likely to be ready for data transmissions, which increases the contention level and thus degrades the network throughput. To address the fairness problem due to the various propagation delay, the window sizes of nodes should be carefully tuned based on the communication distance.

In Fig. 4.6, the throughput performance under different window sizes is investigated. It can be seen that the throughput in both cases increases with the window sizes CW when $N = 40$ but decreases with CW when $N = 20$. When the number of users is large, the contention level in the network is high, and a larger window can efficiently reduce the collisions. When the number of users is small and the contention level is low, an enlarged window leads to unnecessary waiting time which degrades the throughput. Thus, to attain the best throughput performance, window sizes should be carefully tuned according to the traffic demands in the network.

The average number of ready nodes in a random slot is shown in Fig. 4.7. It can be observed that the number of ready nodes increases with the window size. The larger the window size, the lower the transmission probability. According to Fig. 4.3, the node stays in the ready state with higher probability if the transmission probability becomes smaller. Simulation results validate our analytical model.

We further investigate the network throughput in a more complicated network setting, i.e., half of network nodes carry critical data and the other half of network nodes carry non-critical data. As shown in Fig. 4.8a, nodes with non-critical data (case 1) achieve higher throughput than the nodes with critical data (case 2). Nodes that do not need to wait for ACK will access the channel more aggressively compared with those waiting for ACK and thus achieves a higher throughput. This further jeopardizes the network fairness performance. By increasing the window sizes of nodes with non-critical data, the throughput of nodes with critical data improves at the cost of decreased throughput of nodes with non-critical data, as shown in Fig. 4.8b.

We further implement the proposed multi-agent reinforcement learning algorithm in Algorithm 1 so that each node can adapt its access window based on the interactions with the network. The performance of the proposed algorithm is compared with the theoretical upper bound achieved by solving the formulated optimization problem in Eq. (4.21). As shown in Fig. 4.9, in the first 20 k iterations, the average network throughput is lower than the analytical bound, yet the performance of the proposed algorithm becomes stable after 30 k iterations. In each iteration, each

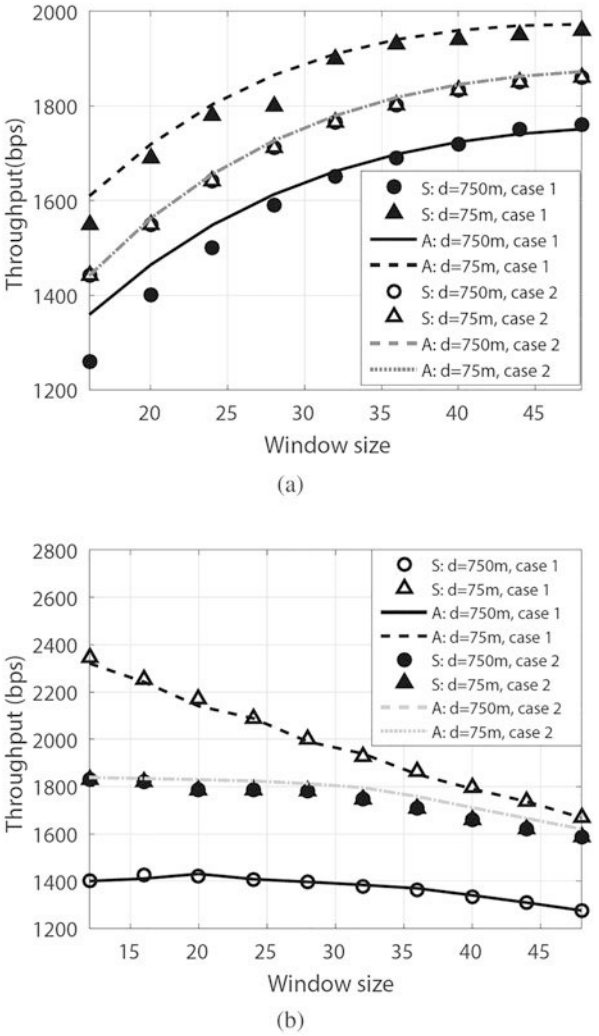

Fig. 4.6 Throughput performance under different window sizes. (**a**) $N = 40$. (**b**) $N = 20$

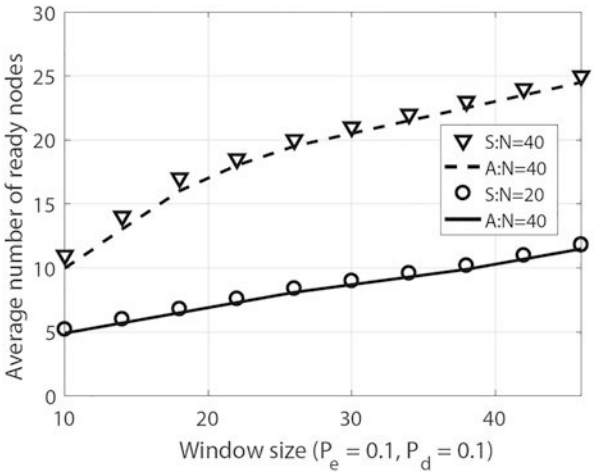

Fig. 4.7 Number of ready nodes

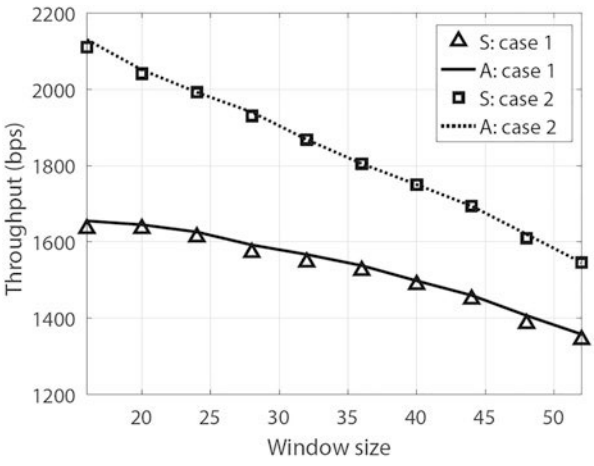

(a)

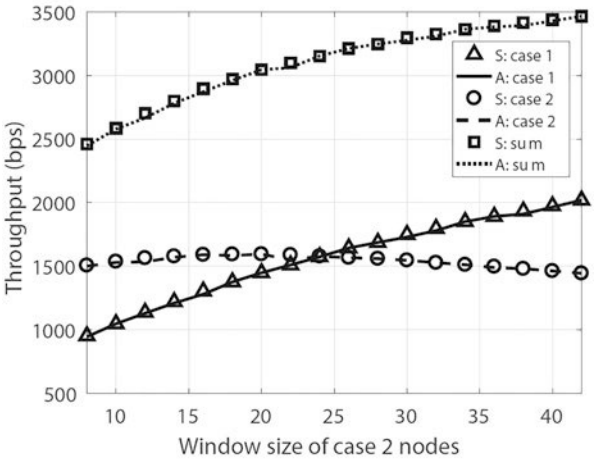

(b)

Fig. 4.8 Network Throughput of co-existed case 1 and case 2. (**a**) Throughput Vs window size. (**b**) Weighted throughput Vs window size

node explores actions randomly or exploits the best action from previous experience. The exploration parameter e decays by iterations, and the throughput becomes stable and closely approaches the analytical upper bound when e decays to zero. Thus, without knowing the detailed network information, an ESUN node can still apply advanced learning technique to attain the sub-optimal network performance.

We further compare the throughput performance of the proposed learning algorithm with some existing solutions in the literature. The first benchmark algorithm uses the fixed window without adaption, as most existing networks implement. The second benchmark algorithm is random algorithm, which selects a window size randomly from [CW_{min}, CW_{max}]. It can be seen in Fig. 4.10a, the fixed algorithm

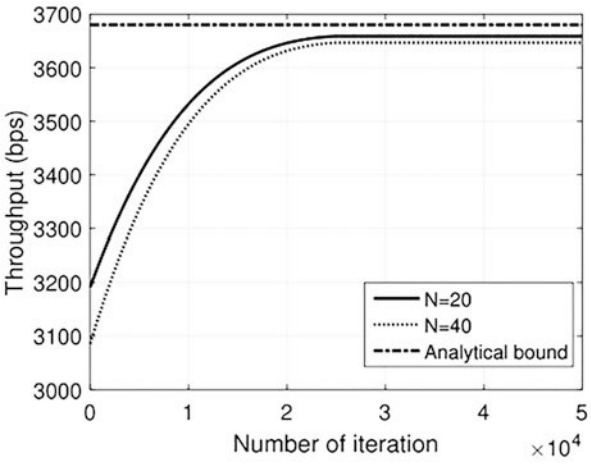

Fig. 4.9 Throughput of the learning algorithm

achieves the lowest throughput among all algorithms, when no fairness constraint is considered. The proposed learning-based algorithm greatly outperforms the other two algorithms and even closely approaches the analytical upper bound. Similar results can be also found in Fig. 4.10b with the fairness constraint.

4.6 Conclusions

In this chapter, we have proposed an analytical model to study the performance of a random access based ESUN by considering the stochastic nature of energy harvesting and the unique feature of acoustic communication channel. It has been found that spatial uncertainty causes severe fairness issue in an ESUN network. By jointly considering the network throughput and fairness, an optimization problem has been formulated. Given the global network information, the optimization problem can be solved using BnB optimization method. In a dynamic network setting where the global network information is not available, a multi-agent reinforcement learning approach has been applied for each node to adapt the access parameter based on the interactions with the dynamic network environment. Numerical results have validated the analysis. It has also been shown that the performance of the proposed learning algorithm can closely approach the analytical bound and outperform some existing solutions.

In our future work, we plan to extend the work in a large-scale ESUN with multiple APs and massive numbers of ESUN nodes operating on multiple acoustic communication channels. Channel allocation and access control under co-channel and cross-channel interference will be jointly investigated.

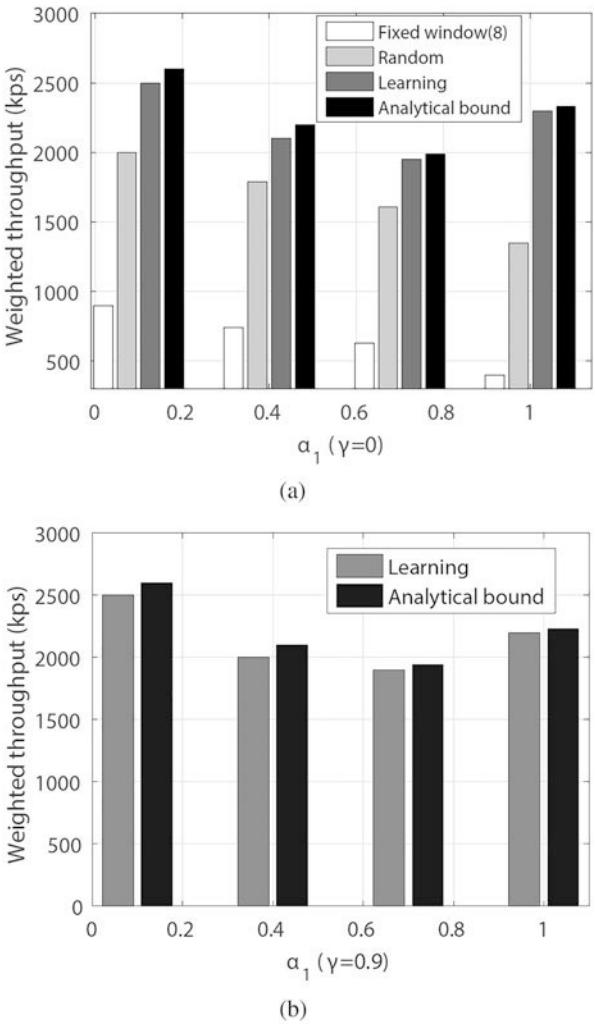

Fig. 4.10 Performance comparisons. (**a**) Without fairness constraint. (**b**) With fairness constraint

References

1. D. J. Cook, A. S. Crandall, B. L. Thomas, N. C. Krishnan, "CASAS: A Smart Home in a Box," Computer, vol. 46, no. 7, pp. 62-69, July 2013.
2. N. Komninos, E. Philippou, A. Pitsillides, "Survey in Smart Grid and Smart Home Security: Issues, Challenges and Countermeasures," IEEE Commun. Surveys Tuts., vol. 16, no. 4, pp. 1933-1954, Fourthquarter 2014.
3. N. E. Cater, T. O'Reilly, "Promoting Interoperable Ocean Sensors the Smart Ocean Sensors Consortium," in OCEANS 2009, Oct 2009, pp. 1-6.

4. H. Chourabi, T. Nam, S. Walker, J. R. Gil-Garcia, S. Mellouli, K. Nahon, T. A. Pardo, H. J. Scholl, "Understanding Smart Cities: An Integrative Framework," in 2012 45th Hawaii International Conference on System Sciences, Jan 2012, pp. 2289-2297.
5. R. Rosli, E. Dimla, "A Review of Tidal Current Energy Resource Assessment: Current Status and Trend," in 2018 5th International Conference on Renewable Energy: Generation and Applications (ICREGA), Feb 2018, pp. 34-40.
6. M. C. Domingo, "An Overview of the Internet of Underwater Things," Journal of Network and Computer Applications, vol. 35, no. 6, pp. 1879-1890, 2012.
7. G. Xu, Y. Shi, X. Sun, W. Shen, "Internet of Things in Marine Environment Monitoring: A Review," Sensors, vol. 19, no. 7, p. 1711, 2019.
8. S. Khairy, M. Han, L. X. Cai, Y. Cheng, "Sustainable wireless IoT networks with RF energy charging over wi-fi (cowifi)," IEEE Internet of Things Journal, vol. 6, no. 6, pp. 10205-10218, 2019.
9. M. Liserre, T. Sauter, J. Y. Hung, "Future Energy Systems: Integrating Renewable Energy Sources into the Smart Power Grid Through Industrial Electronics," IEEE Ind. Electron. Mag., vol. 4, no. 1, pp. 18-37, March 2010.
10. Z. Hou, G. Wang, S. Xu, H. Pan, "The Study on Self-powered Systems for Underwater Sensors Based on Tidal Current Energy," in IOP Conference Series: Earth and Environmental Science, vol. 170, no. 4. IOP Publishing, 2018, p. 042006.
11. P. He, L. Zhao, S. Zhou, Z. Niu, "Recursive Waterfilling for Wireless Links with Energy Harvesting Transmitters," IEEE Trans. Veh. Technol., vol. 63, no. 3, pp. 1232-1241, March 2014.
12. M. K. Park, V. Rodoplu, "UWAN-MAC: An Energy-Efficient MAC Protocol for Underwater Acoustic Wireless Sensor Networks," IEEE J. Ocean. Eng., vol. 32, no. 3, pp. 710-720, July 2007.
13. J. L. Banluta, L. D. Balbuena, N. M. C. Tiglao, J. R. I. Pedrasa, "Comparison of Contention-based MAC Protocols for Underwater Sensor Networks," in 2017 International Conference on Information Networking (ICOIN), Jan 2017, pp. 518-523.
14. S. Shahabudeen, M. Chitre, M. Motani, "MAC protocols that exploit propagation delay in underwater networks," in OCEANS'11 MTS/IEEE KONA, Sep. 2011,pp. 1-6.
15. A. A. Syed, W. Ye, J. Heidemann, B. Krishnamachari, "Understanding Spatio-temporal Uncertainty in Medium Access with ALOHA Protocols," in Proceedings of the second workshop on Underwater networks. ACM, 2007, pp. 41-48.
16. Y. Zhou, K. Chen, J. He, H. Guan, "Enhanced Slotted Aloha Protocols for Underwater Sensor Networks with Large Propagation Delay," in Proc. 1093 IEEE Veh. Technol. Conf. (VTC Spring), May 2011, pp. 1-5.
17. K. Chen, M. Ma, E. Cheng, F. Yuan, W. Su, "A Survey on MAC Protocols for Underwater Wireless Sensor Networks," IEEE Commun. Surveys Tuts., vol. 16, no. 3, pp. 1433-1447, Third 2014.
18. C. Hsu, K. Lai, C. Chou, K. C. Lin, "ST-MAC: Spatial-Temporal MAC Scheduling for Underwater Sensor Networks," in IEEE INFOCOM 2009, April 2009, pp. 1827-1835.
19. F. Alfouzan, A. Shahrabi, S. M. Ghoreyshi, T. Boutaleb, "Graph Colouring MAC Protocol for Underwater Sensor Networks," in 2018IEEE 32ndInternational Conference on Advanced Information Networking and Applications (AINA), May 2018, pp. 120-127.
20. Z. Zhang, W. Shi, Q. Niu, Y. Guo, J. Wang, H. Luo, "A Load-Based Hybrid MAC Protocol for Underwater Wireless Sensor Networks," IEEE Access, vol. 7, pp. 104542-104552, 2019.
21. X. Zhuo, F. Qu, H. Yang, Y. Wei, Y. Wu, J. Li, "Delay and Queue Aware Adaptive Scheduling-Based MAC Protocol for Underwater Acoustic Sensor Networks," IEEE Access, vol. 7, pp. 56263-56275, 2019.
22. F. Alfouzan, A. Shahrabi, S. M. Ghoreyshi, T. Boutaleb, "Performance Comparison of Sender-Based and Receiver-Based Scheduling MAC Protocols for Underwater Sensor Networks," in 2016 19th International Conference on Network-Based Information Systems (NBiS), Sep. 2016, pp. 99-106.

23. F. Alfouzan, A. Shahrabi, T. Boutaleb, S. M. Ghoreyshi, "Efficient Depth-based Scheduling MAC Protocol for Underwater Sensor Networks," in 2017 Ninth International Conference on Ubiquitous and Future Networks (ICUFN), July 2017, pp. 827-832.
24. A. A. Syed, W. Ye, J. Heidemann, "T-Lohi: A New Class of MAC Protocols for Underwater Acoustic Sensor Networks," in IEEE INFOCOM 2008-The 27th Conference on Computer Communications, April 2008, pp. 231-235.
25. N. Chirdchoo, W. Soh, K. C. Chua, "Aloha-Based MAC Protocols with Collision Avoidance for Underwater Acoustic Networks," in IEEE INFOCOM 2007-26th IEEE International Conference on Computer Communications, May 2007, pp. 2271-2275.
26. J. Ahn, B. Krishnamachari, "Performance of a Propagation Delay Tolerant ALOHA protocol for Underwater Wireless Networks," in International Conference on Distributed Computing in Sensor Systems. Springer, 2008, pp. 1-16.
27. Y. Sun, M. Peng, Y. Zhou, Y. Huang, S. Mao, "Application of Machine Learning in Wireless Networks: Key Techniques and Open Issues," IEEE Commun. Surveys Tuts., vol. 21, no. 4, pp. 3072-3108, Fourthquarter 2019.
28. M. Fathi, V. Maihami, P. Moradi, "Reinforcement Learning for Multiple Access Control in Wireless Sensor Networks: Review, Model, and Open Issues," Wireless personal communications, vol. 72, no. 1, pp. 535-547, 2013.
29. N. Ye, X. Li, H. Yu, L. Zhao, W. Liu, X. Hou, "Deep NOMA: A Unified Framework for NOMA Using Deep Multi-Task Learning," IEEE Trans. Wireless Commun., pp. 1-1, 2020.
30. Q. Li, L. Zhao, J. Gao, H. Liang, L. Zhao, X. Tang, "SMDP-Based Coordinated Virtual Machine Allocations in Cloud-Fog Computing Systems," IEEE Internet Things J., vol. 5, no. 3, pp. 1977-1988, June 2018.
31. N. Wu, X. Wang, B. Lin, K. Zhang, "A CNN-Based End-to-End Learning Framework Toward Intelligent Communication Systems",55 IEEE Access, vol. 7, pp. 110197-110204, 2019.
32. P. Belotti, J. Lee, L. Liberti, F. Margot, A. Wachter, "Branching and bounds Tightening Techniques for Non-convex MINLP," Optimization Methods & Software, vol. 24, no. 4-5, pp. 597-634, 2009.
33. R. S. Sutton, A. G. Barto, "Reinforcement learning: An introduction". MIT press, 2018.
34. R. McFarlane, "A Survey of Exploration Strategies in Reinforcement Learning," McGill University, 2018.
35. C. Claus, C. Boutilier, "The dynamics of reinforcement learning in cooperative multiagent systems," AAAI/IAAI, 1998.

Chapter 5
Opportunistic Routing with Q-Learning for Marine Wireless Sensor Networks

In the next generation MWCNs, it is very challenging to monitor the vast marine areas, especially in the deep ocean. To this end, billions of sensors will be deployed over the different depths in the ocean or on the sea surface from Marine Wireless Sensor Networks (MWSNs), to monitor the marine environment and surveil the marine ecosystem. As described in Sect. 1.2.4, energy efficiency is a more difficult challenge for routing in MWSNs due to the harsh marine environment compared with terrestrial wireless sensor networks. In this chapter, we propose an Energy-efficient Depth-based Opportunistic Routing Algorithm with Q-learning (EDORQ) for MWSNs to guarantee the energy-saving and reliable data transmission. It takes the advantages of both Q-learning technique and Opportunistic Routing (OR) algorithm without the full-dimensional location information to improve the network performance in terms of energy consumption, average network overhead, and packet delivery ratio. In EDORQ, the void detection factor, residual energy, and depth information of candidate nodes are jointly considered when defining the Q-value function, which contributes to proactively detect void nodes in advance, meanwhile, to reduce energy consumption. In addition, a simple and scalable void node recovery mode is proposed for the selection of candidate set so as to rescue packets that are stuck in void nodes unfortunately. Furthermore, we design a novel method to set the holding time for the schedule of packet forwarding based on Q-value so as to alleviate the packet collision and redundant transmission. We conduct extensive simulations to evaluate the performance of our proposed algorithm and compare it with other three routing algorithms on Aqua-sim platform (NS2). The results show that the proposed algorithm significantly improves the performance in terms of energy efficiency, packet delivery ratio, and average network overhead without sacrificing too much average packet delay.

This chapter is organized as follows: We present a brief research background in Sect.5.1. The related works are reviewed comprehensively in Sect.5.2. Section 5.3 illustrates the network architecture and Q-learning model in MWSNs. The proposed algorithm is described in detail in Sect.5.4. We report the simulation results and analysis in Sect. 5.5. Section 5.6 concludes this chapter and refers to future works.

B. Lin et al., *Next Generation Marine Wireless Communication Networks*, Wireless Networks, https://doi.org/10.1007/978-3-030-97307-0_5

5.1 Background

With the great application prospects in marine environmental protection, underwater exploration, marine disaster monitoring, offshore operations, and marine military activities, MWSNs have drawn great attention from governments, industry, and academia over the course of the past few years [1, 2]. Routing is a non-trivial task in MWSNs that can ensure fast and reliable transmission of data packets, which becomes one of the most valuable research hotspots recently.

Designing an efficient and reliable routing algorithm is a fundamental but essential research topic in MWSNs. In Chap. 1 we discussed the challenges facing MWCNs at different layers, and the challenges in MWSNs can be summarized in the following.

- The sensor nodes in MWSNs are usually powered by batteries, which are difficult to replace or recharge them because of the harsh and violent underwater environment. Therefore, improving the energy efficiency is one of the most crucial issues that should be considered in the design of routing algorithms for MWSNs.
- Radio signals attenuate rapidly in underwater environment. Larger antennas and higher transmission power are required to propagate at longer distance with extra low frequencies [3–6]. Besides, optical signals are affected by the factors of water clarity, scattering, and precision [6]. Both radio and optical signals cannot meet the requirement of long-distance underwater communication. Thus, acoustic signals are usually adopted in underwater environment to communicate. However, compared with the radio-frequency channel, the bandwidth of an acoustic channel is lower (up to 20 kbps) and the propagation delay is longer (approximately 1500 m/s) [7]. Meanwhile, it may be affected by some unfavorable factors such as path loss, noise, and Doppler spreading, which can cause extremely high packet loss ratio and total energy consumption [2, 6].
- The network topology changes frequently in MWSNs since the sensor nodes move passively with the water currents [8, 9].

Therefore, the inherent features of MWSNs make it difficult to design efficient and appropriate routing algorithms. Due to all the above differences between the terrestrial wireless sensor networks and MWSNs, traditional routing algorithms for terrestrial-based wireless sensor networks are not feasible for MWSNs [10]. Hence specific routing algorithms must be designed to tackle the intrinsic properties in MWSNs.

Underwater OR algorithms have been proposed as a promising paradigm to mitigate these drawbacks and improve the performance of network in an underwater environment [11]. Unlike conventional routing algorithms in which packets are transmitted along the predefined route and a specific neighbor node is selected as the next-hop forwarder, OR algorithms make good use of the broadcast characteristic of wireless channels to select a set of next-hop forwarder candidates [12]. These candidates provide better alternative paths to the destination so that it can adapt to the dynamic underwater topology effectively and reduce the negative effect of weak

links in MWSNs. It can also increase the communication reliability and network throughput by taking advantage of multiple potential relay nodes. However, there are lots of challenges in order to obtain a better performance in MWSNs with the use of OR algorithms [13–15]. A large number of redundant copies can be generated due to the usage of multiple potential candidates during forwarding process, resulting in unnecessary energy losses. Furthermore, the frequently forwarding of some high priority nodes leads to energy exhausted early, which shortens the network lifetime and causes the routing void that occurs whenever the current node has no neighbor closer to the water surface than itself for packet forwarding to the destination. A node is a void node if none of its neighbor nodes makes a positive progress for packet transmission towards the sink on the water surface. Some void-handling approaches are required in OR algorithms to achieve a recovery when the packet reaches a void node [16].

In general, OR algorithms are composed of two main procedures, that is, candidate set selection and candidate set coordination. The candidate set selection procedure is for the purpose of selecting a suitable set of neighboring nodes as potential candidates, which can be further classified into three groups: sender-side-based, receiver-side-based, and hybrid approaches [17, 18]. The candidate set coordination process is responsible to choose relay nodes from candidates and suppress redundant packet transmissions of low-priority nodes. The underwater OR algorithms can be roughly divided into two main categories: localization-based and localization-free. The significant difference between them is whether or not the awareness of location by the sensor nodes [19]. A Focused Beam Routing (FBR) is a localization-based OR algorithm to address energy consumption. It applies the exchanging of Request To Send (RTS) and Clear To Send (CTS) to select forwarders within a cone formed from the source to the destination. It can improve the energy efficiency but it has a low packet delivery ratio in sparse conditions [20].

Due to the accurate three-dimensional information is hard to acquire in an underwater environment, localization-based routing algorithms are difficult to be widely applied. While localization-free algorithms pick out packet forwarders only according to the depth information of the nodes which can be obtained easily [21]. A Depth-Based Routing (DBR) requires water pressure (depth) as a forwarder's selection metric, which achieves great performance improvements in packet delivery ratio and end-to-end delay. However, it has high load on the nodes closer to the water surface [22].

As a classic learning method that interacts with the environment, reinforcement learning is one of the most critical contents in the field of artificial intelligence and machine learning [23]. It does not require agents to grasp the environment model in advance, nor does it require supervision and guidance from supervisors. The Q-learning algorithm is one of the most representative and widely used reinforcement learning algorithms [24]. In the Q-learning algorithm, agents learn continuously to adapt to the environment better according to their received rewards or penalties. Thus, it has great adaptability and flexibility in practical applications [25]. In recent years, several routing algorithms [26–29] based on Q-learning technique are implemented in MWSNs. The Q-learning-based Energy-efficient and

Lifetime-Aware Routing (QELAR) algorithm [26] applies machine learning technique in the distributed underwater routing for the purpose of energy conservation and lifetime extension. But lots of control packets are used to exchange the related information, resulting in unnecessary overhead. The Q-learning based Delay-Aware Routing (QDAR) algorithm for underwater networks aims to extend the lifetime of MWSNs with the aid of Q-learning algorithm. However, the designated routing path needs to be constructed before issuing the data packet, which leading to high end-to-end delay due to the low acoustic velocity. Moreover, the frequent construction of routing paths brings about plenty of additional overheads and energy consumption [27]. The reinforcement learning based data forwarding algorithm with Received Signal Strength (RSS) and Arrival of Angle (AoA) positioning mechanism, to cope with the passive mobility of nodes in underwater routing. By adopting the Q-learning to build the mobile model of sensor nodes, it achieves a good performance in terms of energy consumption but has a low packet delivery ratio [28]. The localization-based routing algorithm based on Q-Learning with additional Kinematics and Sweeping features (QKS) has great adaptability to the dynamic topology by estimating the node velocity and position with the help of Q-learning. However, it is very difficult to realize underwater location [29].

In summary, the depth-based opportunistic routing tackles the harsh underwater environment well but it only focuses on the local optimal selection by employing greedy approaches. Although the aforementioned routing algorithms based on reinforcement learning for MWSNs can improve the network performance in some aspects by observing and learning the environment, some of them cannot control the routing overhead well when exchange the related information about Q-values and the others require position information, in which it is tricky to achieve accurate underwater location. Meanwhile, as far as we know, the Q-learning technique has not been introduced to underwater depth-based OR algorithms basically. Motivated by the above considerations, in this chapter, we propose an EDORQ to further reduce the energy consumption and improve the robustness for MWSNs. Instead of depending on full-dimensional position coordinates for packet delivery, the EDORQ needs only local depth information which can be easily obtained via an inexpensive pressure sensor. Our main contributions in this chapter can be summarized as follows.

- We introduce the Q-learning technique into the underwater OR algorithm, so as to fully utilize their respective advantages. On the one hand, it takes full advantage of the broadcast nature of wireless medium in OR for reliable data packet delivery. On the other hand, global optimization can be achieved through single step Q-value iteration with the aid of Q-learning technique, which overcomes the shortcomings of greedy strategy and local optimization in traditional underwater OR algorithms.
- In our proposal, the void detection factor, residual energy, and depth information of nodes are jointly considered in the reward function of Q-learning, which contributes to proactively detecting and bypassing void nodes in advance as

well as avoids excessive energy consumption for the nodes locating in hot regions.

- We design a simple and scalable void node recovery mode in the candidate set selection phase through a packet backward retransmission manner to recover packets that encounter void nodes unfortunately. Instead of the network topology information, the void recovery mode needs only local depth to go around void nodes, which can further improve the packet delivery ratio, especially in a sparse network.
- We exploit a timer-based candidate set coordination approach to schedule packet forwarding, where a novel method to set the holding time is designed on the basis of Q-value, which helps to reduce the packet collisions and redundant transmissions. Besides, the Q-value is shared in only one hop neighbor, which is beneficial to further decrease overhead and energy cost.

5.2 Related Works

For a special wireless sensor network, the underwater routing algorithm is required to be deliberately tailored to fit the unique characteristics, which poses great challenges to the design of underwater routing algorithms for MWSNs [30]. In this section, we review the related research works on this topic.

In the Vector-Based Forwarding (VBF) routing algorithm for MWSNs [31], a virtual "pipe" from the source to the destination is predefined for the selection of forwarder nodes. The nodes only located in the routing "pipe" can be selected as the qualified candidates. It avoids excessive redundant transmissions since the low-priority nodes are suppressed. However, frequent usage of sensor nodes in "pipe" leads to early death of these nodes. As a result, it will disconnect the routing links and cause the energy distribution unbalanced. A Hop-by-Hop Vector-based Forwarding Algorithm (HH-VBF) is proposed to mitigate the drawbacks of VBF [32]. HH-VBF creates a dynamic virtual routing "pipe" in each hop instead of a fixed vector from the source to the sink. It is less sensitive to "pipe" radius threshold and has a higher opportunity to deliver the packet to the destination in the sparse network. Simulation results show that HH-VBF has better performance of packet delivery ratio and more robustness than VBF. However, more energy is consumed in a dense network due to the dynamic change of the routing "pipe." Furthermore, both VBF and HH-VBF are localization-based OR algorithms, which require sensor nodes to know their own full-dimensional position coordinates information. However, as mentioned before, it is not an easy task for underwater sensor nodes to obtain their location information, which limits the usage of VBF and HH-VBF in practical applications.

The first localization-free routing algorithm is named as Depth-Based Routing (DBR) [22]. As a representative opportunistic routing algorithm, DBR adopts the holding time to schedule packet forwarding. During the holding time, the sensor nodes with the highest priority will suppress the packet forwarding of the other

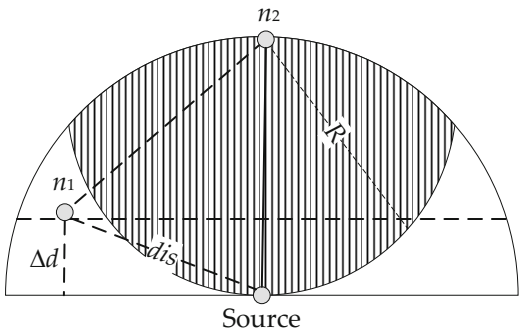

Fig. 5.1 Forwarding zone of Energy-Efficient Depth-Based Routing Algorithm (EE-DBR)

nodes with the lower priority. A fixed depth threshold mechanism is introduced to reduce the number of redundant packets. It requires that the depth difference between the previous hop node and candidate node should be larger than a fixed depth threshold. The mechanism decreases the number of redundant packets to a certain extent in a dense network. However, the defect of this mechanism is that the depth threshold is set to a fixed value even if the underwater nodes are not deployed uniformly. If the value is too large, the packet delivery ratio will be very small in sparse networks. Contrariwise, the number of redundant packets will increase in dense networks if the value is too small. It cannot adapt well to the changing of the senor density.

Aiming at the problem of fixed depth threshold in DBR, the Depth and Energy Aware Dominating Set based algorithm (DEADS) employs an optimized depth threshold mechanism [33]. Three optimal depth threshold values are defined in advance to reduce the scope of candidate set. The source node determines which optimal depth threshold value should be taken on the basis of the number of dead nodes in the network. The algorithm can overcome the defect that the fixed depth threshold only has one value in DBR to a certain extent. However, there are only three optimal values in the dynamic network that cannot adapt to the changing density of sensor nodes well. Furthermore, it needs the whole network information to select the depth threshold that greatly increases the overhead.

In the Energy-Efficient Depth-Based Routing Algorithm (EE-DBR) [34], an underwater Time of Arrival (ToA) ranging technique [35] is introduced to reduce multipath redundancy forwarding. Instead of using the depth threshold mechanism, EE-DBR removes the redundant nodes in the blind zone (nonshaded area in Fig. 5.1) to select the next-hop forwarder candidates. The calculation of blind zone is given as Eq. (5.1).

$$\left(dis^2 - \Delta d^2\right) + (R - \Delta d)^2 > R^2 \tag{5.1}$$

where dis is the minimal distance between node n_1 and source node, which can be obtained by ToA technique. Δd is the depth difference of two nodes and R is the maximum transmission range of one hop. EE-DBR effectively reduces redundancy

energy waste in the blind zone compared with DBR. However, there are still a large number of redundant copies in the non-blind zone in a dense network. What is more, it is challenging to guarantee the synchronization of time when using ToA technique in MWSNs.

Two routing mechanisms of Effective Energy and Reliable Delivery (EERD) and Cooperative Effective Energy and Reliable Delivery (CoEERD) are proposed for MWSNs to improve the energy efficiency and reliability of packet transmissions [36]. EERD is a single path routing mechanism, in which a certain weight function based on residual energy, bit error rate, and shortest distance is designed to prolong the network lifetime and reduce the energy consumption and delay. In order to ensure packet reliability in harsh underwater conditions, the CoEERD, a multiple path routing mechanism, improves the EERD by adding the cooperation of a single relay node between a source–destination pair. However, it increases the energy usage and average delay compared with EERD due to the cooperation of nodes.

Considering the energy balanced localization-free cooperative noise-aware routing for MWSNs, Depth and Noise-Aware Routing (DNAR) and Cooperative DNAR (Co-DNAR) are proposed [37]. DNAR is designed to reduce the energy consumption by combining the extent of link noise with the depth of a node. But only a single link is utilized to send data, which is vulnerable to the harshness of channel. Co-DNAR algorithm proposed to overcome the weaknesses of DNAR. In Co-DNAR, the source–relay–destination triplets in information advancement are applied to reduce the probability of information corruption while with a high data traffic on the relay and the destination nodes.

The above-mentioned OR algorithms can adapt to the MWSNs well but they do not have void-handling techniques to deal with the routing void problem. The Void-Aware Pressure Routing (VAPR) algorithm aims to enhance the performance of opportunistic directional forwarding [38]. The sequence number, hop count, and depth information are used to build a directional trail to the closest sonobuoy, which does not need additional recovery path maintenance. Due to whole network beacon propagation being involved to share the control information, undoubtedly it increases the network overhead.

The Hydraulic-pressure-based Anycast Routing (HydroCast) algorithm is proposed to address the challenges of ocean current and limited resources in MWSNs [39]. HydroCast selects a cluster of candidates with the maximum progress and limited hidden terminals by exploiting the hydraulic pressure level of sensor nodes. A dead-end recovery method is proposed to improve the performance of simple 3D flooding manner. However, as a sender-side-based OR algorithm, it updates the neighbors' information frequently for the selection of next-hop forwarder, which greatly increases the energy consumption.

An Opportunistic Void Avoidance Routing (OVAR) is proposed to handle the void problem and improve the energy efficiency in MWSNs [40]. In OVAR, the adjacency graph is constructed at each hop, which does not require global topology information to impose less overhead. The packet delivery probability and packet advancement are utilized to select the relay nodes, which increases the throughput and reliability in a sparse network. However, the nodes close to the sinks are

frequently involved in packet forwarding, leading to the unbalanced energy consumption of nodes [4].

The Q-learning technique is applied in QELAR so as to learn and adapt to the dynamic underwater environment efficiently [26]. The residual energy of each node is considered into the definition of reward function to prolong the lifetime of network. However, it adopts a large number of "metadata" packets to exchange the information, introducing plenty of overhead and collisions unavoidably. The more sensor nodes in the network, the higher energy will be consumed. Thus, it is unsuitable for dense networks with a great quantity of nodes.

A QDAR is proposed to extend the network lifetime and reduce end-to-end delay [27]. It defines an action-utility function with residual energy-related cost and delay-related cost for routing decisions. The defined "DATA_READY" and "INTEREST" control packets are applied to construct the routing path between sources and sink nodes. However, the designated paths may be easily broken before data packets are sent due to the dynamic topology in MWSNs. Besides, the frequent construction of routing paths results in lots of extra overheads and energy consumption.

In a reinforcement learning-based data forwarding algorithm in MWSNs with passive mobility, the performance of both delay and energy consumption are improved in a specific dynamic scene [28]. AOA and RSS positioning mechanism are used in the phase of orientation determination but the precision is difficult to be guaranteed in UWSNs. What is more, it sacrifices the packet delivery ratio greatly. Thus, it is inappropriate for the delivery ratio sensitive scenarios.

In the underwater routing algorithm based on QKS, the transmission probabilities in Q-value are modeled based on the position and velocity of nodes in order to handle the nodes' high mobility in underwater environment [29]. However, the underwater positioning is a trouble due to the high attenuation of RF and the velocities of nodes in QKS are estimated by Kalman filter, which is also inaccurate underwater.

In conclusion, the aforementioned underwater routing based on reinforcement learning technique enhances the network performance in many aspects, through observing and learning the environment. However, the routing overhead is not controlled well when sharing the related information of Q-values. Besides, it is few and far between for the existing routing algorithms to concentrate on the combination of depth-based OR routing and Q-learning technique in MWSNs, which can make full use of their advantages, respectively. In this chapter, we propose an EDORQ for MWSNs to further reduce the total energy consumption and improve packet delivery ratio. Our algorithm is different from those above as follows. First, the Q-learning technique is utilized in OR algorithm to learn the environment and adapt to the dynamic underwater topology. Second, we take the void detection factor, residual energy, and depth difference information of sensor nodes into account in the construct of Q-value for the void detection and avoidance, which is beneficial to balance the energy distribution, reduce energy consumption, and improve the packet delivery ratio. Next, a simple void recovery mode is designed to select next-hop candidate nodes, which further minimizes the unnecessary energy waste and improves the packet delivery ratio in a sparse network.

Moreover, the timer-based candidate set coordination approach based on Q-value is applied to reduce the collisions of the packets while imposing minimal overhead. Finally, extensive experiments are conducted on the popular Network Simulator Version 2 (NS2) [41] platform. The simulation results demonstrate that our proposal can significantly improve the performance in terms of energy efficiency, packet delivery ratio, and average network overhead.

5.3 System Model

5.3.1 Network Architecture

The MWSN architecture considered in this chapter is depicted in Fig. 5.2, which is composed of underwater sensor nodes, sinks, underwater acoustic channels, and water surface base station. A large number of wireless sensor nodes with acoustic modems are randomly deployed underwater with different depths, operating to collect oceanographic data. Multiple sinks are randomly placed on the water surface and equipped with both radio-frequency and acoustic modems. On the one hand, sinks adopt acoustic signals to receive data packets from underwater sensor nodes. On the other hand, the radio modem is employed by sinks to communicate with the surface base station.

The base station transmits the collected data to the onshore control center for offline information processing. Suppose that with the aid of an inexpensive depth sensor, each sensor node knows its own depth [22], that is, the minimum distance from itself to the water surface. What we discussed is the routing process that data packets are transmitted from underwater sensors to sinks.

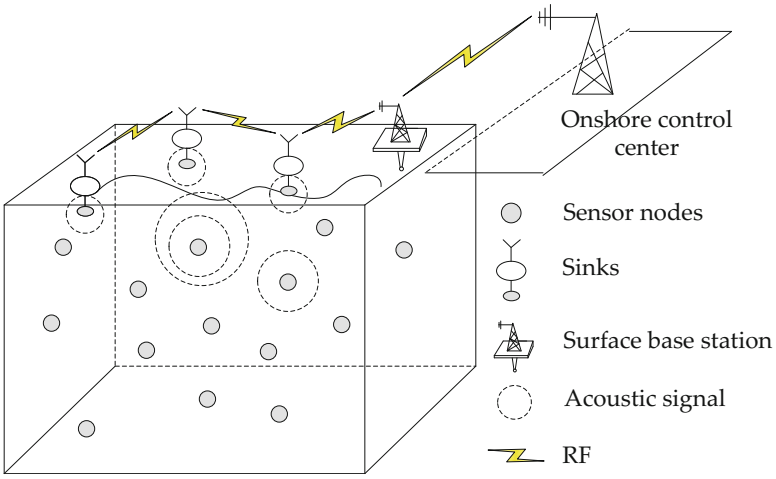

Fig. 5.2 Marine wireless sensor network architecture

5.3.2 Q-Learning Model

5.3.2.1 Markov Decision Process (MDP) Model

The MDP is the optimal decision process of stochastic dynamic system and also the theoretical basis of reinforcement learning. The routing decision process of the entire MWSN can be regarded as a reinforcement learning system. And the routing problem can be formulated as a discrete MDP [23]. The mathematical framework of MDP consists of a tuple of <*S, A, P, R*>, where *S*, *A*, *P*, *R* are the set of discrete states, actions, state transition probabilities, and rewards, respectively. The related definitions in our routing scenario are explained as follows.

Agents Each underwater sensor node is regarded as an independent agent. Sensor nodes distributively learn from the underwater environment to transmit packets, which are described by a finite set of$N = \{n_1, n_2, \ldots\ldots n_j, \ldots\ldots n_m\}$, where $n_j$is the *j*th sensor node and *m* is the total number of sensors.

States $S = \{s_1, s_2, \ldots\ldots s_j, \ldots\ldots s_m\}$ is defined as the states set of the network, where the state s_j represents that the data packet reaches to the node n_j. If a packet is forwarded from node n_i to node n_j, then the state of node transfers from s_i to s_j.

Actions $A = \{a_1, a_2, \ldots\ldots a_j\}$ denotes the set of exploration actions, where the action a_j represents the node n_j is selected as the next-hop forwarder successfully.

Reward $R^{a_j}_{s_i s_j}$ represents an immediate reward (positive or negative) when an agent takes action a_j to make a state transfer from s_i to s_j. The factors to be considered in the construction of the reward function may include energy consumption, network lifetime, average end-to-end delay, and so forth, which depends on the specific task of the scenario.

Probability Transfer Function $P^{a_j}_{s_i s_j}$ indicates the transition probability that node n_i takes the action a_j from state s_i to state s_j successfully, while the failure transition probability is defined as $P^{a_j}_{s_i s_i} = 1 - P^{a_j}_{s_i s_j}$ [26]. In our model, the transition probability can be estimated at run time based on the success or failure history of probability forwarding action.

5.3.2.2 The Basic Q-Learning Technique

Reinforcement learning adopts a "trial-and-error" scheme to interact with the environment, committing to find the optimal behavioral policy to maximize the cumulative rewards [42]. Figure 5.3 depicts the basic pattern of reinforcement learning technique. The agent perceives the current state and the corresponding reinforcement signals (reward or punishment values) from the environment and then to perform an action. The quality of the action selection affects the next state and rewards. If an action makes the environment generate positive rewards, the trend of agent to select

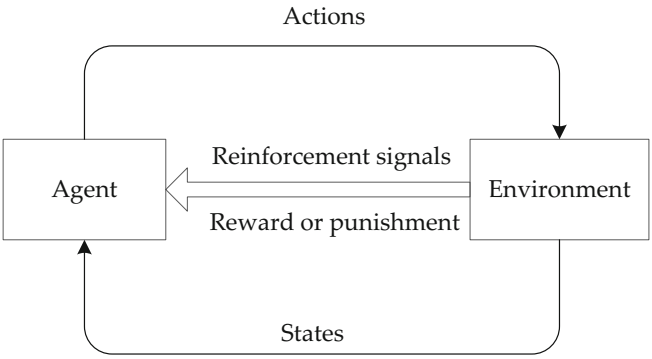

Fig. 5.3 Schematic of reinforcement learning

this action will be strengthened. With the passage of time, the agent will learn an optimal behavioral policy to get a higher reward.

Q-learning is a value-based reinforcement learning technique, which determines an optimal policy to obtain a higher reward in a step-by-step iteration manner. It can evaluate the performance of a given action at a particular state with the aid of the Q-value (action-value), $Q(s_i, a_j)$, which denotes the expected discounted reward for taking an action a_j at the state s_i [24]. The Q-value function satisfies Eq. (5.2):

$$Q(s_i, a_j) = r_i(a_j) + \gamma \sum_{s_j \in S} P^{a_j}_{s_i s_j} \max_a Q(s_j, a). \tag{5.2}$$

where $\gamma (0 \leq \gamma < 1)$ is the discount factor, which is used to determine the importance of future rewards. When γ is small, the agent will pay more attention to the immediate rewards. Conversely, the agent will pay more attention to the future rewards. Typically, to balance the direct and future reward, the value of $\gamma$is within (0.5, 0.99) [26]. $r_i(a_j)$ is the direct reward function, which is critical to Q-learning as it determines the behavior and performance of action $a_j$at the state s_i, which can be defined as follows:

$$r_i(a_j) = \sum_{s_j \in S} P^{a_j}_{s_i s_j} R^{a_j}_{s_i s_j}. \tag{5.3}$$

According to the Bellman's principle of optimality [43] in dynamic programming, once the maximum Q-value function is found, the optimal policy can be obtained. The optimal action a_i^* at state s_i can be acquired as follows:

$$a_i{}^* = \arg\max_{a_i \in A(s_i)} Q(s_i, a_i) \tag{5.4}$$

where $A(s_i)$ is the set of actions that a_i may be chosen at state s_i. A greedy Q-learning algorithm always chooses the action with the highest Q-value, which contributes to the packets being forwarded from source to sinks via the best path.

5.4 EDORQ Algorithm

5.4.1 Overview of EDORQ

The routing process of our proposed algorithm EDORQ includes two phases candidate set selection phase and candidate set coordination phase. The purpose of the first phase is to select a subset of neighbor nodes as candidates to continue forwarding the packet toward the destination. The general candidate set selection method can be divided into two different categories: sender-side-based and receiver-side-based [18]. In the sender-side-based method, the unique ID of candidate nodes is embedded into the data packet by sender to determine the next forwarders. Therefore, lots of control packets are exchanged between nodes to acquire the network topological information. To avoid huge overhead of the network, our proposal employs receiver-side-based candidate set selection method without extra control packets. As a simple and scalable candidate set selection method, it requires that packet receivers decide whether or not to be qualified candidates by themselves. Because of this, energy conservation and channel utilization improvement can be achieved. In EDORQ, the data packet is composed of two parts: packet header and payload data. Its format is illustrated in Fig. 5.4, where the packet header consists of five fields, as follows.

Packet Sequence Number: The unique sequence number of the packet.

Sender ID: Node ID of the node sending the data packet.

Depth: The depth information of the current node.

Q-value: The Q-value of the current node.

Void-flag: A bit information of "0" or "1" identifying whether or not the current forwarder of the packet is a void node. If the node is a void node, the void-flag is filled with "1"; otherwise, the void-flag is filled with "0."

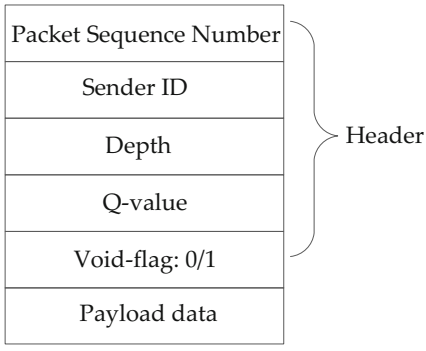

Fig. 5.4 The format of data packets

In the second phase, the candidate nodes will collaborate with each other to decide the forwarding orders with an attempt to suppress the redundant forwarding according to their priorities. To achieve that, the common technique of a timer-based mechanism [17] is applied in EDORQ. However, in order to further minimize the energy consumption and raise the dynamic adaptability, the Q-learning technique is adopted in our proposal to design the holding time mechanism, which is further elaborated in Sect. 5.4.3. The different holding times are assigned to each neighbor node in the candidate set based on Q-value. The potential candidate node with the highest Q-value is first selected as the best forwarder.

5.4.2 Void Detection Based Candidate Set Selection

So as to show the process for candidate set selection clearly, we assume that an intermediate node n_i is the current forwarder aiming to determine the candidate set to continue packet transmission to sinks. $CS(n_i)$ is considered as the candidate set of node n_i. The number of nodes in $CS(n_i)$ has a significant influence on the routing performance. If the number is too small, the packet delivery ratio will be low; otherwise, the energy consumption will be increased. The depth and void-flag information embedded in the data packet header are utilized as the metrics to select the candidate set.

We divide the candidate set selection procedure into two modes of greedy mode and void recovery mode. The greedy mode is first applied to select candidate forwarders, while the void recovery mode is actuated whenever the routing void is encountered. n_i first broadcasts the data packet to its one hop neighbors. After receiving the data packet, each neighbor node extracts the depth d_i and void-flag information of n_i from the packet header and then compares d_i with its own depth. The greedy mode contributes to find a set of candidate nodes closer to the water surface, which can ensure that the data packets are transmitted upwards to the sinks quickly. To this end, the void-flag field in the header of packet is filled with "0," indicating that only the nodes with a smaller depth than the current forwarder can be selected as an eligible candidate. The neighbors with a bigger depth than the current forwarder are not desirable nodes as next forwarders, only discarding the data packet simply. However, one major defect should be properly addressed in the greedy mode is that the data packet may get stuck in a void node, that is, there is no qualified candidate node in its lower depth region. As shown in Fig. 5.5, node n_2 is the next forwarder of n_1. After receiving the packet from n_1, node n_2 first updates the void-flag in packet header with "0" and then sends out it with the greedy mode. If it does not hear that the packet is successfully forwarded during a period of time, then the void recovery mode will be triggered. Subsequently, node n_2 will retransmit the data packet in a void recovery mode, where the void-flag filed is filled with "1," allowing those neighbor nodes with greater depth to be selected as candidate nodes. To suppress duplicate packets, similar to the DBR [22], ideally a node forwards the packet with the same ID only once in a certain time interval. Accordingly, nodes n_3,

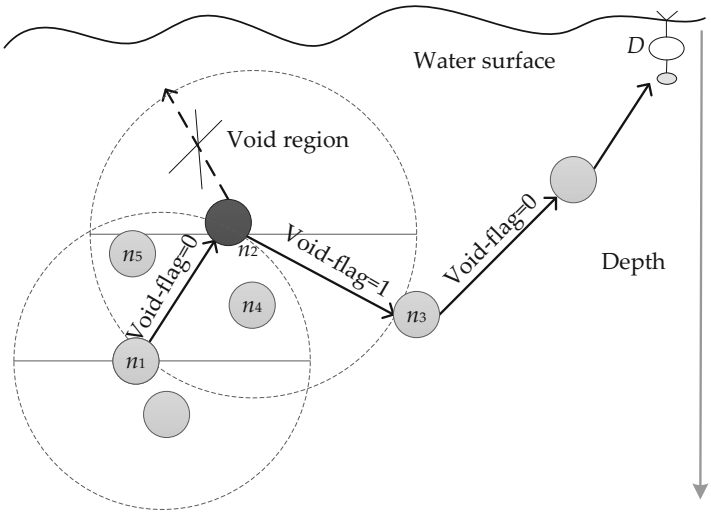

Fig. 5.5 The void recovery mode

n_4, and n_2 form the new candidate set of node n_2. Node n_3 is the optimal next forwarder of n_2 and then it will continue the packet transmission in a greedy mode toward to the sink D until the void node occurs.

The phase of void-detection based candidate set selection is conducted in Algorithms 5.1 and 5.2 describes the switching mechanism of greedy mode and recovery mode.

Algorithm 5.1: Candidate Set Selection
Input: the packet p broadcasted by n_i
Output: $CS(n_i)$ //the candidate set of n_i for packet forwarding

1: $CS(n_i)=\varnothing$
2: **for** each neighbor node of n_i denoted by n_j **do**
3: **if** it has forwarded the packet p **then**
4: drop p
5: **else**
6: extract the depth d_i and n_i.void-flag from p
7: obtain its own depth d_j
8: compute $\Delta d = d_i - d_j$
9: **if** (!n_i.void-flag and Δd > 0) or (n_i.void-flag) **then**
10: $CS(n_i) = CS(n_i) \cup \{n_j\}$
11: **end if**
12: **end if**
13: **end for**

Algorithm 5.2: Forwarding Mode Switch
Input: the packet p received by node n_i
Output: greedy mode or void recovery mode

```
node n_i updates p with d_i
n_i.void-flag=0
BroadcastFlag=True // indicate that whether or not node n_i transmits p
RecoveryFlag=True // indicate whether to activate void recovery mode or not
while (BroadcastFlag) do
   n_i broadcasts p and set a specific timer
      while (timer is not expired) and (RecoveryFlag) do
        overhear the channel
        if n_i overhears p being transmitted then
          RecoveryFlag=False
        end if
      end while
if (RecoveryFlag) and (!n_i.void-flag) then //overhear no transmission of p within
its //timer and it is the first time to activate the void recovery mode
   set n_i.void-flag to 1
else
   drop the packet p
   BroadcastFlag=False
end if
end while
```

5.4.3 Q-Learning Based Candidate Set Coordination

In this subsection, we elaborate on the data forwarding coordination process among candidate nodes based on the Q-value, which is the expected discounted reward for executing an action at a particular state. Some of the main symbols used in this chapter are listed in Table 5.1.

Table 5.1 The main symbols used in the equations

Name	Description
ρ_j	The void detection factor of node n_j
E_j	The energy-related factor of node n_j
D_{ij}	The depth-related factor between nodes n_i and n_j
δ_{ij}	Binary-valued variable
α	Adjustment coefficients of ρ_j
β	Weight factor of rewards E_j and D_{ij}
T_j	The holding time of node n_j

Suppose that node n_j is one of the candidate nodes of current forwarder n_i. In order to make packets detect and bypass the void node in advance as much as possible, meanwhile, minimize energy consumption, we define the immediate reward function $R_{s_i s_j}^{a_j}$ for taking action a_j at state s_i via an exponential function, as follows:

$$R_{s_i s_j}^{a_j} = \left(2 + \alpha\rho_j\right)^{\delta_{ij}\cdot\left[\beta E_j + (1-\beta)D_{ij}\right]} \tag{5.5}$$

$$\text{s.t.}, \delta_{ij} = \begin{cases} 1, & \text{if } n_i \text{ forwards a packet to } n_j \text{ successfully } \left(s_j \neq s_i\right) \\ -1, & \text{otherwise } \left(s_j = s_i\right) \end{cases}, \tag{5.6}$$

where $\rho_j \geq 0$ is designated as a void detection factor, which represents the number of forwarding packets from neighbors with lower depth overheard by node n_j in a period of time. The factor is approximately proportional to the number of potential qualified forwarders of n_j, which is utilized to detect the void nodes in advance. The larger the ρ_j is, the less likely for node n_j to be a void node. We plus two to $\alpha\rho_j$ in order to guarantee the base of exponential function Eq. (5.5) is always greater than 1. $\alpha(0 < \alpha \leq 1)$ is the adjustment coefficients of ρ_j. E_j is the energy-related factor, while D_{ij} is the depth-related factor, which are defined as Eqs. (5.7) and (5.8), respectively. The parameter $\beta \in (0, 1)$ is the weight factor to balance the impact between E_j and D_{ij}.

$$E_j = \frac{e_j^r}{e_j^i}, \tag{5.7}$$

$$D_{ij} = \frac{d_i - d_j}{R_{\max}}, \tag{5.8}$$

where e_j^r and e_j^i are the residual energy and initial energy of node n_j, respectively. Clearly, the more energy node n_j remains, the more rewards it obtains. d_i and d_j are the depth of nodes n_i and n_j, respectively. $R_{\max}$ is the maximum communication range between two sensor nodes. In conventional depth-based routing algorithms [22], the nodes with smaller depth tend to be dead prematurely since they participate in forwarding data packets frequently. Unlike them, our proposed reward function considers both the depth difference and residual energy information of sensors at the same time, which can avoid excessive energy consumption for the nodes with smaller depth. From Eqs. (5.5)–(5.6) we can see that, if the node n_i forwards a packet to n_j successfully, then the immediate reward function $R_{s_i s_j}^{a_j}$ is a monotone increasing function and its value is always more than 1. It indicates that any node with higher residual energy, lower depth, or greater void detection factor has more rewards to be selected as a forwarder node. Otherwise, $R_{s_i s_i}^{a_j}$, the immediate reward function for the case that node n_i fails to forward a packet to n_j is a monotone decreasing function in the range (0,1), which is considered as a penalty for packet delivery failure that is always less than the $R_{s_i s_j}^{a_j}$. For those undesirable candidate

nodes, less residual energy, depth difference, or void detection factor they have, more penalties they will pay. Therefore, the direct reward function for node n_i taking an action a_j is expressed as Eq. (5.9).

$$r_i(a_j) = P^{a_j}_{s_i s_j} R^{a_j}_{s_i s_j} - P^{a_j}_{s_i s_i} R^{a_j}_{s_i s_i}, \tag{5.9}$$

where the state transition probabilities $P^{a_j}_{s_i s_i}$ and $P^{a_j}_{s_i s_j}$ can be estimated by the probabilities of successful and failed packet forwarding, respectively.

The Q-value of n_j can be updated according to Eq. (5.10).

$$Q(s_i, a_j) = r_i(a_j) + \gamma \sum_{s_j \in S} P^{a_j}_{s_i s_j} \max_a Q(s_j, a). \tag{5.10}$$

Suppose that the Q-value of each node is 0 in the initial stage. If the next hop is one of the sinks, n_i transmits the packet with the largest reward in its cache to sink directly.

If all the eligible candidate nodes of n_i take part in forwarding the same packet, then it will result in larger overhead and higher energy consumption. To reduce this waste of energy, we assign a holding time for each candidate node with the principle that nodes with larger Q-value have higher priority and lower holding time. Each candidate node of the current forwarder obtains its Q-value through Eqs. (5.5)–(5.10) and then sets a respective holding time according to the Q-value. The holding time of node n_j can be calculated as follows:

$$T_j = \left[1 - \frac{2}{\pi} \arctan Q(s_i, a_j)\right] T_{\max}, \tag{5.11}$$

where Q(s_i,a_j)is the Q-value calculated by node n_j, $T_{\max}$ is a predefined maximum holding time. In order to further reduce the number of redundant packets, the $T_{\max}$ should be long enough to be able to suppress the duplicate transmission of lower priority nodes before relaying the packet. Thus, $T_{\max}$ can be defined as Eq. (5.12):

$$T_{\max} = \frac{2R_{\max}}{v_s}, \tag{5.12}$$

where v_s is the propagation speed of sound in the water.

The candidate forwarder with a larger Q-value has a shorter holding time, which means that it is preferential to relay the data packet. If a candidate node with a lower priority overhears the same packet transmission of any node with a higher priority within its holding time, then it will discard this packet simply. A simple example is shown in Fig. 5.6, nodes n_2 and n_3 are candidate forwarders of sender n_1. It assumes that the respective Q-value of nodes n_2 and n_3 are 5 and 1. Upon receiving a data packet broadcasted by n_1, nodes n_2 and n_3 start a timer, respectively. After calculating according to Eqs. (5.11)–(5.12), we know that the holding time of n_2 is 0.016 s while n_3 is 0.06 s. Consequently, the optimal action a^* at state s_1 is a_2 and node n_2

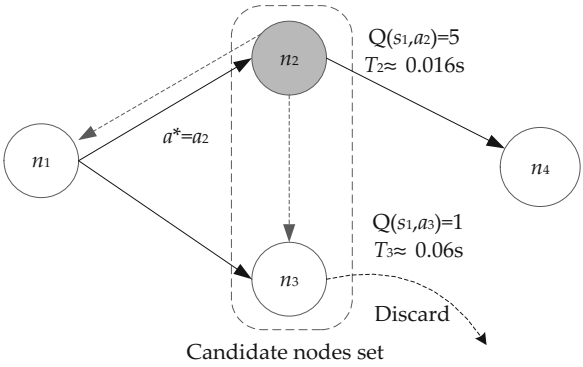

Fig. 5.6 Timer-based candidate coordinate mechanism with Q-learning

will first forwards the data packet when its timer expires. Node n_3 will discard the packet simply when it overhears the same packet transmitted from node n_1 during its holding time. This coordination approach has no additional control or ACK packets and is easy to implement.

In our EDORQ algorithm, a sender node usually has several potential forwarding candidate nodes and each of them has opportunity to forward packets. If the sender overhears no transmission for the same packet from its candidate nodes after the maximum holding time, then the packet retransmission occurs. The sender node will select the new candidate set again in a void recovery mode to expand the range of candidate set. Algorithm 5.3 details the phase of Q-learning based candidate set coordination.

Algorithm 5.3: Candidate Set Coordination
Input: CS (n_i) //candidate set of node n_i
Output: broadcast or drop the packet

```
for each node in CS (n_i) denoted by n_j do
   calculate its Q-value according to Equations (5.5)–(5.10)
   Set its holding time according to Equations (5.11)–(5.12)
   RelayFlag = True // indicates that whether or not a node overhears a packet
within its  // holding time
   while (timer is not expired) and (RelayFlag) do
      if overhear that packet p has been sent by any neighbor then
         RelayFlag = False
      end if
   end while
if (RelayFlag) then
   broadcast the packet
else
   drop the packet
end if
end for
```

5.4.4 Summary

In this subsection, we describe the data packet forwarding process from the perspective of an intermediate receiver sensor node. Upon receiving a data packet, the receiver node determines its eligibility to take part in the packet forwarding or not according to Algorithm 5.1. If it is not selected as a qualified candidate node, then only discards the data packet simply. Otherwise, it will implement the candidate set coordination phase by executing Algorithm 5.3. Firstly, it calculates the Q-value, which is an expect discount reward, on the bases of the void detection factor, depth difference, and residual energy information and subsequently starts a timer with a holding time based on the Q-value to schedule packet forwarding. If the node does not hear that the same packet is forwarded from a higher priority node before itself holding time is expired, then it will relay the packet to continue the routing process in a greedy mode. After that, if it does not overhear the packet be transmitted after a period of time, the void recovery mode will be activated for the reselection of candidate set, in which the forwarding mode switch manner can be referred to Algorithm 5.2.

The main strategy of our proposal is to select a qualified candidate set from one hop neighbor nodes and then to utilize the Q-learning technique for the determination of forwarder nodes with higher priority. In the candidate set selection phase, it takes a time complexity of $O(h)$ at most to select the candidate nodes from neighbors, where h is the size of $CS(n_i)$. The time complexity of the second phase is similar to the algorithm proposed in Reference [28], which is $O(h(h\text{-}1))$. As a result, the complexity of our algorithm can be represented as $O(h^2)$.

5.5 Simulation Results and Analysis

5.5.1 Simulation Setup

In this chapter, we evaluate the performance of the proposed EDORQ algorithm and compare it with VBF [31], DBR [22], and QELAR [26]. All simulations are implemented on the Network Simulator Version 2 (NS2) with an underwater sensor network simulation package (called Aqua-Sim) extension [41]. In our simulations, the source nodes are deployed at the bottom of the network randomly. Unless otherwise specified, four sinks are randomly deployed at the water surface. Each sink is equipped with both radio-frequency and acoustic modems. Once a packet arrives at any sink node successfully, it assumes that the packet reaches the destination. The other sensor nodes are randomly deployed in a 500 m × 500 m × 500 m 3D underwater environment. They follow the random-walk mobility pattern [22]. Each of them moves to a new horizontal direction randomly with a random speed between 1 m/s and 3 m/s, respectively, whereas the vertical movement is considered negligible [22]. Moreover, it adopts LinkQuest UWM1000 [44] as the

Table 5.2 Main simulation parameters

Parameters name	Value
Simulation scene range	500 m × 500 m × 500 m
R_{max}	100 m
Send power	2 w
Receive power	0.1 w
Idle power	0.01 w
Discount factor γ	0.9
α	0.5
β	0.5
Simulation time for each run	800 s

acoustic modem with 10 k bps transmission bit rate and a maximum transmission range of 100 m. These sensor nodes adopt the same propagation model, energy consumption model, and initial energy. The discount factor γ is set as 0.9 [26], while the adjustment coefficients α is set as 0.5. To balance the depth with energy consumption, we set β as 0.5. In order to investigate the effect of node density on the performance of the four algorithms, we perform extensive simulations with different sizes of sensor nodes from 200 to 800, respectively. All of the simulation results are averaged over 20 runs for randomly generated topologies with the 95% confidence interval. For each run, the simulation time is set to 800 s. The main simulation parameters are listed in Table 5.2.

5.5.2 Simulation Metrics

The performances of the four algorithms are assessed by the following four metrics: total energy consumption, packet delivery ratio, average packet delay, and average network overhead.

Total Energy Consumption (TEC) is the total amount of energy consumed by all underwater sensor nodes within the simulation duration, including the energy consumption of nodes in sending, receiving, and idling mode.

Packet Delivery Ratio (PDR) is defined as the proportion of the number of packets successfully received by the sinks to the total number of packets sent by source nodes.

Average Packet Delay (APD) is the average time taken by a data packet transmission from the source to any of the sinks.

Average Network Overhead (ANO) is defined as the ratio of the total number of forwarding packets including data and control packets for all forwarder nodes to the number of data packets successfully delivered to any sink.

5.5.3 Simulation Results

5.5.3.1 Performance Comparison

Figure 5.7 compares the performance of VBF, DBR, QELAR, and EDORQ in terms of total energy consumption for various numbers of nodes. We can observe that the total energy consumptions of the four algorithms increase with an increase of the sensor nodes. The reason is that when the density of nodes increases, the number of qualified forwarding nodes also increases, which causes more energy consumption in sending, receiving, and even idling mode. It is notable that the EDORQ algorithm outperforms other counterparts, followed by QELAR, DBR, and VBF in sequence no matter what the number of sensor nodes. This is attributed to that the use of void recovery mode and void detection factor reduces the chance to encounter a void node, which effectively reduces the energy consumption caused by routing void problem, while neither DBR nor VBF takes it into account. What is more, its holding time based on Q-value of each candidate nodes prevents lots of redundant copies retransmissions that result in less energy consumption than the other three algorithms. In addition, in contrast to QELAR, the EDORQ algorithm does not require too many extra control packets to exchange network information, further avoiding excess energy consumption. QELAR consumes less energy since fewer nodes are involved in the packet forwarding process compared to DBR. The higher energy

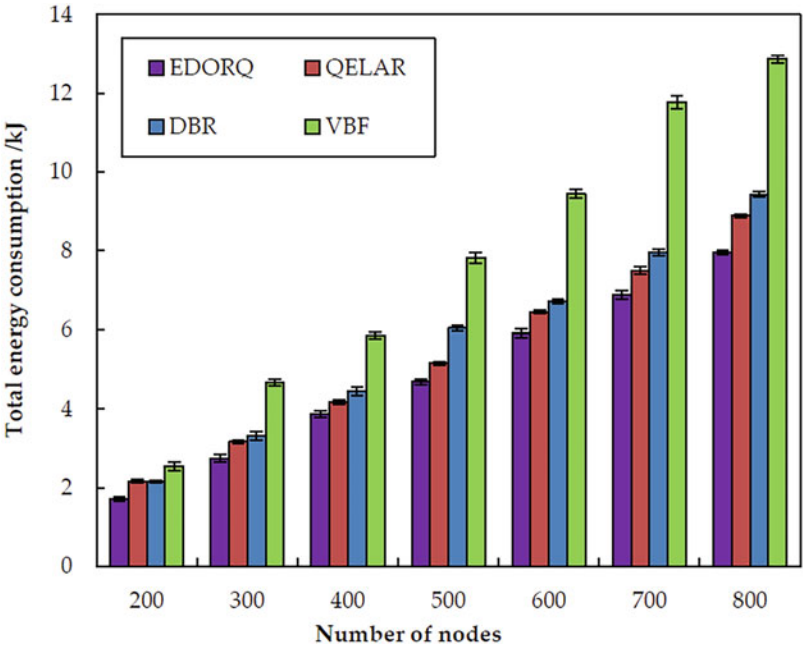

Fig. 5.7 Total energy consumption

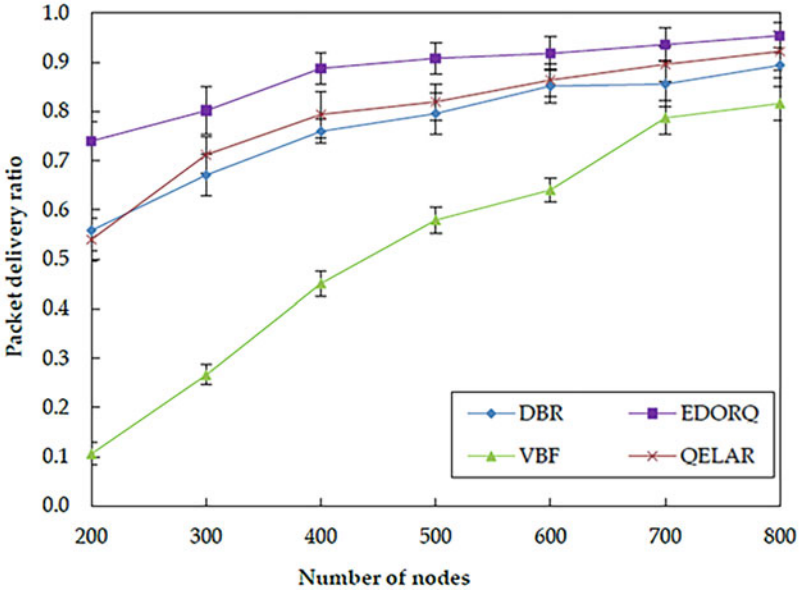

Fig. 5.8 Total energy consumption

consumption result in VBF is mainly caused by a number of redundant transmissions. DBR adopts the fixed depth threshold mechanism to suppress the number of redundant packets, thus it is more efficient at energy saving than VBF.

Figure 5.8 depicts the performance of the four algorithms in terms of packet delivery ratio with different number of nodes. It can be clearly seen that the packet delivery ratio is enhanced as the density being increased. This is because with the number of nodes increasing in the network, the more nodes have opportunity to be selected as suitable forwarder nodes, which leads to a higher packet deliver ratio. It can also be observed that when the number of nodes is greater than 400, DBR, QELAR, and EDORQ can achieve a higher packet delivery ratio (more than 0.75) but this metric of VBF is always at a relatively low level (less than 0.5). The reason is that the packet delivery ratio of VBF is significantly influenced by the radius of routing "pipe" and the location precision underwater. The passive movement of sensor nodes in the networks affects the number of nodes in pipe, thereby reducing the packet delivery ratio of VBF. No matter what the number of sensor nodes, our algorithm has obvious advantages than the other three algorithms and the lower the node density is, the more obvious the advantage is. This is because the void detect factor in Q-value and the void recovery mode in candidate selection phase are used to improve the packet deliver ratio in EDORQ, which can achieve good performance especially in the sparse network.

Figure 5.9 portrays the impact of node density to the average packet delay of the four different algorithms. We can see that the average packet delay of the four algorithms decreases with the increasing of the number of nodes, because the

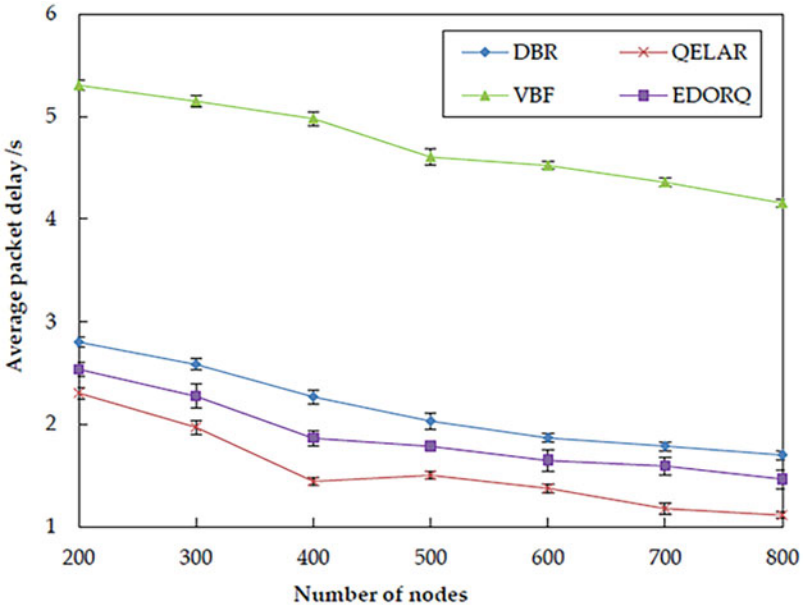

Fig. 5.9 Average packet delay

forwarding node can find more qualified nodes to relay packets in its neighborhoods. Another observation from Fig. 5.9 is that the average packet delay of VBF is higher than other three algorithms. This can be explained by the fact that, in VBF, the packets are delivered only within the routing "pipe" formed from source to sink. However, the nodes located in the "pipe" may not be closer to the surface sink, resulting in higher average packet delay. The average packet delay of DBR is shorter than VBF, it is mainly because that DBR utilizes the multiple-sinks architecture while VBF has only one fixed sink on the water surface. The performance of our proposal in terms of average packet delay is better than DBR but a little weaker than QELAR. Because the Q-leaning based candidate coordination method in EDORQ helps to find the global optimal next-hop forwarder to reduce the packet delay, instead of a local optimal forwarder in DBR, it has a less average latency than DBR. Our method utilizes a holding time based on Q-value to coordinate the forwarding of candidate nodes, in which each packet needs to wait for a moment before it be forwarded, thus causing a slightly higher average packet delay than QELAR.

The results for the average network overhead of the four algorithms at different node densities are illustrated in Fig. 5.10. We can observe that the average network overhead of DBR is smaller than VBF. The reason is that, in VBF, there are too many sensor nodes that are contributed to the process of data forwarding without effective redundant packets suppression technique. Compared to VBF, the utilizing of depth threshold and timer in DBR greatly reduces the number of redundant copies in the network, resulting in the reduction of average overhead. QELAR causes many overheads in the initial stage of routing process when using the Q-learning

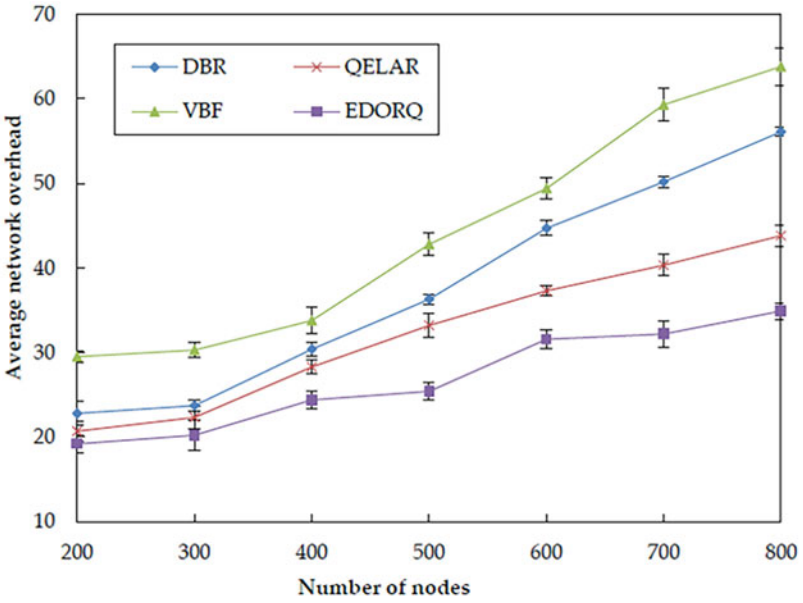

Fig. 5.10 Average network overhead

technique. However, it can find a path of the length near the shortest one; therefore, the overall overhead is smaller than DBR. Compared with QELAR, the proposed EDORQ algorithm applies the timer-based candidate set coordination mechanism based on Q-learning, which decreases the number of packet retransmissions. Meanwhile, it exchanges the related information of Q-value in only one hop neighbor without too many extra control packets, thus it suppresses redundant packet transmissions and avoids causing too much extra overhead. Therefore, the proposed scheme attains superior performance in average network overhead to other three algorithms.

5.5.3.2 Impact of Sink Number

In order to examine how number of sinks impacts the performance of EDORQ, we conduct extensive simulations at varied sink numbers of 1, 2, and 4 under the same operational condition as before. The simulation results for total energy consumption, packet delivery ratio, average packet delay, and average network overhead are shown in Figs. 5.11, 5.12, 5.13, and 5.14, respectively.

From the figures, we can observe that EDORQ has a lower total energy consumption, average packet delay, and average network overhead while a higher packet delivery ratio with more the number of sinks. It is mainly because that the fewer the number of sinks, the greater the probability for a node close to the water surface to be a void node. Thus, with fewer sinks, the void recovery mode will be

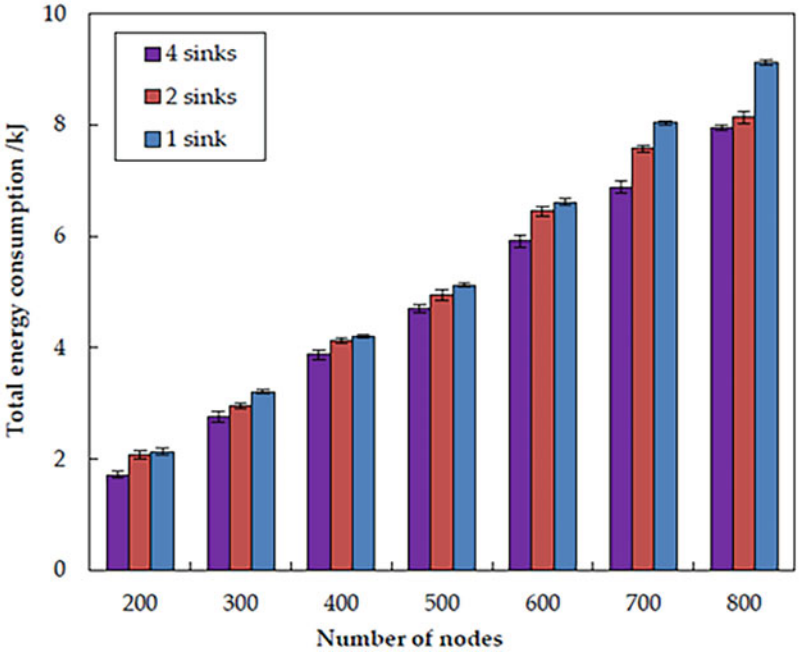

Fig. 5.11 Impact of different number of sinks on the total energy consumption

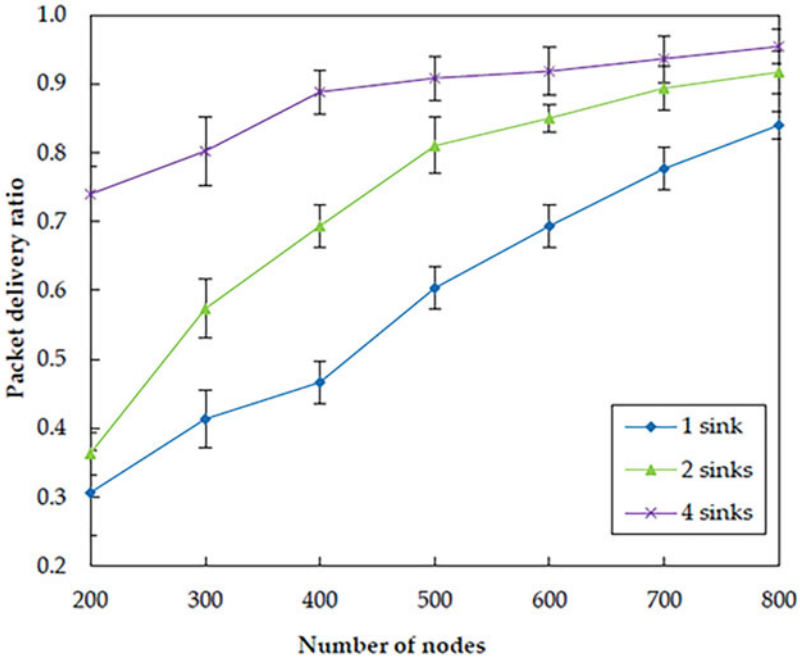

Fig. 5.12 Impact of different number of sinks on the packet delivery ratio

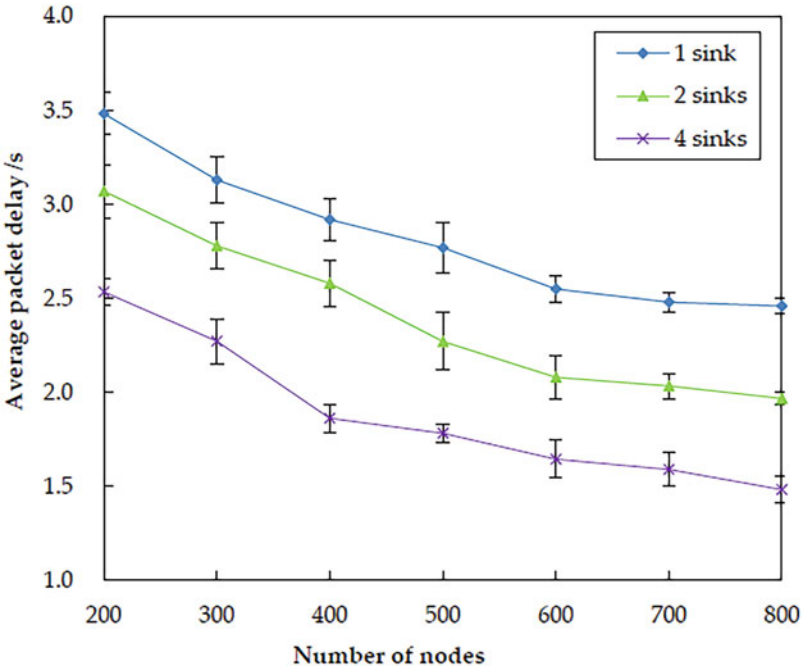

Fig. 5.13 Impact of different number of sinks on the average packet delay

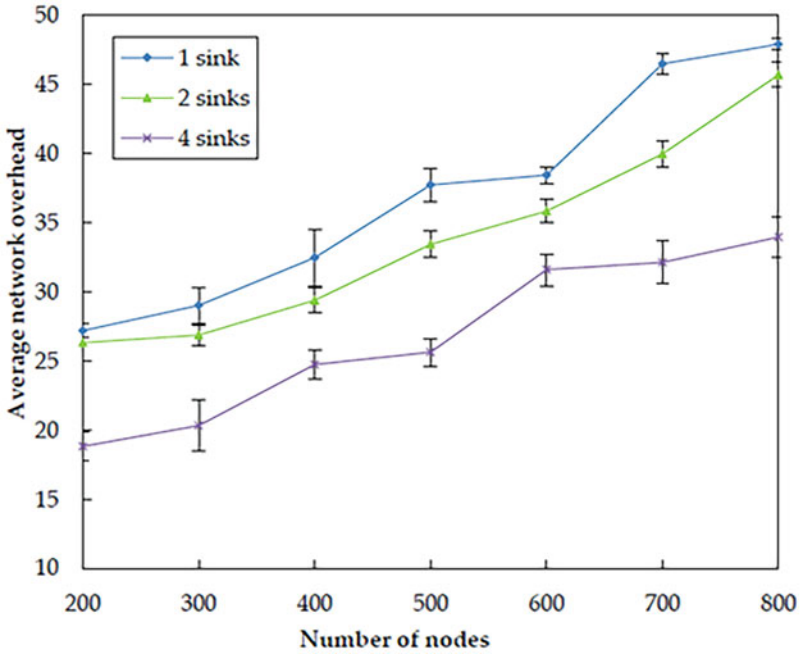

Fig. 5.14 Impact of different number of sinks on the average network

triggered more frequently to recover the data packet suffering from void nodes, which causes plenty of extra energy consumption, delay, and network overhead. On the contrary, more sinks mean an increase in the chance for packets to be delivered to a sink along a shorter path with fewer nodes, which is beneficial to reduce the energy consumption, overhead, and latency. What is more, the increasing of the number of sinks enhances the opportunity for each forwarding node to select more qualified neighbor nodes for packet transmission to any of the sinks, which improves the packet delivery ratio.

5.5.3.3 Impact of Node Mobility

In this subsection, we investigate the impact of node mobility on the performance of EDORQ with different random speed intervals of [1, 3] m/s, [3, 5] m/s, and [5, 7] m/s, respectively, and the other parameters are the same as Sect. 5.5.1. The first number in the bracket is the minimal speed and the second is the maximum speed. Each underwater node randomly selects a horizontal direction and moves with a random speed between the minimal speed and maximal speed. Figures 5.15, 5.16, 5.17, and 5.18 show that how node mobility affects the network performance of EDORQ in terms of total energy consumption, packet delivery ratio, average packet delay, and average network overhead, respectively.

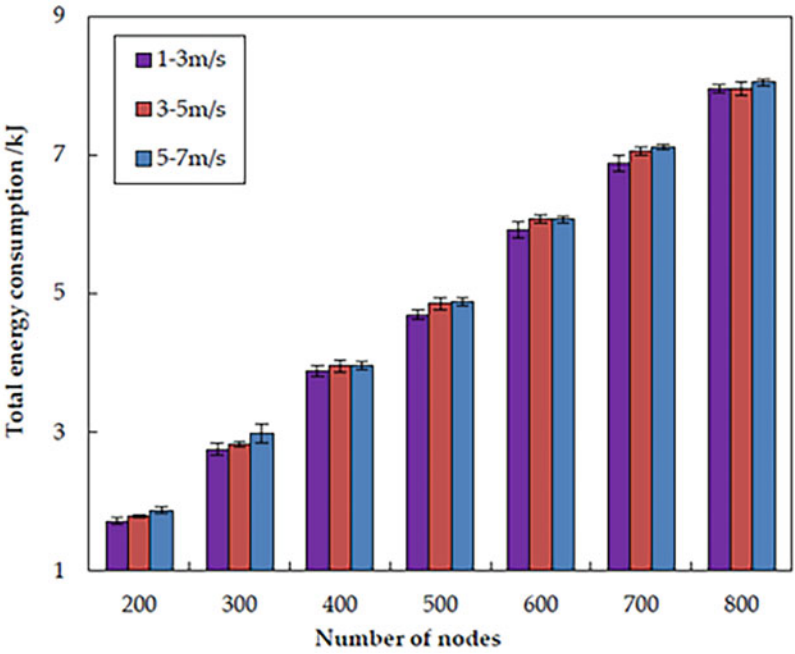

Fig. 5.15 Impact of different node mobility on the total energy consumption

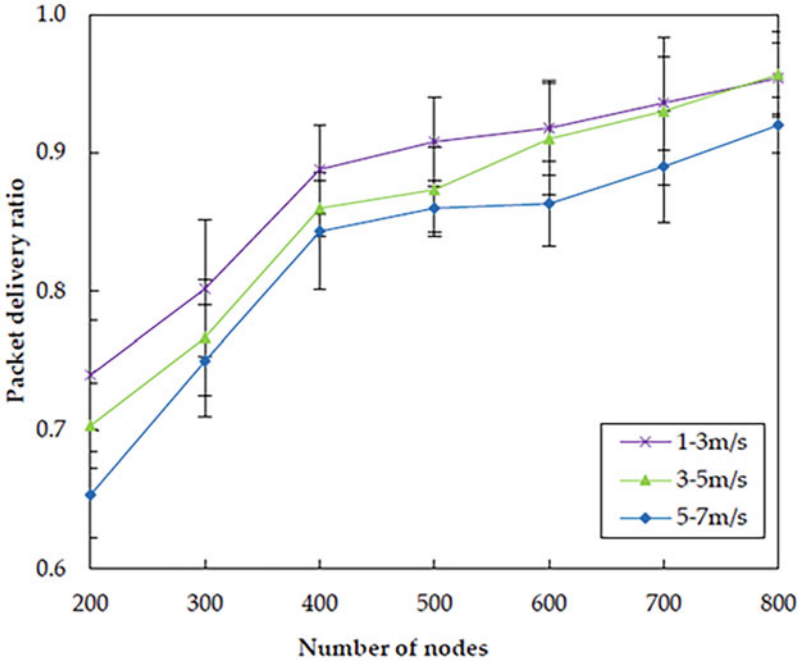

Fig. 5.16 Impact of different node mobility on the packet delivery ratio

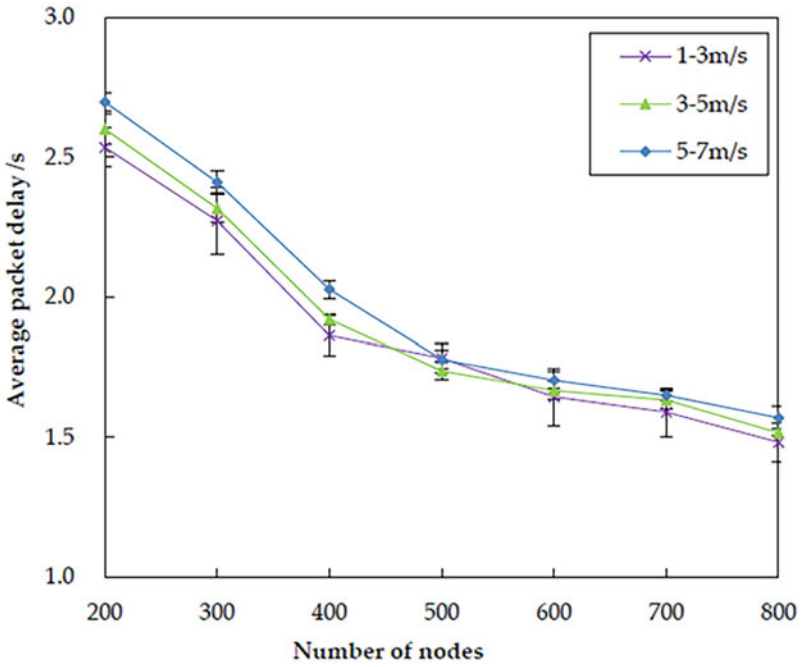

Fig. 5.17 Impact of different node mobility on the average packet delay

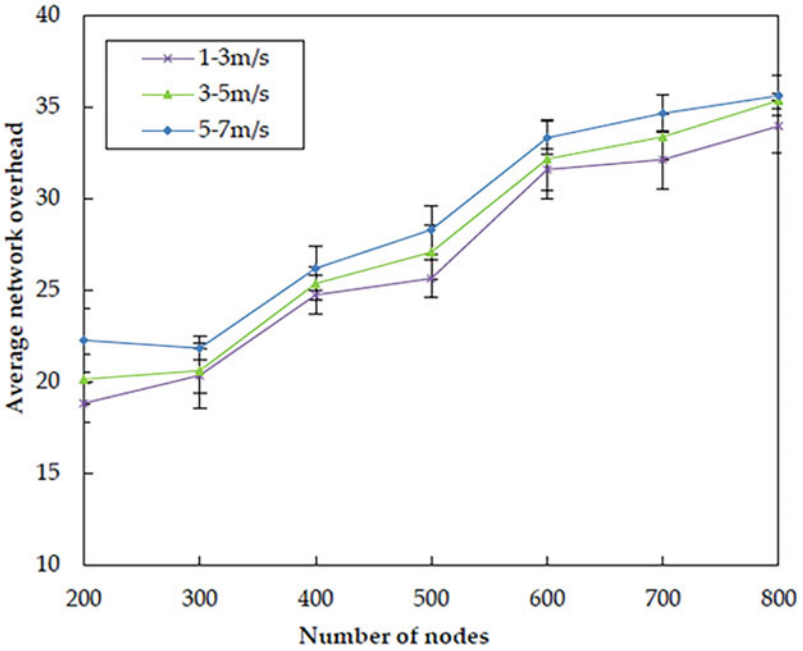

Fig. 5.18 Impact of different node mobility on the average network overhead

As can be observed from the figures, the total energy consumption, average packet delay, and average network overhead will increase slightly while the packet delivery ratio will reduce slightly with the increasing of node speed. It shows that the movement of nodes within a certain speed range does not impact much on the performance of EDORQ algorithm. The reason is that the OR features of our proposal can deal with the dynamic underwater topology to some extent by making the best of multiple potential forwarders. In addition, no exchange of topology or route information is involved among neighbor nodes in EDORQ. Furthermore, the Q-learning technique employed by EDORQ can learn from the network environment and make it have an adaptation to the dynamic underwater topology.

5.6 Conclusions

In this chapter, we have proposed an EDORQ for MWSNs to provide energy-saving and reliable data transmission, which improves the performance of network in terms of energy consumption, average network overhead, and packet deliver ratio by taking the advantages of both OR algorithm and Q-learning technique. It does not need the three-dimensional location information of sensors or other positioning methods like ToA or AOA. In EDORQ, we design the direct reward function with

a joint consideration of a void detection factor, residual energy, and depth difference of sensor nodes to extend the Q-value, which can contribute to detecting and bypassing the void node in advance; meanwhile, minimizing the energy consumption. Furthermore, we design a void recovery mode in the candidate set selection phase to further recover the packet forwarding that is unfortunately trapped in the void nodes. What is more, we propose a novel holing time mechanism based on Q-value to further alleviate collisions and redundant forwarding. Simulation results show that, compared with the DBR, VBF, and QELAR algorithms, our proposed algorithm significantly improves the performance in terms of energy efficiency, packet delivery ratio, and average network overhead without sacrificing too much average packet delay. In the future, we will investigate the novel method to minimize the average packet delay of our proposed EDORQ to make it more flexible to many applications. Additionally, we intend to further extend the Q-value in our EDORQ for different research purposes by considering the influence of ocean currents, channel capacity, and other performance indicators.

References

1. S. Trifunovic, S. T. Kouyoumdjieva, B. Distl, L. Pajevic, G. Karlsson, B. Plattner, A Decade of Research Opportunistic Networks: Challenges, Relevance and Future Directions. IEEE Commun. Mag. 55(1), 168-173 (2017).
2. K. M. Awan, P. A. Shah, K. Iqbal, S. Gillani, W. Ahmad, Y. Nam, Underwater wireless sensor networks: A review of recent issues and challenges. Wirel. Commun. Mob. Comput. 3, 1-20 (2019).
3. G. Han, J. Jiang, N. Bao, L. Wan, M. Guizani, Routing protocols for underwater wireless sensor networks. IEEE Commun. Mag. 53(11), 72-78 (2015).
4. A. Khan, I. Ali, A. Ghani, N. Khan, M. Alsaqer, A. U. Rahman, H. Mahmood, Routing protocols for underwater wireless sensor networks: Taxonomy, research challenges, routing strategies and future directions. Sensors. 18, 1-30 (2018).
5. S. N. Li, W. Y. Qu, C. F. Liu, T. Qiu, Z. Zhao, Survey on high reliability wireless communication for underwater sensor networks. J. Netw. Comput. Appl. 148, 102446 (2019).
6. Z. Q. Zeng, S. Fu, H. H. Zhang, Y. H. Dong, J. L. Cheng, A survey of underwater optical wireless communications. IEEE Commun. Surv. Tuts. 19(1), 204-238 (2016).
7. S. Climent, A. Sanchez, J. V. Capella, N. Meratnia, J. J. Serrano, Underwater acoustic wireless sensor networks: advances and future trends in physical, MAC and routing layers. Sensors. 14(1), 795-833 (2014).
8. L. Li, Y. Qin, X. Zhong, A Novel Routing Scheme for Resource-Constraint Opportunistic Networks: A Cooperative Multiplayer Bargaining Game Approach. IEEE Trans. Veh. Technol. 65(8), 6547-6561 (2016).
9. R. W. L. Coutinho, A. Boukerche, L. F. M. Vieira, A. A. F. Loureiro, Underwater wireless sensor networks: A new challenge for topology control based systems. ACM Comput. Surv. 51(1), 1-19 (2018).
10. M. Zorzi, P. Casari, N. Baldo, A. F. Harris, Energy-efficient routing schemes for underwater acoustic networks. IEEE J. Sel. Areas Commun. 26(9), 1754-1766(2008).
11. W. Bai, H. Wang, K. He, R. Zhao, Path diversity improved opportunistic routing for underwater sensor networks. Sensors. 18(4), 1293 (2018).
12. A. Boukerche, B. Turgut, N. Aydin, M. Z. Ahmad, Routing protocols in ad hoc networks: A survey. Comput. Netw. 55(13), 3032-3080(2011).

13. S. Shaghaghian, M. Coates, Optimal Forwarding in Opportunistic Delay Tolerant Networks with Meeting Rate Estimations. IEEE Trans. Signal Inf. Process. Netw. 1, 104-116(2015).
14. L. F. M. Vieira, Performance and trade-offs of opportunistic routing in underwater networks. In Proceedings of the IEEE Wireless Communications and Networking Conference (WCNC), Shanghai, China, 1-4 April 2012; pp. 2911-2915.
15. R. W. L. Coutinho, A. Boukerche, L. F. M. Vieira, A. A. F. Loureiro, Modeling and analysis of opportunistic routing in low duty-cycle underwater sensor networks. In Proceedings of the 18th ACM International Conference on Modeling, Analysis and Simulation of Wireless and Mobile Systems, Cancun, Mexico, 2-6 November 2015; pp. 125-132.
16. S. M. Ghoreyshi, A. Shahrabi, T. Boutaleb, Void-handling techniques for routing protocols in underwater sensor networks: Survey and challenges. IEEE Commun. Surv. Tutor. 19(2), 800-827(2017).
17. A. Darehshoorzadeh, A. Boukerche, Underwater sensor networks: a new challenge for opportunistic routing protocols. IEEE Commun. Mag. 53(11), 98-107 (2015).
18. R. W. L. Coutinho, A. Boukerche, L. F. M. Vieira, A. A. F. Loureiro, Design guidelines for opportunistic routing in underwater networks. IEEE Commun. Mag. 54(2), 40-48 (2016).
19. N. Li, J. F. Martínez, J. M. M. Chaus, M. Eckert, A survey on underwater acoustic sensor network routing protocols. Sensors. 16(3), 414 (2016).
20. J. M. Jornet, M. Stojanovic, M. Zorzi, Focused beam routing protocol for underwater acoustic networks. In Proceedings of the 3th Workshop on Underwater Networks, San Francisco, California, USA, 15 September 2007; pp. 75-82.
21. T. Wu, N. Sun, A reliable and evenly energy consumed routing protocol for underwater acoustic sensor networks. in Proceedings of the 20th IEEE International Workshop on Computer Aided Modelling and Design of Communication Links and Networks (CAMAD) (2015), pp. 299-302.
22. H. Yan, Z. J. Shi, J. H. Cui, DBR: Depth-based routing for underwater sensor networks. In Proceedings of the 7th International IFIP-TC6 Networking Conference (2008), pp. 72-86.
23. A. Nowé, T. Brys, A gentle introduction to reinforcement learning. in Proceedings of the International Conference on Scalable Uncertainty Management, Cham, Switzerland(2016), pp. 18-32.
24. C. J. C. H. Watkins, P. Dayan, Q-learning. Mach. Learn. 8, 279-292 (1992).
25. M. Tan, Multi-agent reinforcement learning: Independent vs. Cooperative agents. in the Proceedings of the 10th International Conference, Massachusetts, USA(1993), pp. 330-337.
26. T. S. Hu, Y. S. Fei, QELAR: A machine-learning-based adaptive routing protocol for energy-efficient and lifetime-extended underwater sensor networks. IEEE Trans. Mob. Comp. 9(6), 796-809 (2010).
27. Z. G. Jin, Y. Y. Ma, Y. S. Su, A Q-learning-based delay-aware routing algorithm to extend the lifetime of underwater sensor networks. Sensors. 17(7), 1660 (2017).
28. H. T. Chang, J. Feng, C. F. Duan, Reinforcement learning-based data forwarding in underwater wireless sensor networks with passive mobility. Sensors. 19(2), 256 (2019).
29. R. Plate, C. Wakayama, Utilizing kinematics and selective sweeping in reinforcement learning-based routing algorithms for underwater networks. Ad Hoc Netw. 34, 105-120 (2015).
30. M. Ayaz, I. Baig, A. Abdullah, I. Faye, A survey on routing techniques in underwater wireless sensor networks. J. Netw. Comput. Appl. 34(6), 1908-1927(2011).
31. P. Xie, J. H. Cui, L. Li, VBF: Vector-based forwarding protocol for underwater sensor net-works. In Proceedings of the 5th International IFIP-TC6 Networking Conference, Coimbra, Portugal, 15-19 May 2006; pp. 1216-1221.
32. N. Nicolaou, A. See, P. Xie, J. H. Cui, Maggiorini, D. Improving the robustness of location-based routing for underwater sensor networks. In Proceedings of the Oceans 2007 Europe International Conference, Aberdeen, UK, 18-21 June 2007; pp. 1-6.
33. A. Umar, N. Javaid, A. Ahmad, Z. A. Khan, U. Qasim, N. Alrajeh, A. Hayat, DEADS: Depth and energy aware dominating set based algorithm for cooperative routing along with sink mobility in underwater WSNs. Sensors. 15(6), 14458-14486(2015).

34. B. Y. Diao, Y. J. Xu, Z. L. An, F. Wang, C. Li, Improving both energy and time efficiency of depth-based routing for underwater sensor networks. Int. J. Distrib. Sens. Netw. 11(10) 1-9 (2015).
35. Q. L. Liang, B. J. Zhang, C. L. Zhao, Y. M. Pi, TDoA for passive localization: underwater versus terrestrial environment. IEEE Trans. Parallel Distrib. Syst. 24(10), 2100-2108(2013).
36. U. Ullah, A. Khan, M. Zareei, I. Ali, H. Khattak, I. U. Din, Energy-effective cooperative and reliable delivery routing protocols for underwater wireless sensor networks. Energies. 12(13), 2630(2019).
37. J. Qadir, A. Khan, M. Zareei, C. Vargas-Rosales, Energy balanced localization-free cooperative noise-aware routing protocols for underwater wireless sensor networks. Energies. 12, 4263 (2019).
38. Y. Noh, U. Lee, P. Wang, B. S. C. Choi, M. Gerla, VAPR: Void-Aware Pressure Routing for Underwater Sensor Networks. IEEE. Trans. Mob. Comput. 12(5), 895-908(2012).
39. Y. Noh, U. Lee, S. Lee, P. Wang, L. F. Vieira, J. H. Cui, M. Gerla, K. Kim, Hydrocast: pressure routing for underwater sensor networks. IEEE Trans. Veh. Technol. 65(1), 333-347(2015).
40. S. M. Ghoreyshi, A. Shahrabi, T. Boutaleb, A novel cooperative opportunistic routing scheme for underwater sensor networks. Sensors. 16(3), 297(2016).
41. The Network Simulator - ns-2. Available online: http://www.isi.edu/nanam/ns/ (accessed on 9 October 2019).
42. R. S. Sutton, A. G. Barto, Reinforcement learning: An introduction. IEEE Trans. Neural Netw. Learn. Syst. 9(5), 1054-1054 (1998).
43. V. G. Rolla, M. Curado, A reinforcement learning-based routing for delay tolerant networks. Eng. Appl. Artif. Intell. 26(10), 2243-2250 (2013).
44. LinkQuest Underwater Acoustic Modems UWM1000 Specifications. Available online: http://www.link-quest.com/html/uwm1000.htm (accessed on 15 October 2019).

Chapter 6
Conclusions and Future Directions

In this chapter, we summarize the main research results presented in this book and highlight the potential future research directions.

6.1 Conclusions

As one of the Earth's most valuable resources, maritime resources have attracted increasing attention from both academia and industry in the past decades. To support intensive maritime activities, Marine Wireless Communication Networks (MWCNs) are introduced to provide reliable, low-latency, and low-cost communications services. However, the current MWCNs can only meet the needs of limited services and cannot cope with the ever-increasing growth of marine applications. Thus motivated, in this book, we first briefly introduce the background of MWCNs and then present some recent research in network deployment, channel coding, resource management, and routing design to improve the network performance of MWCNs.

In the first research work, we have presented a multi-tier hierarchical network architecture with support of edge computing that includes the underwater acoustic sub-network, the sea-surface wireless sub-network, and the air wireless sub-network. Based on the network architecture, we have formulated an MO problem to minimize the total network deployment cost and to maximize the network lifetime. To solve the MO problem, we have proposed an efficient algorithm, namely AC-ETO, and analyzed its time complexity. The proposed algorithm can approach the optimal solutions under different network scales within polynomial time.

In the second research work, we have proposed a novel OFDM autoencoder, which employs CNN and LSTM layers to facilitate end-to-end learning. The proposed learning-based autoencoder not only works for maritime communications, but also is suitable for a communication system where a precise channel model is either impractical or impossible. Meanwhile, we have also proposed a new channel estimation algorithm for OFDM systems that marries the power of DL with the

B. Lin et al., *Next Generation Marine Wireless Communication Networks*, Wireless Networks, https://doi.org/10.1007/978-3-030-97307-0_6

idea of super-resolution reconstruction. A specially designed Dense-Net architecture is used to reconstruct a low-resolution pilot information image into a high-resolution image.

In the third research work, an analytical model has been proposed to study the performance of a random access based UMWCN network, taking into consideration the stochastic nature of energy harvesting and the unique feature of the acoustic communication channel. It has been found that spatial uncertainty causes a severe fairness issue in a UMWCN. By jointly considering the network throughput and fairness, an optimization problem has been formulated. Given the global network information, the optimization problem can be solved using the BnB method. In a dynamic network setting, where the global network information is not available, a multi-agent reinforcement learning approach has been applied for each node to adapt the access parameter based on the interactions with the dynamic network environment. The proposed learning algorithm can closely approach the theoretical upper bound.

In the fourth research work, we have proposed an opportunistic routing algorithm for UWSNs to improve the network performance in terms of energy consumption, average network overhead, and packet delivery ratio by combining the advantages of OR algorithm and Q-learning technique. Unlike some traditional positioning method like ToA or AOA, the proposed algorithm does not require the knowledge of the three-dimensional location information of sensors or other network information. In EDORQ, we design the direct reward function with a joint consideration of a void detection factor, residual energy, and different depths of sensor nodes to extend the Q-value, which can contribute to detecting and bypassing the void node in advance. Additionally, we design a void recovery mode in the candidate set selection phase to further recover the packet forwarding that is unfortunately trapped in the void nodes. Furthermore, we propose a novel holing time mechanism based on Q-value to mitigate collisions and redundant forwarding.

6.2 Future Research Directions

We close this book with the potential research directions including: (1) large space-time scale heterogeneous network fusion; (2) design of flexible elastic protocol based on SDN/NFV; (3) complex mobility management; and (4) communication security.

- Large Space-Time Scale Heterogeneous Network Fusion

The Space-Air-Ground-Sea Integrated Network (SAGSIN) covers a variety of heterogeneous networks with different time and space spans, including space-based satellite networks, space-based networks, ground-based wireless networks, the Internet, etc. Its architecture is multi-layered, and each network has its own network architecture, protocols, and service scenarios, which poses great challenges to the deep integration of the network. In order to solve this problem, it is necessary to

propose generic network architecture that adaptively integrates large-scale spatial-temporal heterogeneous networks to solve the problems of function deployment of heaven and earth multi-network system and distributed interconnection of large-scale heterogeneous networks. Zhao et al. [1] proposed an Adaptive Aggregation Network (AANet) architecture, which uses network endogenous intelligence to realize the dynamic adaptive aggregation ability of different types of network intelligence, and adaptively meet diversified scenarios and business requirements. Conversely, based on the existing architectures such as TCP/IP and mobile Ad-hoc network, it is necessary to design a network protocol system suitable for the integration scenario of space-air-ground-sea, so as to solve the problems of large-scale heterogeneous node identification, large-scale dynamic routing, multi-dimensional resource allocation, multi-system protocol interconnection, and so on.

- Design of Flexible Elastic Protocol Based on SDN/NFV

Traditional networks are constrained by complex operation logic and physical limited network resources and lack of support for network scalability and service flexibility. For example, the existing network functions are generally realized by the corresponding hardware and are highly coupled with the equipment. Therefore, when the network needs to deploy new functions, the cycle and cost of network update are too high. For SAGSIN, because it covers the future human production and living space, it needs to support a variety of emerging new network architectures, equipment, functions, and services, which puts forward higher requirements for the scalability of the network. In recent years, a series of network generalization and virtualization technologies represented by SDN/NFV provide new possibilities to improve the scalability, reusability, and flexibility of the network. With the help of SDN/NFV, the control surface and data surface of the network can be decoupled, and various network resources and functions can be deployed and allocated more flexibly through virtualization, so as to realize service-oriented and user demand-oriented network control and optimization.

Papa et al. [2] proposed a deployment method of dynamic SDN controller in LEO satellite constellation network to deal with the dynamic changes of network traffic with users' geographical location and time zone. On demand service is an important issue in SAGSIN. Ahmed et al. [3] used SDN/NFV technology to transform SAGSIN from a connection-based model to a service-based model, which has high service customization and adaptability, so as to realize the on-demand allocation of resources. Due to the dynamic nature of resources and the uncertainty of services in the air space integrated network, the traditional methods are not suitable for decision-making tasks with high efficiency and response speed, such as service function chain deployment and mapping. Reinforcement Learning (RL) method, as a self-learning and adaptive decision-making method, has been studied in SDN/NFV network [3–5]. At this stage, the research of RL method in SDN/NFV space earth integrated network requires further investigation.

- Complex Mobility Management

Space-based, air-based, ground-based, and sea-based networks have their own mobile characteristics, resulting in the unique "multi-mobile" characteristics of SAGSIN, which makes their mobile characteristics more complex, more dynamic, and more difficult to describe and predict compared with ground-based networks, which hinders the provision of efficient and coherent service guarantee. Therefore, the mobility management of SAGSIN is an important challenge to be addressed. Among them, designing an efficient switching mechanism is an effective way to solve the service interruption caused by mobility. However, because the received signal strength of satellite signals is usually low, traditional switching methods based on signal strength or bit error rate threshold are no longer applicable. Therefore, it is more suitable for complex SAGSIN environment to consider a variety of judgment criteria and make a switch decision using machine learning algorithm. Foong [6] presents a switching method which takes into account the link quality, QoS, error rate, and signal strength switching indices and uses deep learning networks to blur these indices for different network environments.

Another important task of mobility management in SAGSIN is to design dynamic hybrid network routing protocols to optimize network end-to-end transmission performance. Routing of large-scale space-time transmission services usually requires a combination of a ground-based network, a space-based access network, and a space-based backbone network. Among them, the basic network routing technology is mature, and the space-based network routing protocol with the rise of LEO network and intersatellite communication technology has gradually attracted the attention of the academic community.

- Communication Security

Since SAGSIN integrates various military and civil application systems, we need to ensure the transmissions of a large amount of sensitive data are secure, reliable, and real-time. However, due to the open links, moving nodes, dynamic network topologies, and diverse collaborative algorithms, it is difficult for SAGSIN to efficiently resist jamming, message tampering, malicious attacking, and other security issues.

In addition to the available traditional cryptographic methods, physical layer security, which exploits the physical characteristics of propagation channels to enhance secured wireless links, has been considered as a promising paradigm of the satellite and UAV communication security. How to enhance secure transmission in SAGSIN by utilizing physical layer security mechanisms is an open issue and of great challenges. In this context, jamming and coding may play an important role in adding interference signals to prevent malicious eavesdroppers from decoding the transmitted messages and thus significantly improves quality and reliability of secure communication links between legitimate terminals.

References

1. Y. Zhao, G. Yu, H. Xu, 6G mobile communication network: vision, challenges and key technologies[J]. Scientia Sinica (Informationis), 2019: 963-987.
2. A. Papa, T. Decola, P. Vizarreta, et al., Dynamic SDN controller placement in a LEO constellation satellite network[C]//2018 IEEE Global Communications Conference (GLOBECOM). IEEE, 2018: 206-212.
3. T. Ahmed, A. Alleg, R. Ferrus, et al., On-demand network slicing using SDN/NFV -enabled satellite ground segment systems[C]//2018 4th IEEE Conference on Network Softwarization and Workshops (NetSoft). IEEE, 2018: 242-246.
4. H. J. Ku, J. H. Jung, G. I. Kwon, A study on reinforcement learning based SFC path selection in SDN/NFV[J]. International Journal of Applied Engineering Research, 2017, 12(12): 3439-3443.
5. Y. Xiao, Q. Zhang, F. Liu, et al., NFVdeep: adaptive online service function chain deployment with deep reinforcement learning[C]//The International Symposium on Computer Science, Computer Engineering and Educational Technology. 2019: 1-10.
6. K. C. Foong, Mobility management for satellite/terrestrial multi-service convergence networks [C]//2009 International Conference on Communication Software and Networks. IEEE, 2009: 362-366.

Index

B. Lin et al., *Next Generation Marine Wireless Communication Networks*, Wireless Networks, https://doi.org/10.1007/978-3-030-97307-0